Aus der Klinik für Neurochirurgie der Heinrich-Heine-Universität Düsseldorf

Direktor: Univ.-Prof. Dr. med. D. Hänggi

Study on the therapeutic mechanism of Tumor Treating Fields（TTFields）and Trihexyphenidyl （THP） and identification of clinical predictive expression signature for glioblastoma

Dissertation

zur Erlangung des Grades eines Doktors der Medizin

Der Medizinischen Fakultät der Heinrich-Heine-Universität Düsseldorf

vorgelegt von

Renfei Du

2022

Als Inauguraldissertation gedruckt mit Genehmigung der Medizinischen Fakultät der Heinrich-Heine-Universität Düsseldorf

gez.:

Dekan: Prof. Dr. med. Nikolaj Klöcker

Erstgutachter/in: Prof. Dr. rer. nat. Ulf Kahlert

Zweitgutachter/in: PD Dr. rer. nat. Carsten Berndt

Parts of this work have been published:
Qian C, Xiufu W, Jianxun T, Zihao C, Wenjie S, Jingfeng T, Kahlert UD, Renfei D., A Novel Extracellular Matrix Gene-Based Prognostic Model to Predict Overall Survive in Patients with Glioblastoma, Front Genet. 2022 Jun 17;13:851427

Abstract

Glioblastoma (GBM) is the most common primary brain tumor with has a median survival of only 14 months. Currently, surgery and postoperative adjuvant chemoradiotherapy remain the main treatment for this disease with an average postoperative survival of patients of about seven months due to tumor recurrence. An important factor contributing to postoperative recurrence in patients with GBM are GBM stem cells (GSCs). Hence, inhibiting the proliferation of these cells is of great value for patient overall survival.

In this study, we confirmed that tumor treating fields (TTFields), a new treatment option, can decrease tumor recurrence by inhibiting GSCs adhesion and proliferation, as well as the energy metabolism by using the efficacy test of midfield stimulation (200kHz). RNA sequencing showed that TTFields therapy can lead to dysregulation of several signaling pathways in the tested GBM cell lines. To further explore the inhibitory mechanism, we analyzed AKR1C3, a potential GBM marker, and its involvement in the PI3K-AKT-mTOR-signaling pathway. These results suggested that TTFields might upregulate the expression PTEN through AKR1C3, thereby inhibiting PI3/Akt /mTOR pathway, which then may accelerate the apoptosis in GSCs.

We further analyzed the underlying mechanism of Trihexyphenidyl (THP), which is often used in management of Parkinson's disease and is shown to inhibit the growth of GSCs. To clarify the specific mode of action of this drug on GSCs. CTG-assay revealed that the increase of drug concentration was proportional to the inhibitory effect on the GSCs. In addition, Ki67 proliferation and Annexin V assays confirm that THP inhibit the proliferation and survival of GSCs while not affecting the tumor cell cycle. This was consistent with the observation in xenotransplantation animal experiments. Furthermore, we also attempted to discover the potential targets of the drug on GBM by analyzing the genetic differences between the THP-acting group and the control group. The results suggested that the Cystathionine beta-synthase like (CBSL) gene is a potentially valuable marker candidate. Further study regarding the effect of THP on GBM by targeting CBSL will be explored.

In our third attempt we conducted a bioinformatic analysis to screen prognosis-related extracellular matrix (ECM)-related genes. ECM-related genes can promote tumor development by activating a variety of important pathways and have been confirmed to be associated with the prognosis of GBM patients. We establish a prognostic model for five ECM-related genes (AEBP1, F3, FLNC, IGFBP2, and LDHA), which was further validated in three datasets GSE16011, TCGA-GBM, and GSE83300. We can show that this model can accurately predict GBM patients after surgery 6, 12, 18, 24, 30, and 36 months of survival. To enhance the application scope of the model and to facilitate clinical decision-making, a publicly accessible open-source website (https://ospg.shinyapps.io/OSPG/) was constructed to obtain the survival rates of patients at different time periods.

Overall, in this thesis, we addressed two potential mechanisms by which TTFields and THP inhibit the proliferation of GSCs and demonstrated the potential value of computer-assisted construction of ECM-related gene models to predict patient survival after surgery.

Zusammenfassung

Glioblastom (GBM) ist der häufigste primäre Hirntumor mit einer Überlebenszeit v on nur 14 Monaten. Operative Entfernung des Tumors und die postoperative adjuvante Chemoradiotherapie sind momentan die einzigen Hauptbehandlungen für diese Krankheit, wobei die durchschnittliche postoperative Überlebenszeit der Patienten aufgrund Tumorrezidive etwa sieben Monate beträgt. Ein wichtiger Faktor, der zum postoperativen Wiederauftreten von GBM beiträgt, sind GBM -Stammzellen (GSC). Daher ist die Hemmung der Proliferation dieser Zellen von großem Wert für das Gesamtüberleben der Patienten.

In dieser Arbeit bestätigten wir, dass Tumor Treating Fields (TTFields), eine neue Behandlungsoption, Tumorrezidive verringern können, indem sie die Adhäsion und Proliferation von GSCs sowie deren Energiestoffwechsel bei einer midfield stimulation (200kHz) hemmen. RNA-Sequenzierung zeigte, dass die TTFields-Therapie zu einer Dysregulation verschiedener Signalwege in den getesteten GBM-Zelllinien führt. Unter anderem verifizierten wir AKR1C3, einen potenziellen GBM-Marker und involviert im PI3K-AKT-mTOR-Signalweg. Unsere Ergebnisse deuten darauf hin, dass TTFields die Expression von PTEN durch AKR1C3 hochregulieren und dadurch den PI3/Akt/mTOR-Signalweg hemmt, was wiederum Apoptose in GSCs initiiert könnte.

Weiterhin analysierten wir den zugrunde liegenden Mechanismus von Trihexyphenidyl (THP), ein Parkinson-Krankheit Medikament, welches nachweislich das Wachstum von GSCs hemmt. Wir konnten zeigen, dass der Anstieg der Medikamentenkonzentration proportional zur hemmenden Wirkung auf die GSCs war. Darüber hinaus bes tätigten Ki67 - und Annexin-V-Analysen, dass THP die Proliferation und das Überleben von GSCs hemmt, ohne deren Zellzyklus zu beeinflussen. Dies stimmt mit den Ergebnissen der xenotransplantation Versuche überein. Darüber hinaus analysierten wir die genetischen Unterschiede zwischen der THP-behandelten Gruppe und der Kontrollgruppe, um potenziellen Angriffspunkte des Medikaments auf GBM zu identifizieren. Als potenzieller Markerkandidat wurde das Gen Cystathionin-beta-Synthase-ähnliche (CBSL) gefunden.

In unserem dritten Ansatz führten wir bioinformatische Analysen durch, um prognosebezogene extrazelluläre Matrix (ECM) -verwandte Gene zu untersuchen. ECM-verwandte Gene können die Tumorentwicklung fördern, indem sie eine Vielzahl wichtiger Signalwege aktivieren. Es wurde bereits gezeigt, dass sie mit der Prognose von GBM-Patienten in Verbindung stehen. Wir haben ein Prognosemodell für fünf ECM -verwandte Gene (AEBP1, F3, FLNC, IGFBP2 und LDHA) erstellt, das in drei Datensätzen (GSE16011, TCGA -GBM und GSE83300) weiter validiert wurde. Wir können zeigen, dass dieses Modell die Überlebenszeit nach einer Resektion für 6, 12, 18, 24, 30 und 36 Monate genau vorhersagen kann. Um den Anwendungsbereich des Modells zu erweitern und die klinische Entscheidungsfindung zu erleichtern, wurde eine Open-Source-Website (https://ospg. Shinyapps .io/OSPG/) eingerichtet.

Insgesamt haben wir in dieser Arbeit zwei potenzielle Mechanismen untersucht, die die Proliferation von GSCs hemmen (TTFields und THP), und den potenziellen Wert der computergestützten Konstruktion von ECM -bezogenen Genmodellen zur Vorhersage des Überlebens von Patienten nach der Operation aufgezeigt.

Predictive gene signatures for the clinical course of GBM

- **Background**

Glioblastoma (GBM) is one of the most prevalent brain tumors and is associated with an extremely poor prognosis. Extracellular matrix (ECM)-related genes can promote tumor development by activating many important pathways. Our study aimed to provide an online model to predict the prognosis of GBM by ECM-related genes.

- **Methods**

Firstly, we analyzed the relationship of ECM-related genes with GBM prognosis, and then important genes related to prognosis were used to develop an ECM index in the CGGA dataset. Furthermore, the ECM index is validated on three datasets, namely GSE16011, TCGA-GBM, and GSE83300 to obtain different prognoses, differential expression genes, and potential drugs. A variety of machine learning methods were performed to build a model to predict the survival of GBM patients at 6, 12, 18, 24, 30, and 36 months after diagnosis.

- **Results**

A five ECM-gene signature (AEBP1, F3, FLNC, IGFBP2, and LDHA) was constructed and is proved to be associated with prognosis. GBM patients of the four datasets were divided into high and low ECM-index groups, which showed significantly different overall survival. The prognosis of patients with a high ECM index was worse than that of patients with a low ECM index. The cmap dataset also predicts four small molecules (Podophyllotoxin, Lasalocid, MG-262, and Nystatin) which might reduce the development of GBM. In the independent dataset (GSE83300), the maximum values of prediction accuracy at 6, 12, 18, 24, 30 and 36 months were 0.878, 0.769, 0.748, 0.720, 0.705 and 0.868, respectively. The model constructed by machine learning is provided on a publicly accessible open-source website (https://ospg.shinyapps.io/OSPG/).

- **Conclusion**

Taken together, our findings suggest that ECM genes are prognostic indicators of GBM patients, and this study provides an online server for predicting the survival curves of GBM patients.

Table of Contents

List of Figures

List of Tables

Physical quantities

°C	Degree Celsius
m	Centimeter (10^{-2} m)
eV	Electronvolt
g	Gram
h	Hour
Hz	Herz (1 s^{-1})
K	Kelvin
kDa	Kilodalton (1000 Da = $1.6601 \cdot 10^{-24}$ kg)
kg	Kilogram
kV	Kilovolt
L	Liter
m	Meter
MHz	Megahertz (10^{6} Hz)
min	Minute (60 s)
mL	Milliliter (10^{-3} L)
mm	Millimeter (10^{-3} m)
mmol	Millimol (10^{-3} mol)
mol	Mole (amount of substance, $6.02 \cdot 10^{23}$ particles)
nM	Nanomolar
ppm	Parts per million
rpm	Revolutions per minute
s	Second
µL	Microliter (10^{-6} L)
µM	Micromolar

List of Abbreviations

ACh	Acetylcholine
ANOVA	Analysis of variance
BBB	Blood-brain barrier
BCE	Before the common era
BCSCs	Brain cancer stem-like cells
BTSC233	Glioblastoma cell line
CNS	central nervous system
CT	Computer tomography
CTG	CellTiter-Glo
DLE	Drug loading efficiency
DMEM	Dulbecco's Modified Eagle's medium
DMF	Dimethyl formamide
DMSO	Dimethyl sulfoxide
DNA	Deoxyribonucleic acid
DNP	2,4-dinitrophenyl
DNPH	2,4-dinitrophenyl
e.g.	exempli gratia, for example
hEGF	Human epidermal growth factor
EMT	Epithelial-like-to mesenchymal transition
ESMO	European Society for Medical Oncology
et al.	et alia, and others
etc.	et cetera
FACS	Fluorescence-activated cell sorting
FBS	Fetal bovine serum
FDC	2,5-furandicarboxylate
FGF	Bovine fibroblast growth factor
GABA	Gamma-Aminobutyric acid
GB/GBM	Glioblastoma
GBM1	Glioblastoma cell line
GFP	Green fluorescent protein
GLS1	Glutaminase1 enzyme
GSC(s)	Glioblastoma stem cell(s)

HAADF	High-angle annular dark-field
HEPES	4-(2-hydroxyethyl)-1-piperazineethanesulfonic acid
HIV	Human immunodeficiency virus
HUVE	Human umbilical cord blood stem cells
i.e.	id est, that is
IC50	Half maximal inhibitory concentration
iNSC	Induced neural stem cell
JHH520	Glioblastoma cell line
LDH	Lactate dehydrogenase
LSPR	Localized surface plasmon resonance
MeOH	Methanol
MRI	Magnetic resonance imaging
mTOR	Mammalian Target of Rapamycin
MTT	3-(4,5-dimethylthiazol-2-yl)-2,5-diphenyltetrazo-
NCH644	Glioblastoma cell line
PBS	Phosphate-buffered saline
PC	Propylene carbonate
PD	Parkinson disease
PEG	Polyethylene glycol
PEI	Polyethylenimine
PET	Positron emission tomography
pGBM	Primary glioblastoma
PSMA	Prostate specific membrane antigen
ref.	Reference
rGBM	Recurrent glioblastoma
RL1	Rapalink-1
RNA	Ribonucleic acid
ROS	Reactive oxygen species
RT	Radiotherapy
SEM	Scanning electron microscopy
SERRS	Surface enhanced resonance Raman scattering
SERS	Surface-enhanced Raman scattering
SF188	Glioblastoma cell line

SPECT	Single-photon emission computed tomography
STEM	Scanning transmission electron microscopy
TCGA	The Cancer Genome Atlas
THP	DL-trihexyphenidyl hydrochloride
TMZ	Temozolomide
TTFields	Tumor Treating Fields
U87	Glioblastoma cell line
WHO	World Health Organization
Wnt	Wingless-related integration site

1 Introduction

Glioblastoma is one of the most common malignant brain tumors, patients with this disease have a very poor prognosis, with an average survival of below years. The accompanying decline in neurological function and quality of life can have devastating effects on patients and their families. Traditional surgical methods can not cure gliomas, and with the increase in the number of operations, the malignant degree of glioma will become higher. How close the gap between the lab and patient care is important for all scientists and clinicians. TTF is a new clinical approved treatment, and THP is also a drug newly discovered by our team which can inhibit glioma. Both two types of new treatments are clinically easy to implement, which means I might expand the clinical options to glioma patients in China. To further understand the mechanisms of the new methods, I started the work presented in this thesis.

1.1 Glioblastoma

1.1.1 Overview and cancer stem cells

The incidence of primary brain tumors worldwide is approximately seven per 100,000 individuals per year, accounting for around 2% of all primary tumors. About 7% of the world's population will die of brain cancer before the age of 70. Tumors that arise from glial (non-nerve) cells of the CNS are called gliomas. Gliomas affecting the cerebral hemispheres of adults are termed “diffuse” gliomas due to their propensity to infiltrate, early and extensively, throughout the brain parenchyma[1]. Gliomas with high morbidity and mortality originate from glial or neuronal precursor cells[2], representing approximately 57% of all gliomas and 48% of all primary malignant central nervous system (CNS) tumors[3]. Glioblastoma is the most common malignant brain tumor, patients with this disease have a very poor prognosis, with an average survival of below years[4]. The accompanying decline in neurological function and quality of life can have devastating effects on patients and their families.

In 2016, the World Health Organization (WHO) divided gliomas into four grades to facilitate treatment selection based on this classification: Grade I tumors with low proliferation and curable surgical treatment; Grade II tumors are aggressive and often recur. Grade III tumors are usually malignant, characterized by anaplasia and rapid cell division through mitosis; Grade IV is the most malignant and advanced form of all gliomas. Tumors in the grade IV classification

display the poorest prognosis with high resistance and low survival rate. Grades I and II are summarized into low-grade gliomas, and III and IV into high-grade gliomas[5]. The most common type of malignant tumor in the central nervous system are glioblastomas, which account for 48.3% of all malignant tumors and exhibit a poor prognosis, and are defined as grade IV [3]. Clinical manifestations of glioblastoma include headaches, seizures, and focal neurologic deficits[6].

The identification of cancer stem cells (CSCs) or tumor-initiating cells in brain tumors and their cell-specific surface markers is of importance for the diagnosis and treatment of malignancies[7]. These self-renewing populations of tumor cells express enhanced tumorigenic properties leading to the reoccurrence or spreading of tumors. Most glioma CSC markers were adopted from normal stem cells, but the link between glioma CSCs and normal stem cells remains still to be clarified. Many of the transcription factors or structural proteins essential for normal NSPC function also mark glioma CSCs including SOX2. NANOG, MYC, MUSASHI, and many more. In diagnosis, these factors can help to decide the treatment of the patient. For example, Musashi, an RNA-binding protein expressed in undifferentiated stem/precursor cells at both embryonic and adult stages, is important for grading brain tumors and indicates proliferative activity in gliomas and melanomas. These proteins were shown to control the stem cell state through the translational regulation of target mRNAs[8]. GBMs with an intact expression of the PTEN correlated with increased epidermal growth factor receptor (EGFR) inhibitor response and progression-free survival compared with those tumors lacking PTEN[9].

1.1.2 Discussed causes of glioblastoma development

There are few established risk factors for glioblastoma development. Exposure to ionizing radiation is the strongest risk factor associated with glioblastoma and the only known potentially modifiable risk factor[10]. A negative association between glioblastoma and atopic, allergic, and other immune-related disorders has also been established, although the exact underlying biological causes remain to be determined[11]. Furthermore, rare genetic syndromes associated with glioblastomas, such as Li-Fraumeni syndrome and Lynch syndrome are linked to glioblastoma. However, these account for less than 1% of cases[12]. It is important to note that there is no clear, conclusive evidence of an association between cell phone use and the development of gliomas, but that further research is needed and the association remains controversial[13].

1.1.3 Diagnosis and therapy

The diagnosis of glioblastoma (GBM) usually starts in late-stage disease progression, when a symptomatic patient is presented in a specialized center and subjected to magnetic resonance imaging (MRI). (Figure 1)[14].

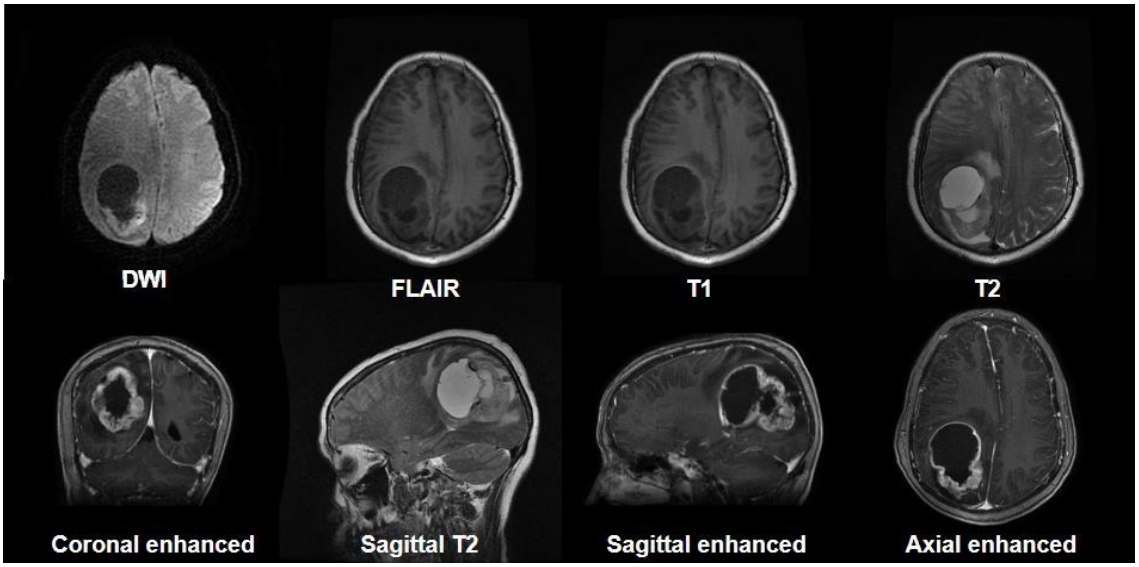

Figure 1: MRI imaging is used for Glioblastoma diagnosis and therapy monitoring.

Current treatment standards include concurrent radiotherapy with temozolomide and adjuvant temozolomide after surgery as well as newer methods including tumor therapy fields that provide low-intensity alternating electric fields combined with adjuvant chemotherapy (temozolomide). This new method will be explained in detail in paragraph 1.2. However, in the event of tumor recurrence, there is no standard treatment or means. Depending on the patient's condition surgery, radiotherapy, systemic chemotherapy (e.g. with bevacizumab), or palliative care with nutritional support may be recommended [3].

Retrospective analysis showed that regardless of the molecular subtype of GBM, maximum surgical resection improved the patients' overall survival[15]. Prospective data from randomized trials of 5-aminolevulinic acid (5-ALA) fluorescently guided resection also showed improvement in patient overall survival[16]. Therefore enhanced MRI scan should be performed within 48 hours postoperatively, which prevents the narrowing of resection and serves as a baseline study for subsequent therapeutic interventions. For situations where surgical or microsurgical resection is not possible, such as medical contraindications or patient refusal, stereo

tactical or open biopsy is also an option[17]. Moreover, TMZ increases GBM sensitivity to radiotherapy[18]. The most effective in O^6-methylguanine-DNA-methyltransferase impaired GBMs, by increasing the degree of radiation-induced double-strand DNA damage[19]. TMZ belongs to a group of anti-cancer drugs that can enter the blood-brain barrier (BBB), which additional could be a limiting factor in the treatment of brain-related diseases, including brain cancers.

The BBB is a protective membrane responsible for brain homeostasis and preventing foreign substances from entering the blood[20]. This barrier normally protects the central nervous system from pathogens or toxins, but it is also a major barrier to the delivery of anti-cancer drugs. It has been shown that most antibodies, proteins, peptides, and small-molecule drugs cannot cross the BBB in pathological conditions. Many drugs fail to treat gliomas because of the BBB[21]. This puts forward very high requirements for our therapeutic drugs. Since TMZ is capable to overcome the BBB it is nowadays used as 'the' standard drug after surgical resection. Despise its action in radio-sensitizing GBM cells, TMZ can also prevent irradiation-induced glioma cell invasion [22] through caspase-mediated prevention of irradiation-induced Focal Adhesion Kinase activation [23]. TMZ also displays antiangiogenic effects in experimental gliomas [24] and has been shown to first induce pro-autophagic defenses in GBM cells [25], a feature that leads to late apoptosis[26]. Thus, although TMZ does not cure GBM patients, it significantly improves GBM patients' survival and quality of life. This effect could also be demonstrated by the still considered benchmark study by Stupp et al. in the year 2005 [18] who assigned 573 GBM patients to different TMZ treatments. Ninety-seven percent (97%) of all patients in the radiotherapy-only group and 89% of patients in the combined radiotherapy/TMZ group died during the five-year follow-up period. Overall survival rates were 27% at 2 years, 16% at 3 years, 12% at 4 years, and 10% at 5 years with TMZ versus 11%, 4%, 3%, and 2% with radiotherapy alone, respectively[18]. A benefit of combined TMZ and radiation therapy was recorded in all clinical prognostic subgroups, including patients aged 60 to 70 years[18]. However, GBMs can present innate resistance to TMZ or develop acquired resistance during treatment [27]. Innate resistance of GBM cells to TMZ includes various underlying causes, such as loss of the phosphatase and tensin homolog, leading to the activation of the phosphoinositide-3-kinase/Akt pathway [28], demethylation or high expression of the O^6-methylguanine-DNA methyltransferase [29], robust base excision repair [30], and deficiency in the DNA mismatch

repair system[31]. All these facts make the treatment of GBM challenging and new treatments are needed such as the tumor treating fields (TTFields). Increased effort on developing this this new technique since the late 2000s, has made considerable progress in the treatment outcome of GBM patients. The successes led to milestone events for the company Novocure, featuring clinical approval in various Western markets including Germany. It is the only more broadly accepted new type of clinical treatment option for GBM for decades.

1.2 Tumor Treating Fields

1.2.1 verview

Exposure to ionizing radiation is the strongest risk factor associated with GBM and the only known potentially modifiable risk factor [10]. Therefore, if we can control the intensity of the electric field can we treat glioblastoma? On that basis, bioelectric therapies show great potential for the treatment of cancer, although they are poorly clinically applied to treat human brain cancers. This technology is getting more accepted and welcomed in the clinics – not only in the context of brain cancer therapy and is known und der the name; tumor treatment fields (TTFields).

In 2011, the United States Food and Drug Administration (FDA) approved the first TTFieldsield device for the treatment of recurrent or refractory GBM. More recently, the FDA approved the TTFieldsield device as an adjuvant treatment for newly diagnosed patients after completing standard-of-care surgery and chemoradiation. The National Comprehensive Cancer Network (NCCN) added the TTFieldsield device as an option for the treatment of newly-diagnosed GBM[32]. These devices generate alternating intermediate electric fields that target tumors or adjacent regions and induce apoptosis through a variety of activation pathways of certain cancer cell types, with little to no side effects [2]. The TTFields device has four transducer arrays, each consisting of nine insulated electrodes, placed on the patient's scalp to deliver a low-intensity, mid-frequency (100-300 kHz) ac electric field [33].

Before clinical application, several preclinical trials have shown the efficacy of TTFields in the inhibition of cancer cell proliferation and their destruction *in vitro*. Many cell lines were tested with TTFields, among them melanoma, glioma, lung, prostate, and breast cancer cells. For some of the cell lines, a specific optimal frequency that demonstrated maximal inhibitory effect was

found, possibly reflecting different cell sizes and shapes [34]. TTFields were also shown to inhibit tumor growth in several mice, rat, and rabbit animal models, probably due to metastasis growth inhibition, migration capability impairment, and primary tumor local control[35]. For that purpose, cancer cell lines were implanted to test the most effective frequency and intensity for *in vivo* treatment. Postmortem analysis of the treated animals showed a significant reduction in tumor size after TTFields-treatment compared with control animals. Furthermore, these *in vivo* experiments proved the delivery of the field to the target region via insulated non-invasive electrodes. Additionally, no abnormality in vital signs, electrocardiograms (ECG), complete blood counts (CBC), chemistry, and coagulation panels was found during the follow-up period of animals treated with TTFields, and no treatment-related pathologies were found postmortem. Interestingly, there was no statistically significant inhibition of tumor growth when a unidirectional TTFields was delivered this way. Only two- and three-directional fields led to statistically significant growth inhibition [36]. However, a dedicated test to investigate the therapeutic potential of TTFields to eradicate cancer stem cells, or investigate differences in the response to this type of treatment depending on what transcriptional [37] or DNA-methylation class [38] the glioblastoma belongs to, is missing. In our study, we thought to address this lack of literature by utilizing in vitro model systems representing GBM stem cells from those different molecular subtypes, as described earlier by our group [39].

The first single-arm clinical trial was conducted on 10 patients by Novocure Ltd. (St. Helier, NJ, USA) [34]. Novocure Ltd. has produced a clinical TTFields device, named Novo TTFields-100A, which uses electrodes configured as a cap that is placed on the patient's shaved scalp and powered by a battery pack[32].

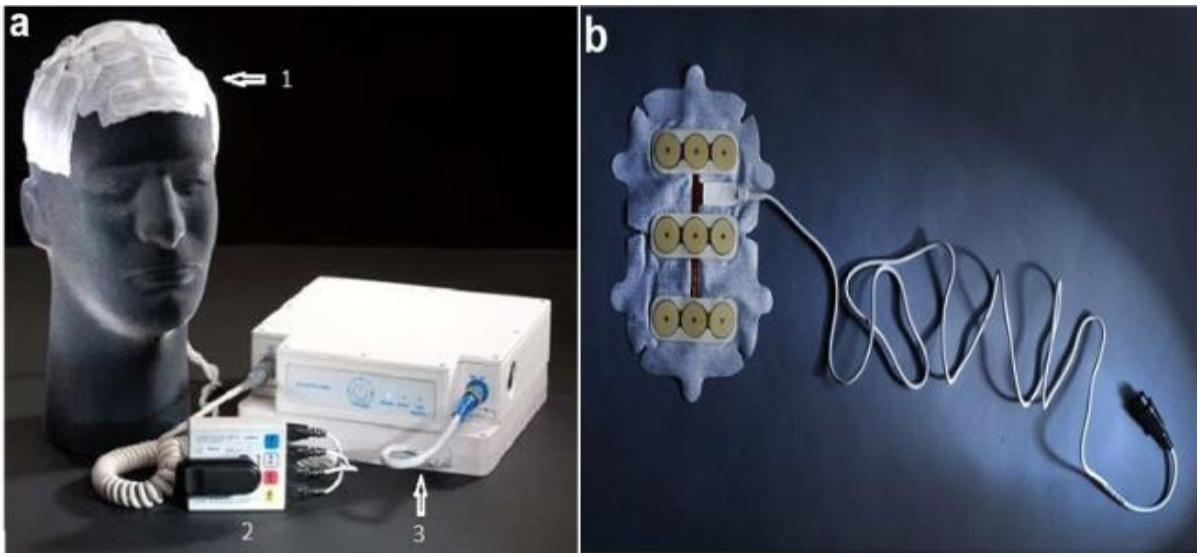

Figure 2: The NovoTTF-100A System components and assembly. (a) The transducer arrays are shown as they are applied to the scalp (1) with the array cables connected to the color-coded sockets on the connection cable and box (2). The box in turn is connected to the

The addition of TTFields low-intensity-alternating electric fields delivered by transducer arrays for antimitotic therapy during temozolomide-maintenance treatment prolonged survival in patients with a supratentorial disease [33]. The phase three trials demonstrated an improvement in progression-free survival (PFS) of 6.7 months for TTFields plus maintenance temozolomide versus 4.0 months for temozolomide alone (HR, 0.63; 95% CI, 0.52-0.76 [P <0.001]). There was also an OS benefit, with a median of 20.9 months versus 16.0 months noted in both groups, respectively (HR, 0.63; 95% CI, 0.53-0.76 [P < 0.001]) [4]. Studies have shown that TTFields not only inhibit the growth of solid tumors but also have clinical benefits in preventing the metastasis and spread of primary tumors [40]. Additional studies on combinational therapy of TTFields plus chemotherapy have shown that cancer cell survival is significantly reduced [41, 42]. This observation was first presented in 2018 and showed that the use of the TTFields device and TMZ improved overall survival out to five years in all three recursive partitioning analysis (RPA) classes [43]. This led to further clinical investigations using TFF and in November 2018, a phase II trial opened comparing a combination treatment with the TTFields and nivolumab with or without ipilimumab in patients with bevacizumab-naive recurrent GBM[44]. Research on the utilization of TTFields in cancer care is also not limited to GBM. A phase 2 pilot study on the safety and efficacy of the TTFields device concomitant with pemetrexed and cisplatin or carboplatin in malignant pleural mesothelioma (STELLER) closed in April 2018. In one study,

150 kHz electrode arrays were placed on the thorax of patients with previously treated malignant pleural mesothelioma in addition to chemotherapy. The preliminary efficacy will be compared to historical cohorts[45]. TFF devices are being now explored for various disease sites such as brain metastasis, non-small cell lung carcinoma, ovarian carcinoma, pancreatic carcinoma, meningioma, and even as an alternative to prophylactic cranial irradiation in small-cell lung cancer [46].

1.2.2 Identified mechanisms of action in TTFields

There are several modes of action in how TTFields act on tumor cells, the main effect will be the disruption of key mitotic proteins, especially on dividing cells. They can exert their antiproliferative effect through three described effects: The antimicrotubular effect, dielectrophoresis, and membrane blebbing. The next chapter will describe the knowledge of most of today's analyzed modes of action in fields.

1. Arrest of mitotic spindle formation and Mitotic furrow destruction[35].

   Each cell contains numerous electrically charged molecules. Under an alternating electric field, these molecules will oscillate according to the changing direction of the field and its density. If the field is uniform, the forces acting intermittently in opposite directions will cause a movement parallel to the direction of the field. When the frequency of the field is high enough, such as in the case of TTFields, this molecular movement will reduce. In the case of dipoles, where there is an electric split between the positive and negative poles of a molecule, it will align with the direction of the electric field and remain at the same place. All charged molecules, including dipoles, will move toward the higher field density in a non-uniform alternating electric field. Within a nondividing cell, the field is mostly uniform and the net force on charges and dipoles will, therefore, yield minimal movement. Non-uniform electric fields, on the other hand, force polar molecules to move toward higher field intensity, in a process called dielectrophoresis[47, 48]. Such fields are characteristic of a dividing cell when a narrow furrow connects the two forming daughter cells[35]. The macromolecular machinery that divides chromosomes among the two daughter cells during mitosis is called the mitotic spindle. It consists of several compartments but the main compart-

ments are the microtubules, which are formed by tubulins dimers (α- and β-tubulin). Microtubules are in a dynamic state of polymerization-depolymerization that is important for cytoskeletal remodeling during mitosis. As noted before, the electric field is uniform within non-dividing cells, but the tubulin subunits will tend to align according to the direction of the field. Finite element simulations (FEA), a method, to control and improve the segmentation speed by calculating various FEA models, showed that the electrical forces acting on the tubulin subunits prevent them from attaining the orientation required for efficient polymerization, therefore, mitosis becomes arrested for an abnormally long time [35, 36]. When this process takes place, cells could either complete mitosis or disintegrate. interestingly, not all cells seem to be affected by mitotic furrow destruction. In general, the membranes of cells that complete metaphase will start dividing into two daughter cells, pulling the daughter chromosomes to each of the cells' poles. During the final step of mitosis, the cytokinesis, a cleavage furrow is eventually formed, which completes the process of cell separation. This narrow membranous link results in an hourglass-shaped, non-uniform electric field, in contrast to non-dividing cells, in which the electric field is uniform. Like mentioned earlier, the electric field is densest in the narrow center during cytokinesis. By focusing the field, all-electric charges and dipoles are directed to the furrow due to the unidirectional nature of the electric force (dielectrophoretic force) under these conditions. Finite element simulations have shown that polarized molecules and organelles within the cell will be affected by forces large enough to move toward the furrow to disrupt the internal cell structure and cause cell destruction seen under TTFields therapy [35, 36].

2. Another, simpler explanation for the mode of action of TTFields is occurring during the prophase of mitosis, TTFields interfere with mitotic cells, resulting in plasma membrane contraction, instability, and blistering. TTFields inhibit spindle tubulin formation during the middle cell cycle, affecting spindle cell formation and prolonging tumor cell division. During anaphase and telophase, TTFields disrupt cell structure, inhibit the location of spindle midline and hydrodynamic groove, and alter physiological function [49]. Taken together, one mode of action of TTFields will be the disturbance of the electrical dipole moment of microtubules, leading to abnormal mitosis and spindle formation [36] [42].

   Several studies have shown that autophagy is involved in cancer cell death following TTfields treatment in lung cancer and glioma cell lines [50, 51]. It is thought that TTFields

inhibit early tumor growth through autophagy [52] and also cause daughter cells to form aneuploidy[53]. This is associated with the induction and regulation of autophagy and lysosomal gene expression[50]. Kim et al. reported that autophagy was activated via the Mir-29B-AKT2-mTOR axis after GBM treatment at TTFields. RNAi inhibition of Beclin1 and Atg5 significantly restored the number of TTFields-induced cell death, suggesting that autophagy is a key cell death pathway triggered by TTFields. However, different findings have been reported. Increased levels of autophagy flux in TTFields treated cells were not associated with decreased mTOR activity in U87MG cell lines, as detected by western blotting analysis of p70S6K phosphorylation. Thus, inhibition of autophagy sensitizes tumor cells to TTFields therapy, leading to increased apoptotic cell death[54].

3. Delayed DNA repair and enhanced DNA replication stress

   After exposure TTFields to four different cancer cell lines, ingenuity pathway analyses revealed a significant down-regulation of BRCA1, a well-known tumor suppressor involved in DNA double-break repair and maintaining genomic stability through cell cycle checkpoints, and was confirmed by immunoblotting[55]. Furthermore, BRCA1 and BRCA2 also are known to mediate homologous recombination and non-homologous end joining up on double-strand break[56]. In TTFields exposed cells, DNA DSB repair foci were increased and chromosomal aberrations appeared. TTFields not only slow down DNA damage repair dynamics but also induce replication stress since a decrease in replication fork speed was observed after TTFields treatment [52]. This shows that TTFields cause cell death by interfering with the DNA repair machinery. A key role of TTFields in DNA damage responses was first reported by Karanam *et al* and subsequent studies in different experimental Settings have reached similar conclusions[57]. Giladi *et al*. also demonstrated that TTFields may synergically enhance the effect of radiotherapy on glioma cells and reduce colony formation by blocking homologous recombination repair [54].

4. Impact on cell migration and metastasis

   Tumor cell migration and metastasis are considered one of the most crucial cancer hallmarks and remain one of the major obstacles to obtaining therapeutic success[58]. It is generally believed that GBM cannot be resected by surgery because of infiltrative characteristics[59]. The inevitable recurrence of GBM may be attributed to a small number of residual

tumor cells that invade the normal brain tissue, thus surviving from multi-modality therapies[34].TTFields exposure, resulting in interference with the directionality and robustness of cancer cell migration[60]. It is shown that TTFields reduce known drivers of cell migration such as MMP2 and MMP9 activities via downregulation of p38, ERK, JNK, and AKT phosphorylation, thus inhibiting the MAPK and PI3K/AKT pathway. Downstream involvement of NF-kB/p65 was also proposed in the study [61].

5. Induction of immune response

   The microenvironment of GBM exhibits immunosuppressive conditions [62]. TTFields have been observed to trigger antitumoral immunity in various investigations. Immune and inflammatory response pathways were dramatically affected after 48 hours of TTFields treatment compared to the control group, according to microarray gene expression data [60]. This is of great interest for anti-PD-L1 treatment therapy since the programmed death-1/programmed death ligand 1 (PD-1/PD-L1) pathway have improved clinical outcomes in patients with cancer. The PD-1/PD-L1 pathway plays an important role in suppressing the function of T cells in eradicating tumor cells[63]. The combination of TTFields and anti-PD1 therapy leads to significantly decreased tumor volume compared with the monotherapy by each drug in an orthotopic LLC lung cancer mouse model[64]. It was shown that the combination of TTFields with anti-PD-1 therapy might enhance PD-L1 expression in infiltrating dendritic cells and macrophages to further enhance anti-tumor immunity.

6. Reversible increase of cell membrane and blood-brain barrier permeability

   Scanning electron microscopy (SEM) studies showed that after TTFields treatment an increase in the number and size of holes in the GBM cell membrane as well as altered morphology[65]. GBM cells exposed to TTFields, therefore, are more permeable to substances ranging from 4kDA to 20 kDa. Interestingly, this phenomenon does not occur in normal human fibroblast cells, and the holes are gradually recovered after TTFields withdrawal. Therefore, this TTFields -induced effect may serve as a tumor-specific, reversible event and can be manipulated for treatment purposes[61]. Correspondingly, the BBB integrity, which hampers delivery of therapeutics to the brain tumor core can be disrupted by the TTFields application [66]. Combined with the increasing cellular membrane permeability effect, this phenomenon provides insights into future novel applications utilizing TTFields to deliver

drugs generally unable to cross the BBB. Hence, these findings may explain the additive and synergistic effects presented above by altered sensitivity to anticancer drugs[67].

7. Impairment of tumor aberrant glycolysis

   Patel et al. recently discovered that TTFields impaired GBM aberrant glycolytic metabolism through downregulated pyruvate kinase M2 (PKM2) expression. Cancer cells take advantage to shift the metabolism towards the anabolic phase by reduced pyruvate kinase activity and the resulting accumulation of upstream glycolytic intermediates. PKM2 is found in many tissues as well as in primary brain tumors. While grade I to III gliomas have slightly increased levels of PKM2 RNA and protein than healthy brain cells, GBM is depicting a 3- to 5-fold increase in PKM2 RNA and protein expression compared to even grade III gliomas. PKM2 is an important regulator of the Warburg effect and an increased level of dimeric PKM2 in cancer cells contributes to anabolic glucose metabolism, which supports rapid cell proliferation and ultimately promotes cancer cell proliferation and growth [68]. To identify the effect of TTFieldsield on glycolysis Patel et al. used a novel radiotracer, [18F]DASA-23, to measure the PKM2 expression and to detect the TTFields-induced effect. A 6-d TTFields exposure led to a reduction in uptake of [18F]DASA-23 and indicated that TTFields cause the above-mentioned shift in GBM metabolism from glycolysis to oxidative phosphorylation [69]. Despite the promising prospect of TTFields in clinical settings, only limited knowledge has been gained of its underlying molecular mechanism[70].

Based on that, the current knowledge of this therapy form on a plethora of cellular processes proves the fundamental impact and potential of TTFields. However, the full action of TTFields, particularly on influencing the differentiation features of malignant, poorly differentiated cancers, and particularly on tumor stem cells, is only poorly understood.

1.2.3 PI3K-AKT pathway

A recent retrospective analysis of the patients who received TTFields therapy demonstrated that the genetic background was strongly associated with the efficacy of TTFields therapy. A common pattern of alterations including CDKN2A/2B co-deletion, MTAP deletion, and PIK3 mutations was observed in the patients who recurred within 12 months and did not occur in those who recurred after 12 months [71]. PI3K/AKT/mTOR signaling pathway is one of the classic

pathways regulating the cell cycle and plays an important role in regulating cell division, differentiation, survival, and tumor genesis. More and more studies have found that the PI3K/AKT/mTOR signaling pathway also plays various important roles in the central nervous system, and its abnormality is closely related to many diseases of the central nervous system [72, 73].

The PI3K/AKT/mTOR signal transduction pathway is mainly composed of three parts. First, the phosphatidylinositol 3-kinase (PI3K) acts as the leading startup system. PI3K is an intracellular phosphatidylinositol kinase. Growth factors and neurotrophic factors can activate PI3K by binding to their extracellular domains. [74]. RTKs, as well as other receptors, undergo autophosphorylation upon binding to these growth factor signals, and PI3K is recruited to the receptor phosphorylation site, catalyzing phosphatidylinositol-4,5-bisphosphate (PIP2) synthesis. PIP2 then generates phosphatidylinositol-3,4,5-trisphosphate (PIP3), which acts as a second messenger to further activate downstream AKT signaling molecules and initiate the PI3K/AKT pathway [73].

The second part and the core regulatory node are the AKT/mTOR pathways. Protein kinase B, also known as AKT, is an intracellular Ser/Thr protein kinase. By activating PI3K, PIP3 is produced on the plasma membrane, which binds to intracellular AKT and activates it by phosphorylation from the cytoplasm to the membrane. Once activated AKT can phosphorylate a series of substrates in the cytoplasm and the nucleus, among which one of the most important substrates is the mammalian target of rapamycin, mTOR [75]. AKT activates mTOR by directly or indirectly phosphorylating mTOR [73]. After activation of mTOR, the mammalian target of Rapamycin Complex 1 (TORC1) is formed, which is the downstream core component of PI3K/AKT [75].

mTOR regulates a variety of proteins that play an important role in the translation process, such as eukaryotic translation initiation factor 4E binding proteins (eIF4EBP) and the p70S6 kinase, as well as it will activate various protein synthesis [76]. Part three of this complex pathway is the negative regulation mechanism dominated by the phosphatase and tensin homolog (PTEN). PTEN is a natural inhibitor of the PI3K/AKT/mTOR pathway. It can dephosphorylate PIP3 into PIP2, thus inhibiting the initiation of the PI3K/AKT pathway on the membrane [77]. A decrease

in PTEN activity increases the activation of this pathway, which results in increased cell survival and proliferation [74], and, therefore, PTEN is one of the most important negative regulatory mechanisms of this pathway. [78]

Activation of the PI3K/AKT/mTOR pathway can activate as well as inhibit phosphorylation of various intracellular proteins and regulate neuronal cell survival/apoptosis, autophagy, neurogenesis, neuronal cell proliferation, and synaptic plasticity[79], depending on the given circumstances. For example, PI3K/AKT/mTOR is the main node of autophagy regulation, upon activation, it will inhibit autophagy[80].

Activated mTORC1 catalyzes the phosphorylation of a series of autophagy initiation proteins (e.g. ULK1 complex), thereby inhibiting signaling molecules for autophagy activation. In addition, mTORC1 can also inhibit transcription factors involved in the synthesis of autophagy-related proteins and reduce the occurrence of autophagy[81]. Therefore, when the PI3K/AKT/mTOR pathway is not inhibited, the peri-cellular phase of neural progenitor cells accelerates and rapidly enters the division phase, thus accelerating the proliferation and differentiation of neuronal cells and playing an important regulatory role in neurogenesis and neural cell proliferation and differentiation[82].

The PI3K/AKT/mTOR signaling pathway is the classic signaling pathway for various central nervous system tumors, and both mTOR1 and mTOR2 pathways are abnormally activated in glioma patients[83]. Glioblastoma is usually accompanied by PTEN variation, mTOR overactivation, and overexpression of EGF (one of the activating molecules of PI3K)[84]. PI3K/AKT/mTOR signaling pathway inhibitors are one of the leading directions of anti-tumor drug development. PI3K/AKT/mTOR pathway inhibitors, however, can only limit the growth of tumor cells to a certain extent, and their specificity is low. Compared to traditional treatment methods like surgery, radiotherapy, and chemotherapy, they can only be used as adjuvant therapy[85]. There is a great need for cytotoxic and specific inhibitors of the PI3K/AKT/mTOR signaling pathway or for methods to inhibit the pathway for the treatment of a variety of nervous system tumors and even other cancers.

1.2.4 AKR1C3

The aldo-keto reductases (AKRs) comprise a functionally diverse family of NAD(P)(H)-dependent oxidoreductases [86]. It becomes increasingly clear that the AKR1C family is intimately linked with cancer biology. In humans, four AKR1C isoforms have been characterized, which include AKR1C1, AKR1C2, AKR1C3, and AKR1C4[87]. Studies suggest that deregulated expression of AKR1C3 occurs in multiple types of cancers and contributes to the development of human cancer and drug resistance[87].

AKR1C3, also known as 17b-hydroxysteroid dehydrogenase type 5, is capable to produce testosterone and 17b-estradiol by reducing the androgen precursors and estrone, respectively [38]. This will lead to the activation of the nucleus androgen- and estrogen-receptor [39]. In prostate cancer cells, some studies have shown a negative interaction and selective dominance between PTEN and androgen receptors [40]. In glioma cells, hypoxia leads to upregulation of AKR1C3 [88], and AKR1C3 was found to be associated with chemoresistance by inactivation of doxorubicin and oracin[43] [89]. AKR1C3 was also found to play a pivotal role in prostate cancer resistance to enzalutamide[44, 90]. AKR1C3 was upregulated to varying degrees in different cancer types according to resistance analysis. It may be important for the development of future clinical medications to conduct a comprehensive evaluation of AKR1C3 and related pathways[91, 92].

However, the above-mentioned mechanism of resistance mediated by AKR1C3 is not clear, and there are very few articles on the role of AKR1C3 and PI3K/AKT/mTOR pathway in glioblastoma. One of the main research objectives of this project is to investigate the role of AKR1C3 and PI3K/AKT/mTOR in glioblastoma.

1.3 Trihexyphenidyl

1.3.1 Overview

Anticholinergic drugs are the first drugs used to treat Parkinson's disease (PD)[93]. The molecular basis of the therapeutic effect in PD is not completely understood. Anticholinergics appear to improve symptoms by modulating the central anticholinergic action in the neostriatum and ameliorating the state of cholinergic hypersensitivity that occurs as a consequence of dopamine

depletion [94]. With the introduction of newer drugs for the treatment of PD, anticholinergic drugs remain among the most commonly used medications worldwide [92, 95]. These drugs are often used in combination therapy with levodopa (LD) rather than used as monotherapy[95].

The anticholinergic agent trihexyphenidyl (also known as benzhexol) is described to be able to block the central cholinergic receptors on receiver cells, helping to balance cholinergic transmission in the basal ganglia. It also may block dopamine reuptake and storage in central sites thus increasing dopaminergic activity[94]. There is also literature suggesting that THP is also used in psychiatric comorbidities, schizophrenia emerged as the most recorded, followed by depression, substance use disorder, schizoaffective disorder, delusional disorder/psychotic disorder, antisocial personality disorder and/or conduct disorder, borderline personality disorder, adjustment disorder, and obsessive-compulsive disorder[96].

The onset of action of this medication occurs within an hour of oral administration. It has a peak effect 2 to 3 hours after administration, and the duration of action can last from 6 to 12 hours[97].

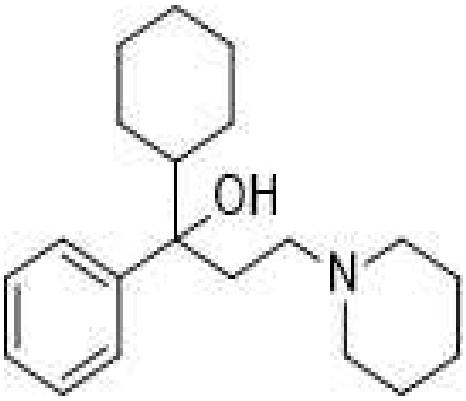

Figure 3: Trihexyphenidyl

The main mechanism of action of trihexyphenidyl may be that the pathophysiology of dystonia is associated with dysfunction of the basal ganglia. The pathway between the basal ganglia and the cortex is influenced by neurotransmitters that act on various receptors in the feedback loop and produce positive or negative effects.

By treating dystonia and its associated impairments, clinicians hope to improve activity and decrease associated pain and discomfort[97]. In addition, THP can significantly reduce the excitatory toxicity of glutamate to nerve cells, reducing the content of NO and malondialdehyde, and increasing the content of superoxide dismutase [98]. It can promote the recovery of brain electrical activity, relieve cerebral edema caused by middle cerebral artery occlusion (MCAO), reduce the accumulation of calcium in brain tissue, and has a protective effect on ischemic reperfusion brain injury. In addition, Peroxidate-induced oxidative stress damage of PC12 cells can be alleviated[99].

Previous reports by our laboratory in *vitro* research have shown that THP has therapeutic potential for glioblastoma tumors, suggesting that neurotransmitter targeting compounds can be used to treat brain tumors[100]. This would be well in line with merging evidence [101], that tumor cells can form synapsis with neurons of the surrounding microenvironment and thereby enhance neurotransmitter release, that itself in paracrine fashion support tumorigenesis[102]. The field is one of the most attractive and innovative areas of current cancer research, and global science opinion makers have recently designated the specific term Cancer Neuroscience to describe activities in research and development in this area[103].

We consider the results of this work associated with this exciting new field of research, with a translational-oriented focus on repurposing clinical treatment. Interestingly, THP is a Parkinson's disease-approved treatment with a Mach/ACh modulating mode of action. These molecular signaling cascades have been described as glioblastoma disease modulators in recent literature [104]. Our work described here aimed to further validate the therapeutic potential of THP in the context of brain cancer, interrogating confirmatory assays of our previous work with multiple cell models of different molecular tumor subtypes, as well as *in vivo* validation of a xenograft rodent model.

1.3.2 Cystathionine β-synthase (CBS)

The cystathionine β-synthase (CBS) is a metabolic enzyme that catalyzes the reaction of homocysteine with either cysteine or serine to form cystathionine and either hydrogen sulfide or water, respectively[105]. CBS is the first rate-limiting enzyme in the trans-sulfuration pathway and by utilizing homocysteine (Hcy) produces H2S and the cysteine precursor cystathionine[106].

Besides cellular uptake of cysteine, cysteine synthesis is the rate-limiting step for glutathione (GSH) production, the ubiquitous antioxidant[107]. In the brain, CBS is expressed by glia and astrocytes[108], which are the cells from which gliomas arise. Neural stem cells also express CBS and the addition of the substrate L-cysteine to culture media stimulated the in vitro differentiation of neural stem cells to neurons and astroglia, whereas knockdown of CBS expression by small interfering RNA suppressed L-cysteine-induced stem cell differentiation[109]. CBS may function to either promote or suppress tumor growth, depending on the cancer cell type[110].

The pathway catalyzed by the tandem CAT/MPST enzyme can play a role in the production of hydrogen sulfide from cysteine, particularly in the glioblastoma cell line U87MG and the neuroblastoma cell line SHSY5Y, and the pathway from methionine to cysteine via the CBS and CTH reactions appears to play a more important role in neuroblastoma cells compared to astrocytoma cells. In contrast, there is a higher activity and expression of enzymes involved in the generation of H2S from cysteine in neuroblastoma cells, which provides an opportunity for a more rapid response to H2S production [111].

Furthermore, in colorectal cancer increased CBS expression in tumors was observed, which was mediated by short hairpin RNA (shRNA). Silencing of the CBS expression in colon cancer cell lines results in decreased proliferation, migration, and invasion that was attributable to decreased hydrogen sulfide production[112]. In contrast, CBS gene expression is silenced by promoter hypermethylation in gastric cancer[113].

Sanjib Bhattacharyya et.al reports an important role of CBS in promoting ovarian tumor growth and maintaining the drug-resistant phenotype by controlling cellular redox behavior and regulating mitochondrial bioenergetics[107]. Taken together sever studies have shown that overexpression of CBS can inhibit proliferation and migration in various types of cancer cells in vitro[114]. Interestingly, CD44, a transmembrane glycoprotein and an important biomarker of CSCs, that is essential to many tumor cell activities, including proliferation and metastasis is inhibited by CBS overexpression[115]. Probably via attenuating the activation and nuclear translocation of the transcription factor SP-1[114]. Molecular analysis showed that CBS knockdown was associated with increased HIF2α protein expression and HIF2α-dependent expression of ANGPTL4 and VEGF. These have been shown to protect against anoikis from other cancer cell lines [116, 117].

2 Material and Methods

2.1 Cell Culture

2.1.1 Material

Cell lines	Origin	Organism	Growth Properties
GBM1	A. Vescovi, San Raffaele Hospital, Milano, Italy	Human	Suspension
NCH644	C. Herold-Mende, Heidelberg University, Heidelberg, Germany	Human	Suspension
SF188	E. Raabe, Johns Hopkins, Baltimore, MA, USA	Human	Suspension
BTSC233	M.S. Carro, Freiburg University, Freiburg im Breisgau, Germany	Human	Suspension
JHH520	G. Riggins, Johns Hopkins, Baltimore, MD, USA	Human	Suspension
U87	ATCC No.: CVCL_0022	Human	Adherent
HUVE	Promocell company Order No.: C-22010	Human	Adherent

Table 1: Cell lines

GBM1/NCH644/SF188/BTSC233/JHH520		
Amount	Name	Manufacturer
340 mL	DMEM,(+) 4.5g/L D-glucose, (-)Pyruvate	Thermo Fisher, 41965-039
150 mL	F-12 supplement	Thermo Fisher, 21765-029
10 mL	B27 Supplement	Thermo Fisher, 17504001

500µL	Human EGF	Peprotech, AF-100-15-1mg
500µL	FGF	Peprotech, 100-18B-1mg
500µL	Heparin	Sigma, H0878-100KU
5 mL	Penicillin-Streptomycin	Sigma, P4333-100 mL
U87		
Amount	Name	Order No.
500 mL	DMEM,(+) 4.5g/L D-glucose, (+)Pyruvate	Thermo Fisher,41965-039
50 mL	Fetal Bovine Serum (FBS)	Merck, S 0615
5 mL	Penicillin-Streptomycin solution	Gibco, 15140122
HUVE		
Amount	Name	Order No.
500 mL	Endothelial Cell Growth Medium	C-22010
12.2 mL	Supplemen tMix	C-39215

Table 2:Medium

2.1.2 Methods

All cell lines were incubated under standard conditions (SCs, humidified 37℃, 5% carbon di-oxide (CO_2)). Cells were regularly tested for mycoplasma accumulation and authenticity using the short tandem repeat assay, as previously described [37]. All cell lines were passaged every other day.

2.2 Passaging cells

2.2.1 Passaging cells (GBM1/NCH644/SF188/BTSC233/JHH520)

Material		
Amount	Name	Manufacturer
1 pcs	Cell culture in culture flask	
	Medium	Gibco, ThermoFisher
1 btl	PBS-d	Gibco, ThermoFisher
	Water bath (37°C)	
	Sterile pipettes	
1 pcs	15 mL Falcon Tube or 50 mL Falcon tube	
1 or more	New culture flask for suspension cells	Greiner Bio-One
1 pcs	Inverted Phase-contrast microscope	
	Vacuum pump with Pasteur pipettes	

Methods	
Step	Description
1	Let clean bench run for 15 min.
2	Get cell culture in culture flask out of the incubator.
3	Transfer cell culture to a Falcon tube.
4	Centrifuge the cell suspension for 5 min at 500 x g.
5	Remove supernatant with a pipette or vacuum pump with Pasteur pipettes.
6	Resuspend cell pellet in a fresh medium.

7	Split medium into 2 or more culture flasks, top flasks off with an additional medium

Table 3:Passaging cells (GBM1/NCH644/SF188/BTSC233/JHH520)

2.2.2 Passaging cells(U87/HUVE)

Material		
Amount	Name	Manufacturer
1 pcs	Cell culture in culture flask	
	Medium	Gibco, ThermoFisher
1 btl	PBS-d	Gibco, ThermoFisher
	Water bath (37°C)	
	Sterile pipettes	
	Inverted Phase-contrast microscope	
	Vacuum pump with Pasteur pipettes	
	TrypLE	Gibco, ThermoFisher
1 pcs	15 mL Falcon Tube or 50 mL Falcon tube	
1 or more	New culture flask for suspension cells	Greiner Bio-One
1 pcs	15 mL Falcon Tube or 50 mL Falcon tube	
	Centrifuge for falcon tubes (500 G)	
	Cell counter (Neubauer chamber+ trypan blue)	

Methods	
Step	Description
1	Prewarm PBS-d and Medium to 37℃, warm TrypLE at RT

2	Let clean bench run for 15 min.
3	When passaging: Put ~8 mL medium in T25 flask, ~21 mL medium in new culture flask(s), Then put flasks in the Incubator (37°C, 5% CO_2).
4	Get cell culture in culture flask out of the incubator
5	Remove medium with a sterile pipette or vacuum pump with Pasteur pipettes
6	Put 2 mL PBS-d in a T25 flask
7	Remove PBS-d with a sterile pipette or vacuum pump with Pasteur pipettes
8	Add 2 mL TrypLE to the cells in a T25 flask, incubate for up to 3 min at 37°C, 5% CO2 Wait until ~50% of the cells are detached (check with Phase-contrast microscope)
9	Add the double volume of medium to stop the TrypLE reaction. Flush flask with medium repeatedly to detach the cells from the surface
10	Transfer the whole volume of cell suspension into a falcon tube according to volume
11	Centrifuge the cell suspension for 5 min at 500 x g
12	Remove supernatant with a pipette or vacuum pump with Pasteur pipettes.
13	Resuspend the cells in fresh medium
14	Transfer desired amount of cells to the new culture flask with fresh medium
15	Incubate at 37°C, 5% CO_2

Table 4:Passaging cells(U87/HUVE)

2.3 TTFields treatment using the inovitro™ system

To test the effect of TTFields on the different cell types, the inovitro™ preclinical laboratory research system (Novocure, Saint Helier, Jersey) was applied. 40,000 cells in 2 mL of complete media were plated into each of the special inovitro™ dishes as well as into standard 35 mm cell culture dishes, our considered lab ware control condition. In total 15 dishes per experimental group and the control group were prepared. The experimental group's dishes were exposed to TTFields (1.7 V/cm RMS) via the inovitro™ system by using perpendicular pairs of transducers insulated by a high dielectric constant ceramic. TTFields were applied at a frequency of 200 kHz, the optimal frequency established clinically for glioblastoma patients at a final temperature of 37°C , in a humidified incubator with 5% CO_2. The control group dishes are directly placed into a humidified incubator with 5% CO_2 at 37°C . Three dishes from the control group and the experimental group were removed at 0h/24h/48h/72h/96h. 100 µL of the cells were taken from each of the 6 samples and counted using Trypan blue staining and an inverted phase-contrast microscope. MTT Assay is performed on the remaining dishes as described in table 6. Three biological replicates were performed for each cell line.

2.4 Cell Growth (Trypan blue staining and MTT Assay)

2.4.1 Trypan blue staining

Material	
Amount	Name
1 pcs	Resuspended cells of cell culture (see *CC-001*)
300 µL	Trypan blue
1 pcs	Pipette filter tips (20 µL and 1000 µL)
1 pcs	Neubauer chamber with cover glass
1 pcs	Phase contrast microscope
Methods	
Step	Description
1	After resuspending the cell pellet for splitting, take 100 µL cell suspension and transfer it to a 1,5 mL reaction tube

2	Add 300 µL trypan blue using a filter tip, to avoid contaminating the pipette with trypan blue. Mix the suspension by pipetting up and down a few times
3	Breathe onto the cover glass, to moisture the surface
4	Lay cover glass onto the Neubauer chamber. Move it around a bit, until you see newton rings forming (looks like the pattern on oil film)
5	Pipette 15 µL of trypan blue cell suspension underneath the cover glass by holding the pipette on the edge of the cover glass at a low angle
6	Use 100 x magnification of the phase-contrast microscope to count living (white) and dead (blue) cells in the four corner squares of the microscope
7	Calculate the concentration of living and dead cells: Cells per mL = counted cells $*10^4$ The chamber factor of 10^4 is only applicable, when a Neubauer/Neubauer improved chamber and the described volumes of cell suspension and trypan blue are used.
8	Calculate Vitality: $$vitality = \frac{livingcells * 100\%}{living\ cells + dead\ cells}$$
9	Dispose trypan blue in special trypan blue waste (hazardous waste)

Table 5:Trypan blue staining

2.4.2 MTT Lysis Buffer

Material		
Amount	Name	Manufacturer
45 mL	99% Isopropanol	VWR,20839.297
5 mL	Triton X-100	Sigma, X100
330 µL	25% HCl	Roth, 6331.1

1 pcs	50 mL Falcon tube

Methods	
Step	Description
1	Mix all ingredients in a 50 mL Falcon tube, and add HCl as last

Table 6:MTT Lysis Buffer

2.4.3 MTT Assay

Material	
Amount	Name
1 pcs	Cell culture in flask / plate
10 µL	MTT reagent aliquot
	PBS
100 µL	MTT lysis buffer
1 pcs	Paradigm or Saphire plate reader
1 pcs	96-well cell culture plate

Methods	
Step	Description
1	Thaw MTT reagent in Waterbath
2	Plate 100 µL Cell culture per well (treated / untreated / control / blank) in triplicates. Mix cells before plating, because cells will quickly sink to the bottom, resulting in inconsistent plating amounts.
3	Add 10 µL MTT per Well and incubate the plate at RT in the dark between 2 h, formazan crystals are visible under the microscope
4	Add 100 µL MTT lysis buffer per well and mix the plate at 350 rpm, RT for 20 min

5	Read the absorbance at 570 nm and background absorbance at 650 nm
6	For analysis subtract the background absorbance from the absorbance values, then subtract the averaged blank values from all measurements

Table 7:MTT Assay

2.5 CellTiter-Glo (CTG)

To detect the cell survival and cell growth for the THP project the luminescence-based CTG assay was applied as indicated in table 8.

Material		
Amount	Name	Manufacturer
100 mL	CellTiter-Glo® Buffer	
1 vial	CellTiter-Glo®Substrate (lyophilized)	
	THP	Sigma Aldrich,MO,USA
	Methanol	
	96-well black plate	NuncA/S, Roskilde, Denmark
Methods		
Step	Description	
1	1 × 100 mL Celltiter -Glo ® Buffer and 1 vial Celltiter-Glo ® Substrate (Lyophilized) are fully mixed to prepare Celltiter-Glo ® solution.	
2	Celltiter-Glo ® reagent: 1:1, V: V dilution of CTG solution with PBS	
3	THP was resuspended to a final concentration of 50 mM in methanol, MeOH, It is then diluted to the desired concentration as needed; It is then stored at +4°C .	
4	Each cell line was dissociated with TrypLE, washed once with PBS, adjusted to 2000 cells in 100 µL complete media per well, and pipetted in technical triplicates on black 96-well plates, resulting in concentrations of10, 20, 30, 40, and	

	50 µM of THP and a MeOH control. All assays were performed in biological triplicates.
5	Cells were then incubated with the drugs for 0,2,4,6day, in standard culture conditions (humidified 37°C , 5% CO2).
6	Cell line trays are removed at 0,2,4, and 6 days respectively. CTG Reagent 50ul for each well.
7	Shake in the Dark,300 RPM - 3 min
8	Leave for 10 min in the dark
9	CTG assay was performed as described.
10	All assays were performed in a biological bat.

Table 8:CellTiter-Glo(CTG)

2.6 qPCR with BioRad thermo cycler

2.6.1 RNA extraction with Trizol Reagent

Material		
Amount	Name	Manufacturer
	TRI Reagent	Sigma, T9424
	Chloroform (pure, without isoamyl alcohol traces)	Roth, 3313.1
	Isopropanol, 100%	VWR, 20839.297
	Ethanol, 70%	Pharmacy University Medical Center Düsseldorf (UKD)
	PBS	ThermoFisher,14190094
Methods		
Step	Description	

1	Centrifuge 5-10*10^6 cells in a falcon tube, remove supernatant
2	Add 1 mL TRI Reagent to the cell pellet, pipette up and down repeatedly to lyse cells, transfer to reaction tube or falcon tube
3	Let samples rest at RT for 5 min, ad 200 µL Chloroform to each sample, and cover it tightly
4	Shake sample vigorously for 15 sec and let it rest RT again for 10 min
5	Centrifuge at 12,000 RCF and 4℃ for 15 min
6	Each sample should now be separated into three phases
7	Transfer the aqueous (upper, colorless) phase into a fresh 1.5 mL reaction tube
8	Add 0.5 mL Isopropanol per 1 mL of TRI Reagent originally used and mix
9	Incubate at RT 10 minutes
10	Centrifuge at 12,000 RCF at 4℃ for 10 minutes to pelletize RNA
11	Remove the supernatant and add 1 mL 70% Ethanol per mL TRI Reagent added originally to wash pellet. Vortex Sample and centrifuge 7,500 RCF and 4℃ for 5 min
12	Remove supernatant and air dry pellet for 5-10 min
13	When the pellet is dry (no ethanol residues), add 25 µL of RNase-free water, to resuspend the pellet. Pipette up and down to homogenize the suspension
14	Quantize Sample with NanoDrop

Table 9:RNA extraction with Trizol Reagent

All samples were diluted to 100 ng/ul and sent to the in-house facility（BMFZ, Biologisch-Medizinisches Forschungszentrum） for RNA sequencing.

2.6.2 cDNA synthesis

Material		
Amount	Name	Manufacturer
	RNA extract	
1 µL	Random Hexamer Primers	Thermo Scientific, SO142
5 µL	5x cDNA buffer	Promega, M531A
2.5 µL	dNTP mix aliquot	Thermo Scientific, R0182
1 µL	RNase inhibitor	Thermo Scientific, EO0384
1 µL	M-MLV Reverse Transcriptase	Promega, 9PIM170
Min 175 µL	Nuclease free water	
1 pcs	BioRad CFX Connect Real-Time System qPCR cycler	

Methods	
Step	Description
1	Dilute RNA extract to 80 ng/µL in a total volume of 14 µL in a 0.2 mL PCR Tube
2	Add 1 µL random hexamer primers
3	Heat to 70℃ for 5 min in the qPCR cycler
4	In the meantime prepare the RT-master Mix: 5x buffer: 5 µL dNTP mix: 2,5 µL RNase inhibitor: 1µL Reverse transcriptase: 1 µL
5	Put in qPCR cycler with the following protocol: 25℃ – 10 min 42°C – 60 min 70°C – 10 min 10°C – hold
6	Add 175 µL nuclease free water to dilute the cDNA to ~ 10 ng/µL

Table 10:cDNA synthesis

2.6.3 qPCR with BioRad thermo cycler

Material		
Amount	Name	Manufacturer
15 µL	2x SYBR Green qPCR Master Mix	Absource, B21203
0,5 µL	Primer	Sigma-Aldrich
10 ng	cDNA	
	Nuclease free water	
1 pcs	Hard-Shell PCR Plate	BioRad, HSP9601
1 pcs	Microseal 'B' Film	BioRad, MSB1001
1 pcs	BioRad CFX Connect Real-Time System qPCR cycler	

Methods	
Step	Description
1	Dilute cDNA with Nuclease free water to 10 ng/µL
2	Prepare qPCR working solution, prepare enough solution for n + 2 samples (use duplicates of triplicates): 2x SYBR Green MM 10 µL FWD Primer 1 µL REV Primer 1 µL ROX reference Dye 0 µL* Nuclease free water 7 µL *ROX reference is not supported by CFX Connect cycler
3	Pipette 1 µL (= 10 ng) cDNA per sample (use duplicates of triplicates). To a Hard-Shell PCR Plate
4	Add 19 µL of qPCR working solution, mix by pipetting
5	Seal plate with Microseal Film
6	Run a three strep PCR cycle program with an additional melt curve on the CFX Connect cycler: 95°C 5 min

	95℃	15 sec	←
	60-67℃	30 sec	Repeat 39 times
	72℃	30 sec	
	Melt curve 60°C -95°C		
7	Analyze the results with the Bio-Rad CFX Manager software		

Table 11:qPCR with BioRad thermo cycler

The sequence of the primers used for SSCP analysis. The size of the PCR product and the annealing temperature of each primer set are indicated.

Primers	Sequence	Size (bp)	Temp (°C)
HEY1 F	TCTGAGCTGAGAAGGCTGGT	20	64.3
HEY1 R	CGAAATCCCAAACTCCGATA	20	63.6
HES F	CTCTCTTCCCTCCGGACTCT	20	63.8
HES R	AGGCGCAATCCAATATGAAC	20	63.7
Gli1 F	ACCCGGGGTCTCAAACTG	18	65.1
Gli1 R	GGCTGACAGTATAGGCAGAGC	21	62.9
SMO F	GAGACTCTGTCCTGCGTCATCA	22	66.9
SMO R	AGGCATAGGTGAGGACCACAA	21	65.7
Lgr5 F	CACCTCCTACCTAGACCTCAGT	22	60.2
Lgr5 R	CGCAAGACGTAACTCCTCCAG	21	66.0
Axin2 F	AGCCAAAGCGATCTACAAAAGG	22	65.3
Axin2 R	GGTAGGCATTTTCCTCCATCAC	22	65.5
CBS F	CGGCTTCGACTGGGTGTACT	20	64.8
CBS R	GCAGCCTCCCGATTTGG	17	69.5
HIF2α F	CCGCAGTTGTGCTCCTGAA	19	64.8
HIF2α R	ACCTTGGCGGTCTCGTAGCT	20	63.9
HIF1 F	CCACAGGACAGTACAGGATC	20	64.7
HIF1 R	TCAAGTCGTGCTGAATAATACC	22	63.8
ZEB1 F	AAGAATTCAGTGGAGAGAAGCCA	25	64.6
ZEB1 R	CGTTTCTTGAGTTTGGGATT	22	

			63.2
CBF1 F	TGCCTCAGGAACAAAGGTGG	20	67.4
CBF1 R	TGCCATGCCAGTAACTGAGC	20	66.3
SNAI1 F	GCTGCAGGACTCTAATCCAGA	21	63.4
SNAI1 R	ATCTCCGGAGGTGGGATG	18	65.1
TWIST1 F	TCCGCGTCCCACTAGCA	17	67.0
TWIST1 R	TTCTCTGGAAACAATGACATCTAGGT	26	64.8

Table 12:Primer-Sequences

2.7 Guava®Muse®Cell Analyzer

60mL of cell fluid with a concentration of 100,000 cells/mL was prepared for each cell line, and 5 mL was added to each T25 flask after mixing. The cells were randomLy divided into two groups with six bottles in each group. One group was treated with THP at a final concentration of 10 μM. For the analysis, three bottles were randomLy removed from each group at 48h and 72h, respectively.

2.7.1 Ki67 Proliferation Kit

Material		
Amount	Name	Manufacturer
100 tests/vial	Muse® Hu Ki67-PE Antibody	4700-1667
100 tests/vial	Muse® Hu LgG1-PE Antibody	4700-1669
50 mL/vial	5×Assay Buffer	CS202124
10 mL/vial	Permeabilization Buffer	CS202125
Two 3-mL vials	5×Fixation Solution	4300-0340
	Guava®Muse®Cell Analyzer	Luminex

1.5 mL	Microcentrifuge tubes with screw caps	16466-030
	1×Phosphate -buffered saline (PBS)	
	Micropipettes	

Methods

Step	Description
1	The cells were transferred into a 15 mL Olecranon centrifugal tube.
2	Centrifuge 1080 rmp 5 min, remove supernatant
3	Add 500ul TrypLE 3 min,then add 500ul medium
4	Cell count, then take 100,000 cells to a 1.5 mL tube
5	Centrifuge 1080 rmp 5min, remove supernatant
6	Add 1 mL PBS, Centrifuge 300G 5min, remove supernatant
7	Add 50uL of 1×Fixation solution (200uL 5×Fixation Solution buffer +800uL PBS)to each tube.Mix and incubate for 15minutes at room temperature.
8	Add 150 uL of 1×Assay buffer (200uL 5×Assay Buffer + 4 mL H_2O, Centrifuge 300 x g 5min, remove supernatant
9	Add 100uL of Permeabilization Solution to each tube. Mix and incubate for 15 minutes at room temperature.
10	Add 100uL of 1×Assay Buffer, Centrifuge 300 x g 5min, re-move supernatant
11	Add 50uL of 1×Assay Buffer to each tube. Mix and incubate for 15 minutes at room temperature.
12	Add 10uL of either Muse®Hu lgG1-PE or Muse®Hu Ki67 PE Antibody to each tube. Mix and incubate for 30 minutes at room temperature.

13	Add 150 µL of 1×Assay Buffer to each tube and run on the Guava®Muse®Cell Analyzer

Table 13:Ki67 Proliferation Kit

2.7.2 Cell

Cycle Kit		
Material		
Amount	Name	Manufac-turer
	Guava®Muse®Cell Analyzer	Luminex
	Micropipettes	
	Ethanol 70%	
	Muse®Cell Dispersal Reagent	MCH100 106
	Vortex Mixer	
1.5 mL	Microcentrifuge tubes with screw caps	16466-030
	1× PBS	

Methods	
Step	Description
1	The cells were transferred into a 15 mL Olecranon centrifugal tube.
2	Centrifuge 2 x g 5min, remove supernatant
3	Add 500ul TrypLE 3min, then add 500ul medium
4	Cell count, then take 100,000 cells to a 1.5 mL tube
5	Centrifuge 1080 rmp 5min, remove supernatant

6	Add 1 mL PBS, Centrifuge 300G 5min, remove supernatant
7	While mixing cells, slowly add 1 mL ice-cold 70% ethanol.
8	Incubate overnight at -20℃.
9	Add 200 uL of fixed cells to a new tube.
10	Centrifuge 300 x g 5min, remove supernatant
11	Wash once with 300uL PBS, Centrifuge 300G 5min, remove supernatant
12	Add 200 uL of Muse®Cell Dispersal Reagent to each tube and incubate for 30 minutes at room temperature in the dark, then run on the Guava®Muse®Cell Analyzer

Table 14:Cell Cycle Kit

2.7.3 Annexin V & Dead Cell Kit

Material		
Amount	Name	Manufac-turer
	Guava®Muse®Cell Analyzer	Luminex
	Micropipettes	
	Muse®Cell Dispersal Reagent	MCH100105
	Vortex Mixer	
1.5 mL	Microcentrifuge tubes with screw caps	16466-030
	1×Phosphate -buffered saline (PBS)	

Methods

Step	Description
1	The cells were transferred into a 15 mL Olecranon centrifugal tube.
2	Centrifuge 1080 rmp 5min, remove supernatant
3	Add 500ul TrypLE 3min, then add 500ul medium
4	Cell count, then take 1,000,000 cells to a 1.5 mL tube
5	Centrifuge 1080 rmp 5min, remove supernatant
6	Add 1 mL PBS, Centrifuge 300G 5min, remove supernatant
7	Add 100uL of Muse® Annexin V & Dead Cell reagent to each tube.
8	Add 100ul of cells in suspension to each tube.
9	Incubate for 20 minutes at room temperature in the dark and analyze on the Guava®Muse®Cell Analyzer

Table 15:Annexin V & Dead Cell Kit

2.8 Western Blot

2.8.1 Protein extraction from tumor cells

Material		
Amount	Name	Manufacturer
	Cell pellets in 1.5 mL tubes, or cell cultures on 6 well plates	
20 – 50 µL	RIPA-buffer	
	Proteinase Inhibitor	
2 pcs	Precooled 1.5 mL tubes	
1 mL	PBS (only when cells have not been washed prior pelleting)	

Methods

Step	Description
1	When gathering proteins from adherent cells in 6 well plate: Remove medium and wash each well with 1 mL ice cold PBS Remove PBS afterwards
2	Prepare a RIPA and proteinase inhibitor (PrI) solution. Dilution is 1: 25. 1 µL of PrI and 24 µL RIPA.
3	Put 20 - 50 µL of RIPA-buffer with PrI in each 1.5 mL tube/well of 6 well plate
4	Pipette up and down, to lyse cells then incubate for 30 - 45 minutes on ice and vortex every 10 – 15 min
5	Transfer the whole suspension into precooled 1.5 mL tubes
6	Centrifuge the suspension at 13000 rpm and 4°C for 10 min to pellet DNA
7	Put supernatant in fresh precooled 1.5 mL tube

Table 16:Protein extraction from tumor cells

2.8.2 Measure protein concentration with Bio-Rad DC Assay

Material		
Amount	Name	Manufacturer
1 pcs	Bio-Rad DC Assay	Bio Rad, 500-0116
1 pcs	BSA Protein standard	Bio Rad, 500-0112
1 pcs	Microtiter plate	
1 pcs	Plate reader (750 nm)	

Methods	
Step	Description
1	Prepare working solution by mixing 20 µL reagent S to 980 µL of reagent A. This solution can be stored up to 7 days at RT
2	Prepare 6 dilutions of protein standard from 1.5 mg/mL to 0.25 mg/mL and an empty control in

	the same buffer as the protein extract.
3	Pipet 2 µL of your lysate in a new 1.5 mL reaction tube and add 18 µL of RIPA.
4	Pipet 5 µL of standard or sample in a well of the microtiter plate
5	Add 25 µL of the working solution
6	Add 200 µL of reagent B. Gently agitate the plate to mix the reagents
7	Incubate 15 – 30 mins at RT in the dark
8	Read absorbance at 750 nm
9	Create a standard curve using linear regression
10	Read values for the samples

Table 17:Measure protein concentration with Bio-Rad DC Assay

2.8.3 Western blot with precast gels

Material		
Amount	Name	Manufacturer
10-20 mg	Protein extracts	
	4x LaemmLi buffer	
	1x Western blot running buffer	
	1x Western blot transfer buffer	
	TBS-T	
~5 mL	Ponceau S solution	
2 µg	Bio-Rad Dual Color Marker	
4 µL	PageRuler Prestained ladder	
	Primary + secondary (marked) antibodies	
2.5 g	Milk powder or BSA	
1 pcs	Hybridization box	
	Ice bucket with ice	
1-2 pcs	Readymade BAA gel	
1 pcs	Electrophoresis chamber with gel holder and power supply	

1 pcs	Transfer chamber with cassette and power supply
2 pcs	Sponges
~4 pcs	Filter paper
1 pcs	Transfer membrane (nitro cellulose)
1 pcs	Heat shaker (95°C)
1 pcs	Shaker (RT or 4°C)
1 pcs	Scalpel

Methods

Step	Description
1	Preheat the heat shaker to 95°C
2	Mix 10-20 µg of protein extracts with ¼ volume of 4x LämmLi buffer in a 1.5 mL reaction tube
3	Heat the mix to 95°C for 5 min, then store on ice
4	Take a readymade BAA gel out of the fridge and unwrap it
5	Put either 2 gels or a gel and a dummy into the gel holder
6	Put the gel holder into the electrophoresis chamber and slowly fill western blot running buffer between the two gels, avoid bubbles
7	Check if no buffer is leaking into the electrophoresis chamber, then fill the chamber with running buffer to the marked line
8	Remove the comb from the readymade gels and flush every slot with running buffer
9	Fill marker and samples with loading buffer into the slots
10	Start the electrophoresis at 60 V to see if samples run at the same speed
11	Otherwise after 15 minutes of electrophoresis at 60 V, increase to 110 V and let run for ~60 min, or until the running front reaches the end of the gel
12	Take the gels out of the chamber and remove the loading slots with a scalpel

13	Prepare transfer stack: wet sponges, filter paper and membrane in western blot transfer buffer
14	Starting from the black side of the cassette stack sponge, filter, gel, membrane, filter sponge and remove air bubbles and close the cassette
15	Put the transfer chamber into the ice bucket and fill the bucket with ice
16	Put the sandwich case into the transfer chamber containing transfer buffer
17	Transfer at 250 mA for 2 h
18	Put the transfer buffer back into its bottle. It can be reused for up to 5 times
19	Optional: Color the membrane with Ponceau solution to visualize the protein bands. Afterward, wash the membrane with desalted water until its colorless again
20	Cut the membrane to size and put it into the hybridization box
21	Incubate the membrane with blocking buffer for 1 h
22	Put antibody dilution in 7 mL of blocking buffer. For dilution factor check the antibodies protocol
23	Put the antibody solution on the membrane and incubate on a shaker at RT for 1 h or at 4°C overnight
24	Wash the membrane 3 times with TBS-T for 5 min
25	Prepare the secondary antibody solution in 7 mL TBS-T
26	Put the secondary antibody solution of the membrane and incubate it on the shaker at RT for 1 h
27	Wash the membrane 3 times with TBS-T for 5 min
28	Detect the secondary antibody

Table 18: Western blot with precast gels

2.8.4 OxyBlot™ Protein Oxidation Detection Kit

Material		
Amount	Name	Manufacturer
	OxyBlot™ Protein Oxidation Detection Kit	Merck Millipore No. S7150
	1X 2,4-Dinitrophenylhydrazine (DNPH) Solution	
	1X Derivatization-Control Solution	
	Neutralization Solution	
	12% SDS	
Methods		
Step	Description	
1	The protein concentration was measured and adjusted to 5ng/µL for all samples.	
2	Transfer 5 µL of a protein sample (crude or purified) into each of 2 eppendorf tubes (0.5-1.5 mL).	
3	Denature each 5 µL aliquot of protein by adding 5 µL of 12% SDS for a final concentration of 6% SDS.	
4	Derivatize the sample by adding 10 µL of 1X DNPH Solution to one of the tubes. To the aliquot designated as the negative control, add 10 µL of 1X Derivatization-Control Solution instead of the DNPH solution.	
5	Incubate both tubes at room temperature for 15 minutes. Do not allow the reaction to proceed for more than 30 minutes, as side reactions other than hydrazone linkage may occur.	
6	Add 7.5 µL of Neutralization Solution to both tubes. If reduction of the protein sample is desired and a reducing reagent was not present during lysis, add 2-mercaptoethanol to the sample mixture to achieve a final concentration of 0.74 M solution (1-1.5L; 5%v/v).	
7	Both the treated sample and the negative control are ready to load into a polyacrylamide gel.	

Table 19:Derivatization of Protein Mixture

Material		
Amount	Name	Manufacturer
	Transfer Buffer	
	Blocking/Dilution Buffer: 1% BSA/PBS-T	
	PBS-T: PBS (Phosphate buffered saline, pH 7.2-7.5) containing 0.05% Tween-20.	
	DNP-lated molecular weight standard protein.	90450
	First Antibody: dilute first Antibody stock to 1:150 with Blocking/ Dilution Buffer	90451
	2°Antibody: dilute 2°Antibody stock (90452) to 1:300 with Blocking/ Dilution Buffer	
	Chemiluminescent reagent	

Methods

Step	Description
1	Upon first use, warm the standard protein mixture to room temperature. Transfer the amount necessary for the first experiment into one tube and divide the remaining mixture among several tubes. Store the aliquots from excessive freeze-thaw and heating cycles. Combine 2.5 µL of the molecular weight standard with attached DNP residues and 20 µL of 1X Gel Loading Buffer before loading onto the gel.
2	Electroblot proteins to a membrane.
3	Incubate the membrane in Blocking/Dilution Buffer for 1 hour with gentle shaking. Use 0.3 mL/cm2 of membrane.
4	Dilute the 1°Antibody stock 1:150 in Blocking/Dilution Buffer just before use. Use enough solution so that the membrane is completely immersed in the solution (15 mL for a 10 x 10 cm^2 membrane). Incubate the membrane in the 1°Antibody solution for ~1 hour at 18°to 25°C with gentle shaking.
5	Rinse the membrane 2 times with 1X PBS-T. Wash the membrane with 1X PBS-T once for 15 minutes, then twice for 5 minutes each at 18°to 25°C.
6	Dilute the antibody stock 1:300 in Blocking/Dilution Buffer. Incubate the membrane in the 2°C Antibody solution (15 mL for a 10 x 10 cm^2 membrane) for ~1 hour at 18°C to 25°C with gentle shaking.
7	Wash the membrane as in step 5.
8	Drain the excess buffer from the membrane, place it on a plastic sheet with

the protein side up, and cover the membrane. The final reagent volume required is 0.125 mL/cm^2. Incubate for 1 minute at 18˚ to 25°C.

9	Drain off excess reagent by holding the membrane vertically and touching the edge against filter paper. As an alternative, the membrane may be dried by placing it between sheets of filter paper. Place the membrane inside a plastic page protector. Remove air pockets.
10	Place the membrane, protein side up, in a film cassette. Make sure that there is no free reagent in the cassette.
11	In a darkroom, carefully place an autoradiography film on top of the membrane.
12	Expose the film for 30 seconds, then develop. When all the procedures are correctly performed, the bands of molecular weight standard proteins should be readily visible after a 30-second exposure.
13	Place a second film on top of the membrane. Expose the film for the appropriate amount of time.

Table 20:SDS-PAGE, Western Transfer, and Immunodetection

2.9 Animal experiment

All animal experiments were performed in cooperation with Chifeng Municipal Hospital, Chifeng, Inner Mongolia, China, which was approved by the animal ethics committee（ approval number：CFMH-LAEC-202103-08）. The experimental procedures are listed in table 21.

2.9.1 Xenograft model generation from human U87 cells

Material		
Amount		Manufacturer
	U-87 MG	ATCC No.: CVCL_0022
	SPF Balb/C nude mice, 6-8 weeks old, 20~25g, male,	Taconic, Cologne, Germany
	Ultra-clean table	VS-1300， Eppendorf，Germany
	Pipette	Research Plus Series, Eppendorf, Germany

	High speed skull drill	ZH-GSZ, Germany
	Brain stereotactic injection instrument	JK023, Germany
	Pure Water Meter	ELIX3, Millipore, USA
	Various models of a centrifugal tube, nozzle, and cryogenic storage tube	Axygen, USA

Methods

Step	Description
1	The animal room alternates day and night from 12h to 12h, and the animals are kept free to drink and eat at 23-25℃. After one week of adaptive feeding, the experiment is carried out.
2	Inhalation anesthesia is performed with Isoflurane (4% induction, 2-2.5% for maintenance).
3	The hair from the head of the mouse is removed and fixed in the ste-reolocator. Wipe the scalp with alcohol.
4	The anterior fontanelle is marked by a coronal incision of about 1cm in the scalp using pointed forceps.
5	3 μL suspensions containing 1.0×10^{7} tumor cells were prepared in the microinjector.
6	The skull is opened 0.4 mm forward and 2.0 mm to the right from the anterior fontanelle to reach the dura mater
7	The microinjector is vertically passed through the skull defect into the white matter at a depth of 3.0 mm, and the tumor cell suspension was injected at a rate of 0.2μL/min for 5 minutes.

8	After the injection, the needle was held for 5 min at the same place and afterward withdrawn slowly for 1mm, followed by 1mm/min. Disinfect the scalp and suture it.
9	The mice were resuscitated on a 37 ℃-resuscitation pad and then placed in the original cage with adequate food and water.
10	The experiment began on the second day.

Table 21:Animal model

2.9.2 In vivo therapeutic trial

A: THP (general dosage group);

B: THP (maximum dose group for extraspinal diseases);

C: THP (maximum drug dosage group);

D: TMZ medication group;

E: normal saline (inoculated tumor group);

F: Normal saline (uninoculated tumor group).

	A	B	C	D	E	F
1-3 day; 2 times/day	0.05mg/ Kg/time	0.05mg/ Kg/time	0.05mg/ Kg/time	2.0mg/ Kg/time	1.0ul/ Kg/time	1.0ul/ Kg/time
4-6 day; 2 times/day	0.1mg/ Kg/time	0.1mg/ Kg/time	0.1mg/ Kg/time	2.0mg/ Kg/time	1.0ul/ Kg/time	1.0ul/ Kg/time
7-9 day; 3 times/day	0.1mg/ Kg/time	0.1mg/ Kg/time	0.1mg/ Kg/time	1.33mg/ Kg/time	1.0ul/ Kg/time	1.0ul/ Kg/time
10-16 day; 3 times/day	0.1mg/ Kg/time	0.17mg/ Kg/time	0.3mg/ Kg/time	1.33mg/ Kg/time	1.0ul/ Kg/time	1.0ul/ Kg/time
17 day	Remove the	specimen				

Table 22:Grouping and administration

We firstly consulted the clinical generic dose of THP, the maximum dose for extra vertebral systemic diseases, and the maximum dose for Parkinson's disease, according to the clinical dosing instructions for THP and the relevant literature[118, 119]. All mice were then grouped according to a simple practice guide for dose conversion between animals and humans[120, 121].

On day 17, the mice were anesthetized and sacrificed by cardiac perfusion. The brains were collected and stored in 4% paraformaldehyde. After 48 hours, the brains were transferred to 30% sucrose solution and frozen at -80℃.

2.10 Computational development of prognostic gene expression signature for predicting the clinical course of GBM patients

This work was primarily performed in cooperation with the Department of Molecular and Experimental Surgery (MES), Faculty of Medicine, Otto-von-Guericke University Magdeburg, Germany. We first obtained expression data with clinical annotated information from publicly available, consensus molecular tumor datasets.

This includes n=237 patients from the Chinese Glioma Genome Atlas (CGGA), 150 GBM-related prognostic data from Gene Expression Omnibus (GEO), and another 159 cases from the GSE16011 dataset, which was used to validate the GBM prognostic model obtained from GSE83300, which includes 50 GBM samples.1936 extracellular matrix (ECM) related genes are sourced from 47 ECM gene sets. single-factor Cox regression and lasso regression was used to select prognosis-related ECM genes. With the results of multifactorial Cox regression, we constructed prognostic models based on regression coefficients and gene expression and calculated model scores to obtain ECM indices. We further compared the survival difference between patients with high and low ECM index and externally validated the prognostic model.

The relationship between ECM index and the degree of tumor immune infiltration was also calculated, and we also demonstrated the difference in the distribution of ECM index among tumor-infiltrating immune cells. To further test the predictive efficacy of the model, five machine learning algorithms, namely support vector machine (SVM), random forest (RF), generalized linear models (GLM), and artificial neural network (ANN), were used to evaluate the model in the intended assay. Lastly, to support dissemination and application of our newly

identified diagnostic marker by other, non-infmatic experts, a web page developed which can be assessed under (https://ospg.shinyapps.io/OSPG/)[122].

3 Results

3.1 TTFields

3.1.1 TTFields inhibit the cell growth of glioblastoma stem cells (GSCs)

We used established GSC models to confirm the effect of TTFields in our models. All cell lines were classified accordingly by other institutions and verified by our lab using RNA sequencing data and short-tandem-repeat (STR) analysis from ongoing projects[37]. The use of such patient-derived chronic cell systems for the described work has been approved by the local ethical committee of the medical faculty of Heinrich-Heine-University Düsseldorf.

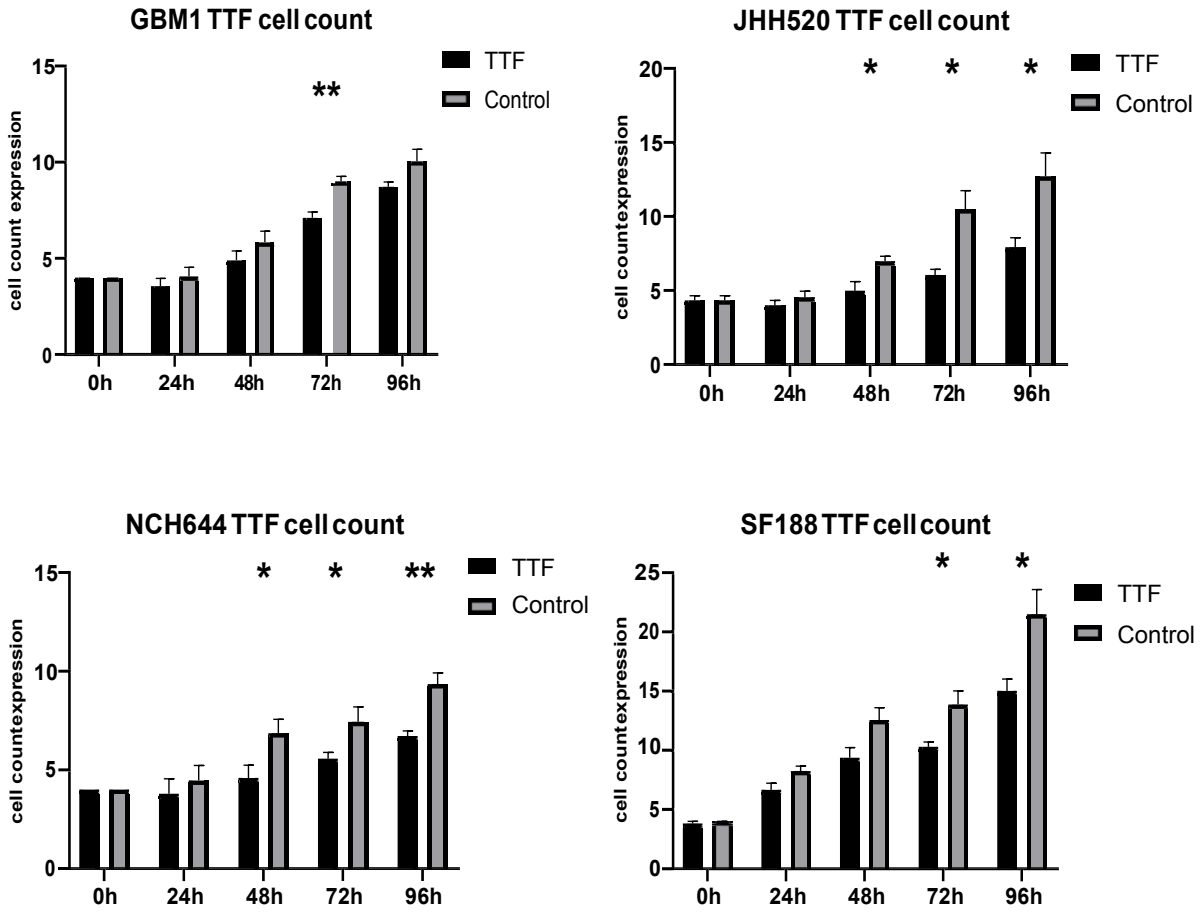

Figure 4:TTFields system implementation and establishment of therapy model (200kHz, three independent repetitions)(Cell Count). The statistical test performed was one-way ANOVA. The significance of the difference between groups was described as * $p < 0.05$, ** p

Cell counting was used to observe the response to TTFields (200 kHz) in each tumor cell line at 0, 24, 48, 72, and 96 hours (Figure 4). The results showed that of all four cell lines treated with TTFields, two cell lines (JHH520, NCH644) showed a significant difference in cell growth at 48 hours, whereas the other two cell lines (GBM1, SF188) showed a significant difference in cell growth at 72 hours. The results of these experiments suggest that TTFields have a significant therapeutic effect on the growth of glioblastoma.

MTT was then used to observe the response of TTFields (200 kHz) to the metabolic response in each of the tumor cell lines at 0, 24, 48, 72, and 96 hours (Figure 5). This was done in concordance with a personal consultation with the research lead of the manufacturer of the TTF research device, as other studies using this tool have found differences when scoring the effect of the treatment depending on the used assay to score cellular viability. The results showed similar results as the manual counting. All four cell lines treated with TTFields, JHH520 and NCH644 showed a significant difference in cell growth at 48 hours, while GBM1 and SF188 showed a significant difference in cell growth at 72 hours. Notably, the pediatric glioblastoma model SF188, which showed a significant difference in cell count at 72 hours, was the most sensitive cell line used. The results of these experiments further reveal that TTFields do have a significant therapeutic effect on glioblastoma cell growth and prove its therapeutic activity extends to GSC, a cell population notoriously resistant to other (more classical) therapies.

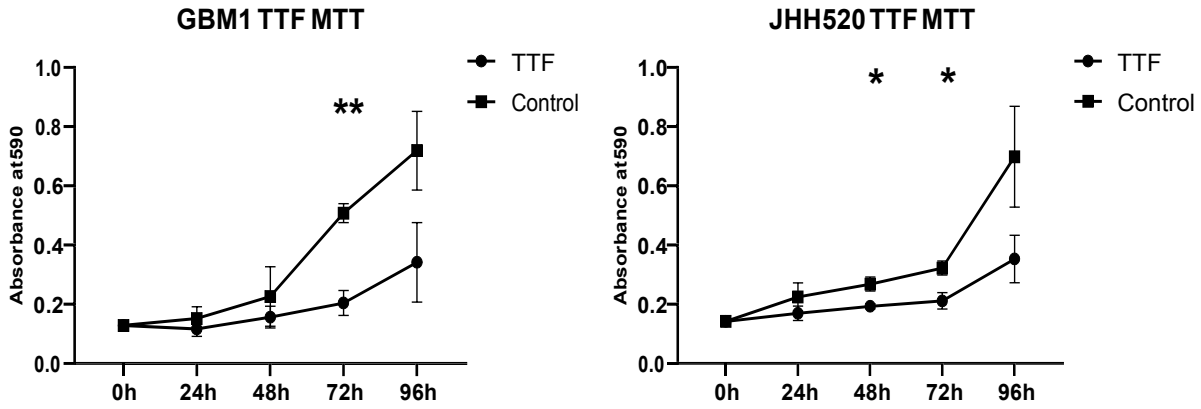

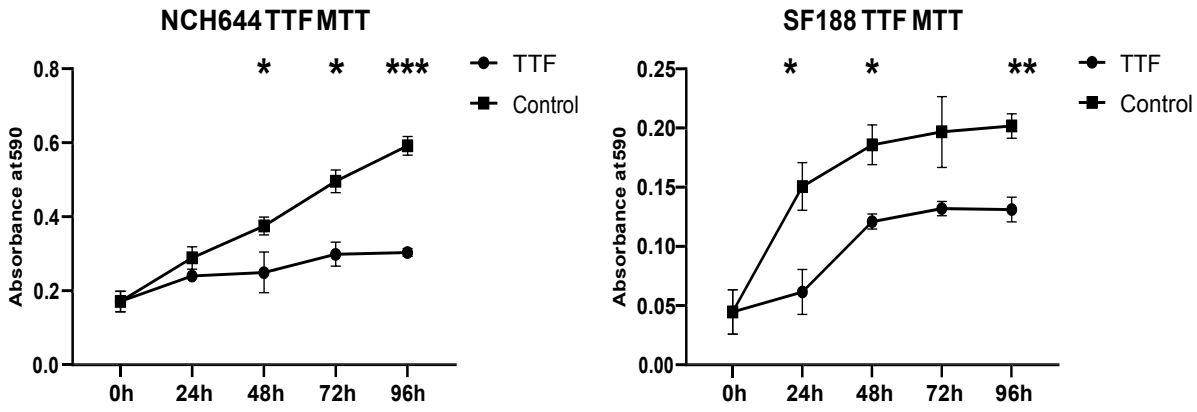

Figure 5:TTFields system implementation and establishment of therapy model (200kHz, three independent repetitions) (MTT). The statistical test performed was one-way ANOVA. The significance of the difference between groups was described as * $p < 0.05$, ** $p < 0.01$.

3.1.2 qPCR results after TTFields 48h

Then qPCR was used to examine the response of TTFields (200 kHz) to the different primers for each tumor cell line after 48 hours (Figure 6). The results showed that all four cell lines treated with TTFields showed varying degrees of up- or down-regulation after 48, especially HES and ZEB1 both showed a significant up-regulation trend in all four cell lines, and there was a significant difference in JHH520. These experimental results further showed that TTFields did have significant effects on many genes of many pathways during the growth of glioblastoma cells, especially the Notch pathway, and some genes of the EMT signaling pathway were significantly up-regulated.

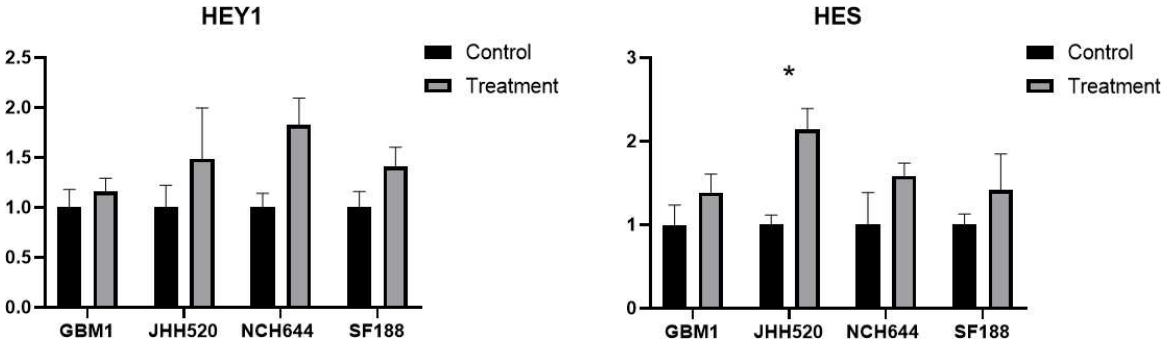

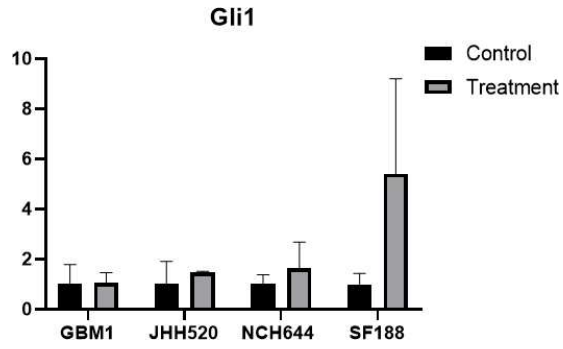
Gli1
Control
Treatment
10
8
6
4
2
0
GBM1
JHH520
NCH644
SF188

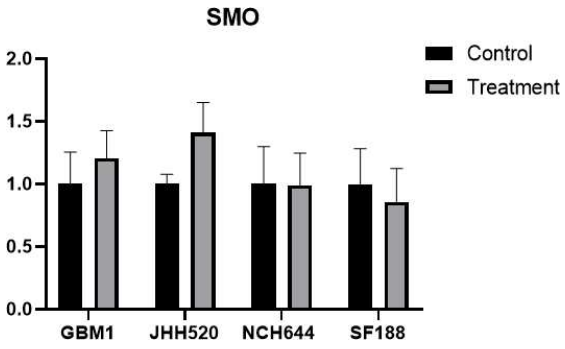
SMO
Control
Treatment
2.0
1.5
1.0
0.5
0.0
GBM1
JHH520
NCH644
SF188

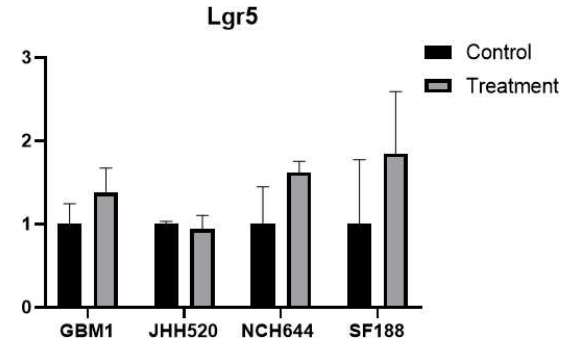
Lgr5
Control
Treatment
3
2
1
0
GBM1
JHH520
NCH644
SF188

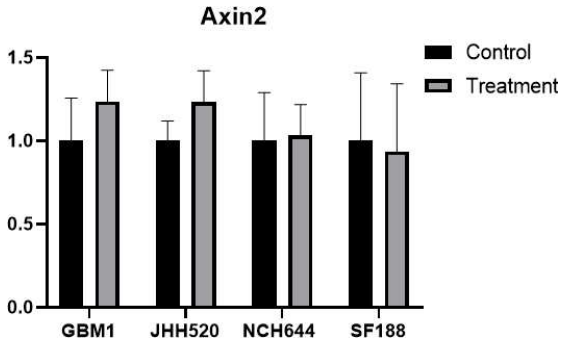
Axin2
Control
Treatment
1.5
1.0
0.5
0.0
GBM1
JHH520
NCH644
SF188

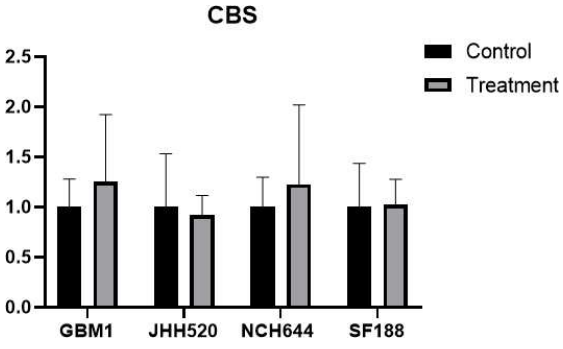
CBS
Control
Treatment
2.5
2.0
1.5
1.0
0.5
0.0
GBM1
JHH520
NCH644
SF188

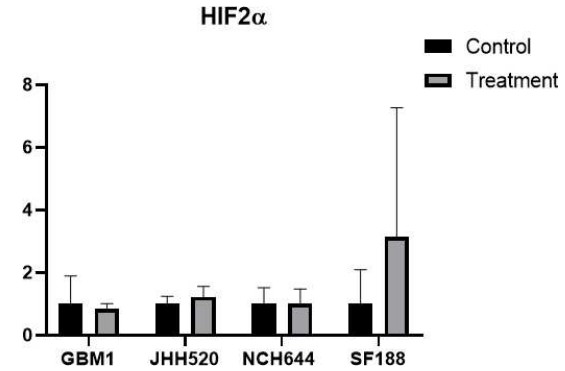
HIF2α
Control
Treatment
8
6
4
2
0
GBM1
JHH520
NCH644
SF188

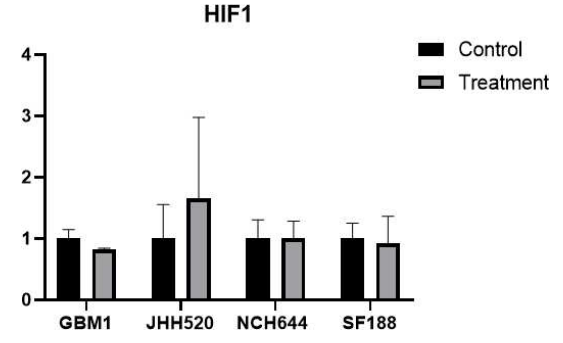
HIF1
Control
Treatment
4
3
2
1
0
GBM1
JHH520
NCH644
SF188

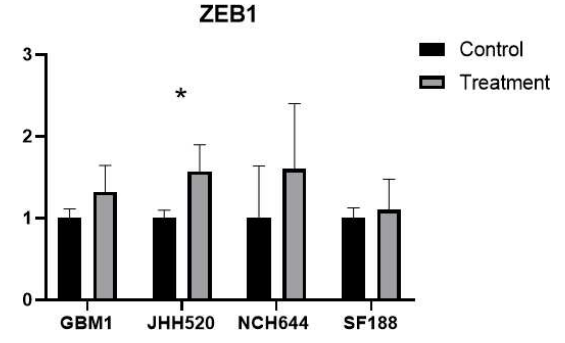
ZEB1
Control
Treatment
*
3
2
1
0
GBM1
JHH520
NCH644
SF188

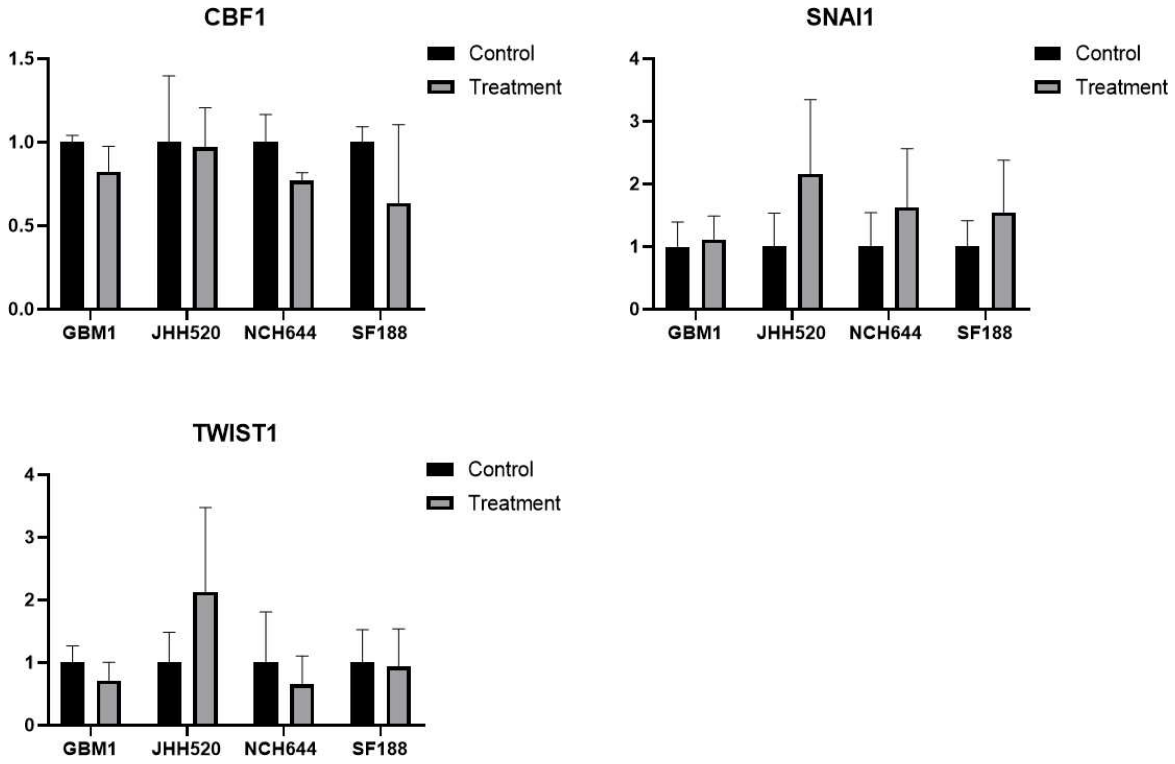

Figure 6:TTFields system implementation and establishment of therapy model (200kHz, three independent repetitions) (qPCR). The statistical test performed was one-way ANOVA. The significance of the difference between groups was described as * $p < 0.05$

3.1.3 Oxyblot blot results after TTFields

Oxyblots were then performed to examine oxidative protein damage in different tumor cell lines upon TTFields (200 kHz) treatment (Figure 7). We first used three cell lines, GBM1, NCH644 and JHH520, after 48h of TTFields treatment to examine the carbonylated proteins, and the results showed that all three cell lines treated with TTFields showed different degrees of reduction in carbonylated proteins after 48h. Subsequently, we performed three replicate experiments with GBM1 cell line after 48h and 72h, respectively, and the results also showed a decrease in the carbonylated protein, but without any statistical significance.

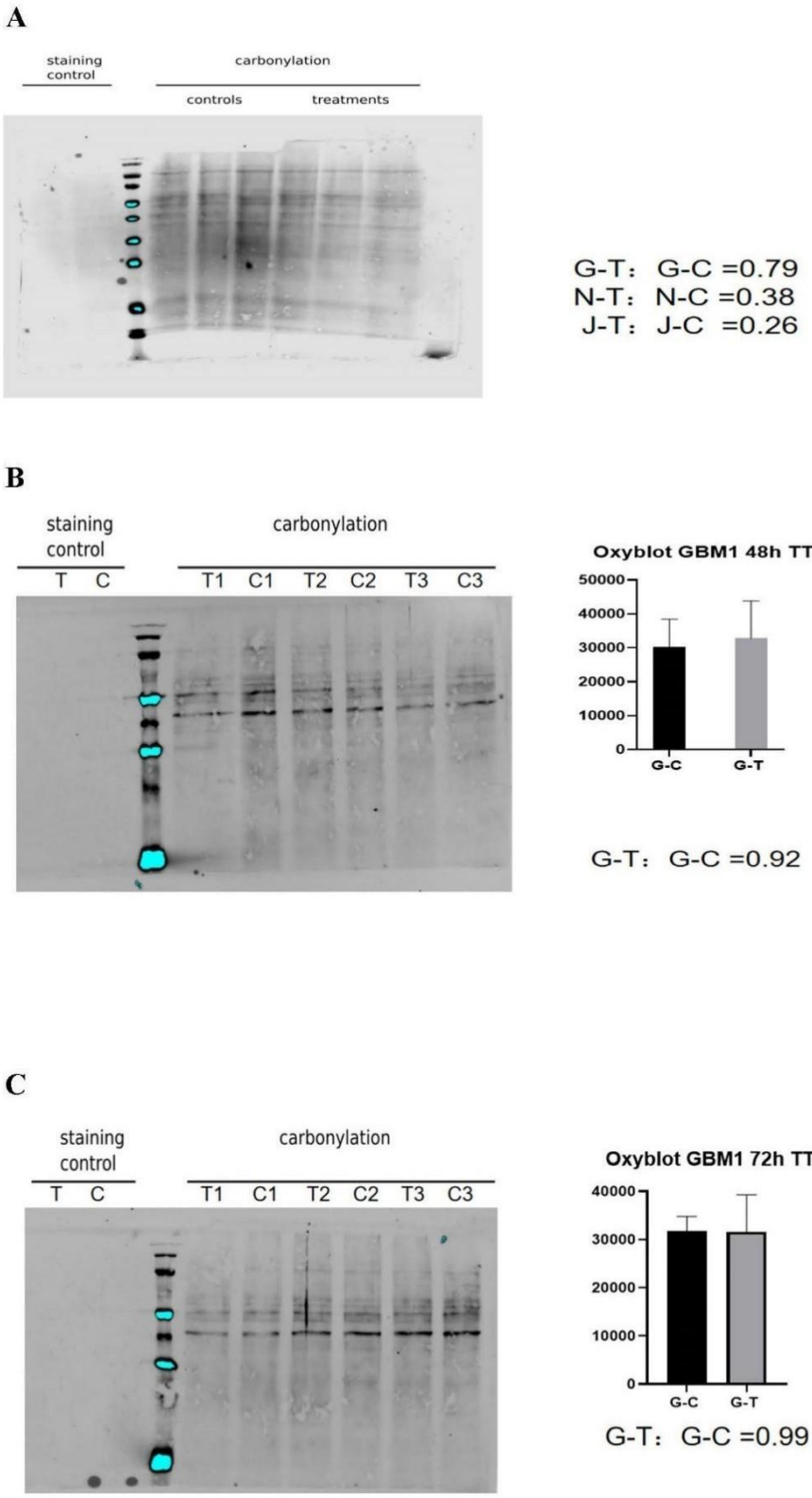

Figure 7: Oxyblots were used to examine the effect of TTFields (200 kHz) treatment on the carbonylation of proteins in different GBM cell lines (Figure 7). Three cell lines after 48h of TTFields treatment to examine the persulfated proteins（A）. Three replicate experiments with GBM1 cell line after 48h（B） and 72h（C）.

3.1.4 RNA sequencing results after TTFields 48h and 72 h

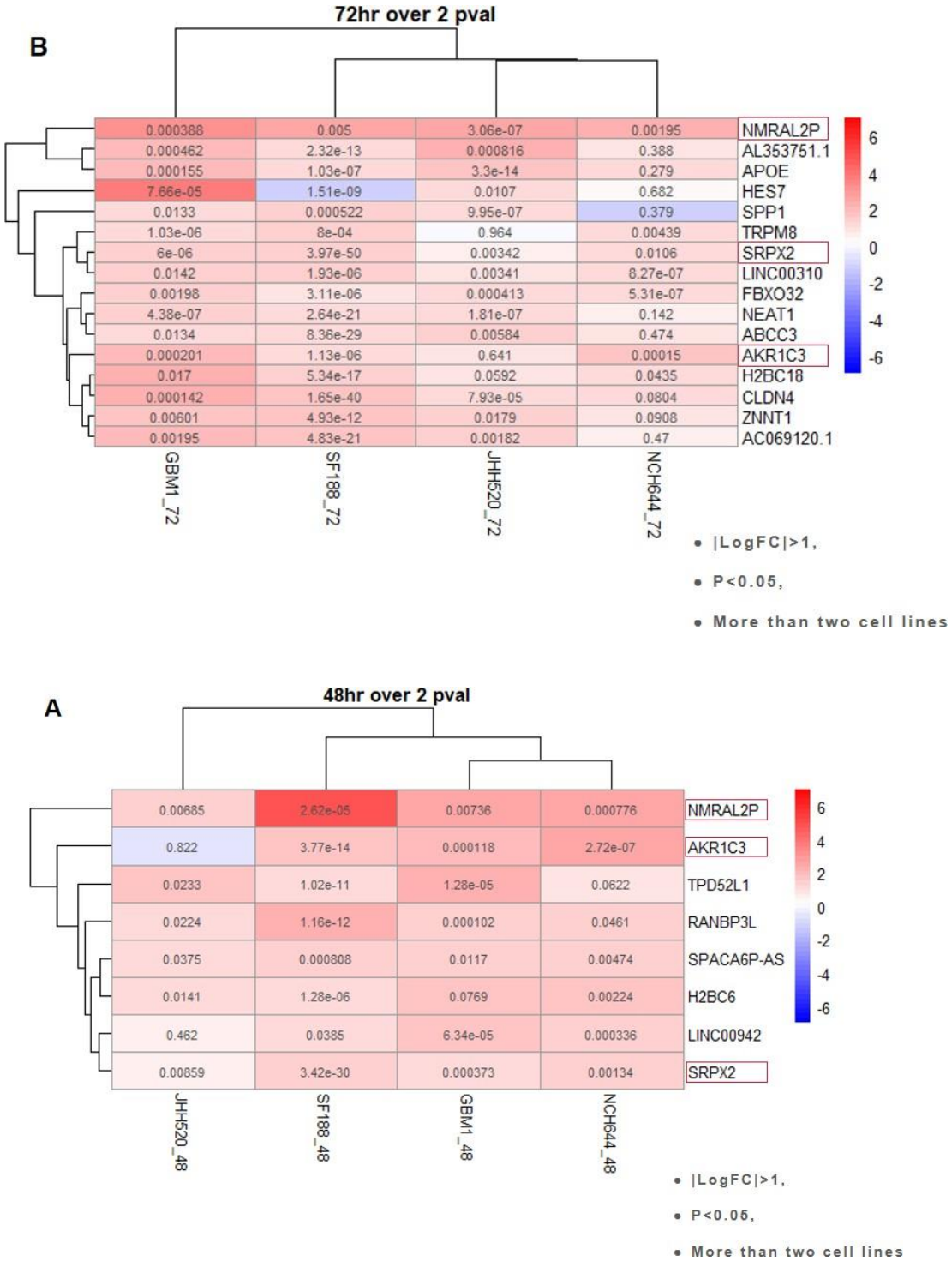

Figure 8:DEGs of significance after TTFields treatment 48 hours (A) and 72 hours(B). Red represents the up-regulation of genes and blue represents the downregulation of genes.

Differential analysis after 48 and 72 hours of TTFields treatment was performed by RNAseq and evaluated using the R package limma to detect possible underlying mechanisms and possible treatment targets. The screening condition was set at |LogFC|>1, P<0.05. The results suggested a total of eight genes that are significantly upregulated after 48 hours of TTFields action. These genes were NMRAL2P, AKR1C3, TPD52L1, RANBP3L, SPACA6P-AS, H2BC6, LINC00942, and SRPX2 (stand for Sushi repeat-containing protein 2). 72 hours of TTFields application, a total of 16 different genes were detected to be upregulated in the cell lines, namely NMRAL2P, AKR1C3, AL353751.1, APOE, HES7, SPP1， TRPM8， SRPX2, LINC00310, FBXO32, NEAT1, ABCC3, H2BC18, CLDN4, ZNNT1, and AC069120.1. Further analyzing the results, we found that a total of three genes (NMRAL2P, AKR1C3, and SRPX2.) were significantly upregulated in gene expression after TTFields action either at 48 or 72 hours (Figure 8).

We further analyzed the data using a HALLMARK pathway enrichment analysis on the differential expressed genes (DEGs) and the results suggested that after 48 hours of TTFields action, a total of seven pathways in the four cell lines were simultaneously inhibited (Figure 6). These seven pathways are MYC_TARGETS_V1, E2F_TARGETS, G2M_CHECKPOINT,DNA_REPAIR,MYC_TARGETS_V2,MITOTIC_SPINDLE,and PI3K_AKT_MTOR_SIGNALING. The results of HALLMARK pathway enrichment analysis of differential genes after 72 h of TTFields action suggested that a total of 12 pathways were inhibited simultaneously in four cell lines, and they were MYC_TARGET_V1, E2F_TARGETS, G2M_CHECKPOINT, MTORC1_ SIGNALING, OXIDATIVE_PHOSPHORYLATION, MYC_TARGETS_V2, SPERMATOGENESIS, ANDROGEN_RESPONSE, PI3K_AKT_MTOR_SIGNALING, MITOTIC_SPINDLE, CHOLESTEROL_HOMEOSTASIS and DNA_REPAIR (Figure 9). Combining the above results, we found that the PI3K_ AKT_ MTOR_ SIGNALING pathway could be significantly inhibited at both 48 h and 72 h of TTFields action. Therefore, this pathway may be related to the mechanism of action of TTFields.

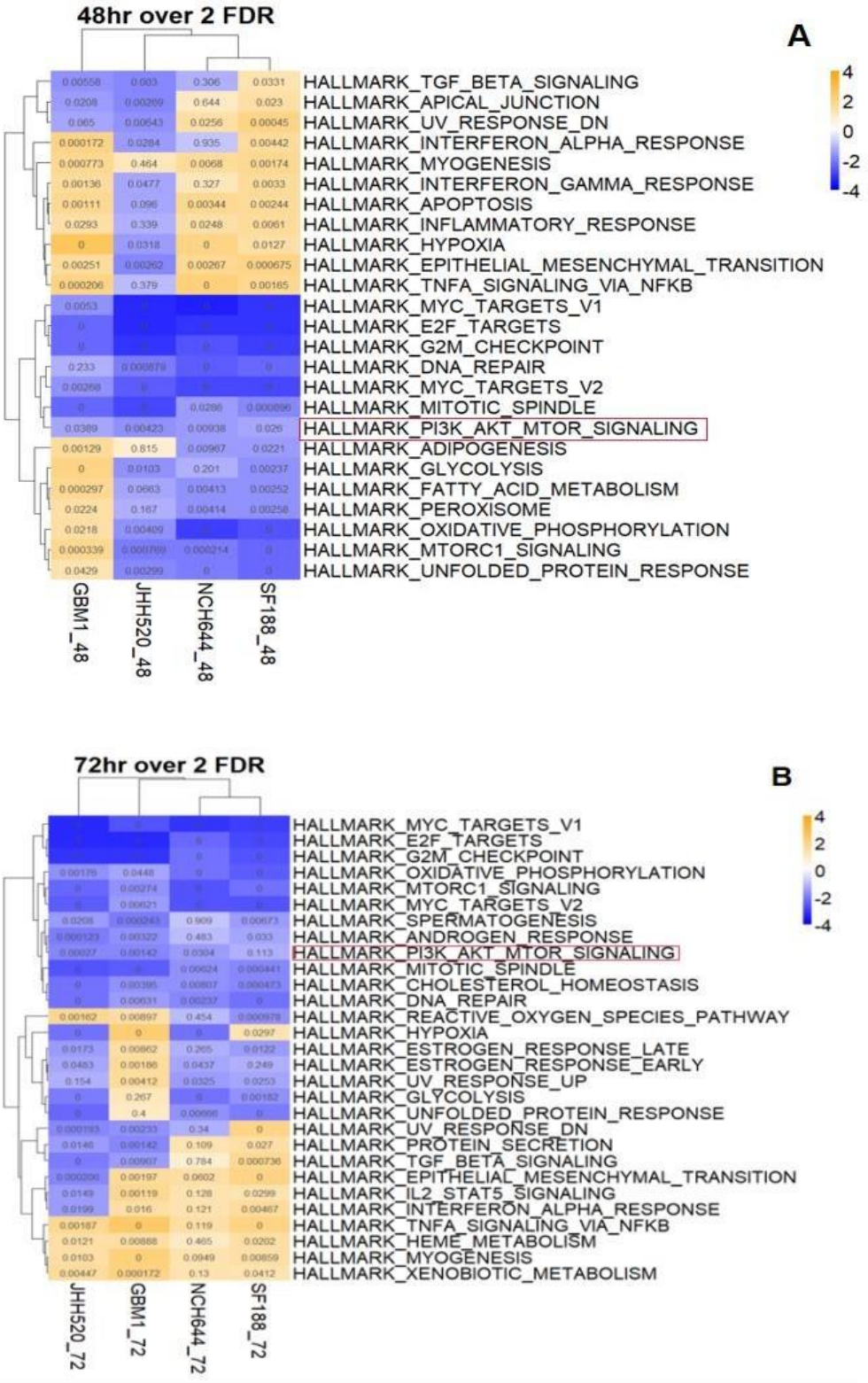

Figure 9:GSEA enrichment analysis results after TTFields treatment 48 hours (A) and 72 hours(B). Yellow represents the upward adjustment of the pathway and red represents the downward adjustment of the pathway.

3.1.5 Alignment of our data with public consensus molecular tumor database

We first screened out the core genes related to the pathogenesis of glioma by differential analysis of the sequencing data. Among the candidate genes, we found NMRAL2 to be a pseudogene and therefore not considered for follow-up studies. Next, we further verified whether the expression trend of candidate genes in cancer was consistent with the expression trend in the public database, and those genes with the opposite expression trend in the public database were also excluded from the cohort. For example, SRPX2, the results of public database analysis suggested that it was highly expressed in tumor tissues, but this was the opposite of our analysis (Fig. 10). After the above screening, AKR1C3 is considered to be a valuable research object. By reviewing the literature, we found that AKR1C3 is closely related to the regulation of the AKT pathway. Our previous results also suggested that the PI3K pathway was significantly inhibited by TTFields. Therefore, we speculated that TTFields might regulate the PI3K pathway by regulating AKR1C3.

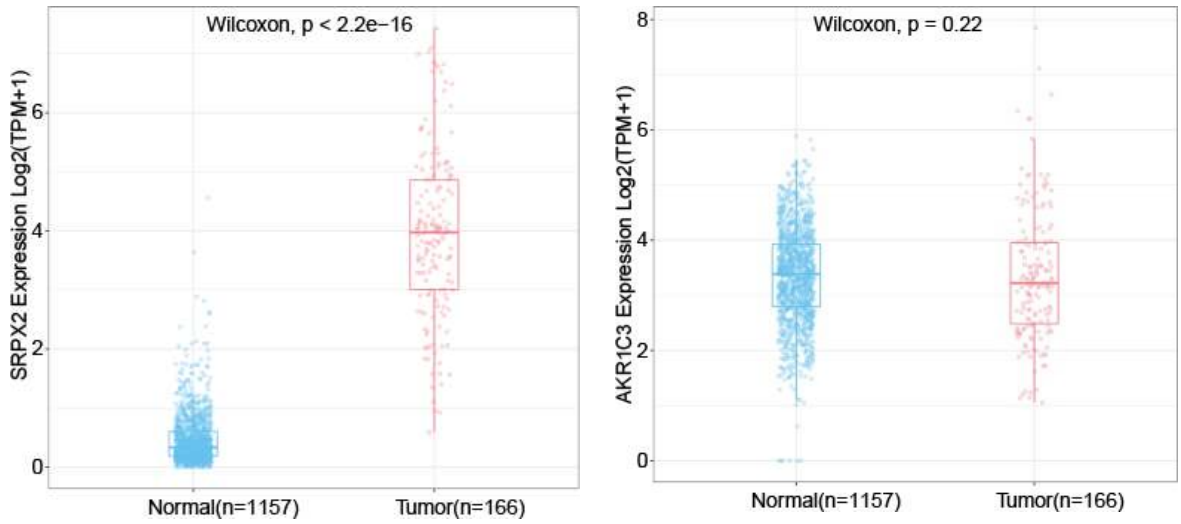

Figure 10: Public database validation reveals high expression of SRPX2 in tumor tissues

To further explore the possible mechanisms by which TTFields regulate AKR1C3 and thus the PI3K pathway, we first demonstrated that glioma patients with high AKR1C3 expression usually obtained worse clinical prognosis, both in terms of OS, DSS, and PFI, compared with the group with low AKR1C3 expression (Figure 11). Indicating that AKR1C3 is possible closely

related to the prognosis of patients. In addition, we also indirectly confirmed the possible involvement of AKR1C3 in the regulation of the PI3K pathway by analyzing the correlation between AKR1C3 and PTEN, a key gene in the PI3K pathway. These results suggested that AKR1C3 was positively correlated with PTEN with a correlation of 0.252 (Figure 11D).

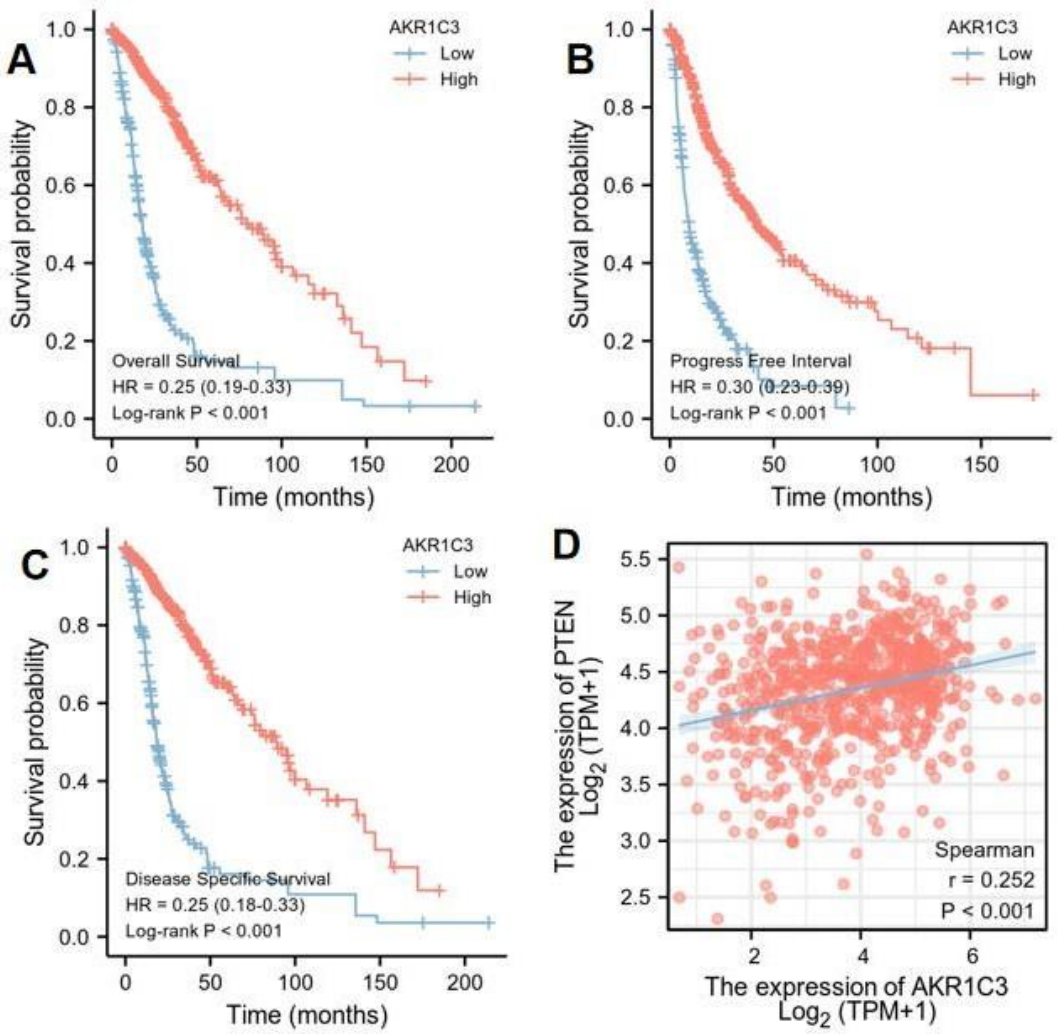

Figure 11: Glioma patients with high AKR1C3 expression usually obtained worse clinical prognoses in terms of overall survival (A), progress-free interval (B), and disease-specific survival. (D) Correlation between AKR1C3 and PTEN.

Assessment of drug repurposing potential of THP to putatively support future neuro-oncological care.

3.2 Trihexyphenidyl

3.2.1 Confirmatory study: THP therapeutic potential - replicated in all tested models independently of the molecular subclass of glioblastoma they represent

The responses of different concentrations of THP in all tumor stem cell models as well as on the control cells HUVE were observed by the CTG method on days 0, 2, 4, and 6. The results showed that under THP treatment, the number of living tumor cells decreased significantly with increasing drug concentration (Figure 12). This difference gradually became more pronounced with increasing time. Furthermore, the effect of THP on HUVE cells was less when the drug concentration of THP was 10 μM, and interestingly, the number of HUVE cells under treatment with 10 μM of THP was surprisingly higher than that of the negative control group on day 6. The experiment showed that THP was less toxic to normal cells at 10 μM. These experimental results suggest that THP has a significant therapeutic effect on the growth of glioblastoma with putatively low side effects on non-cancer cells.

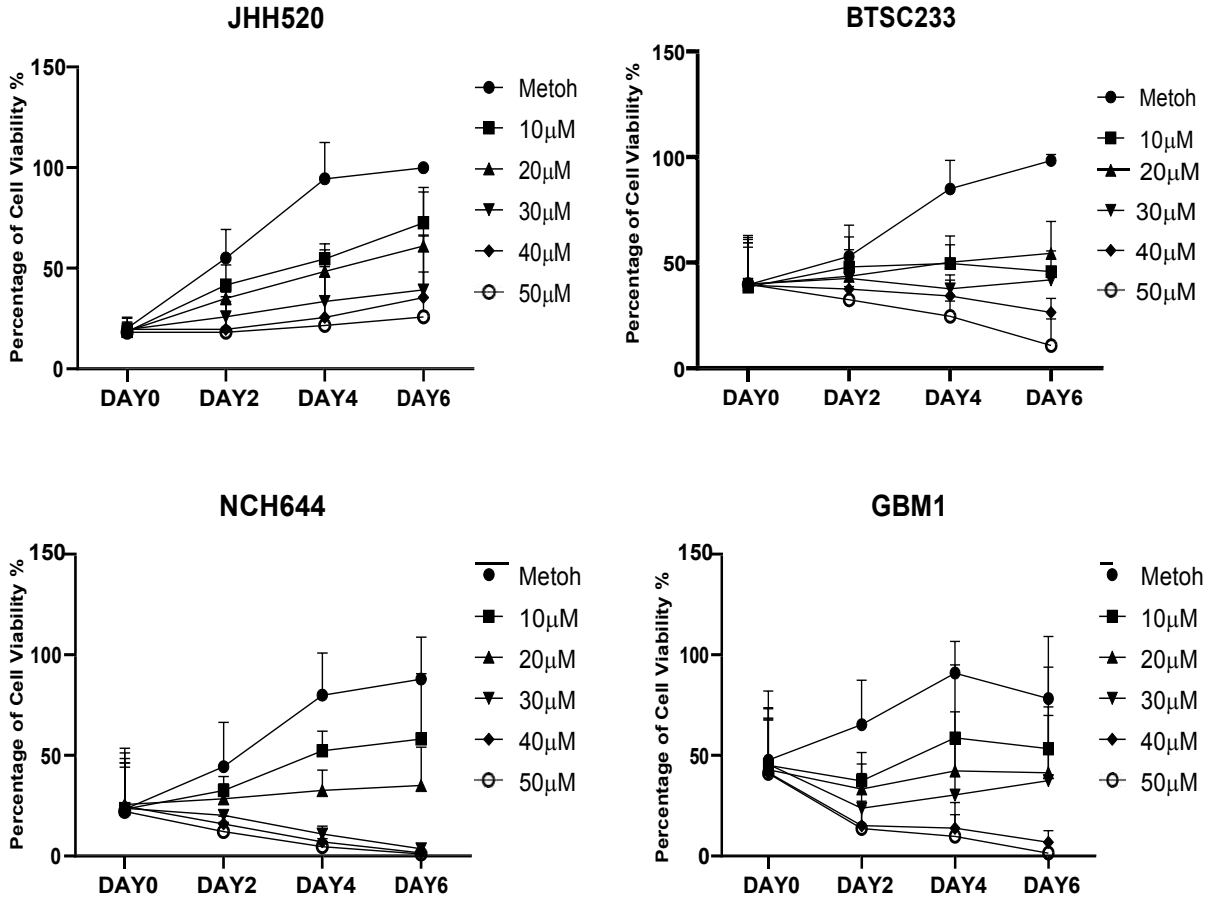

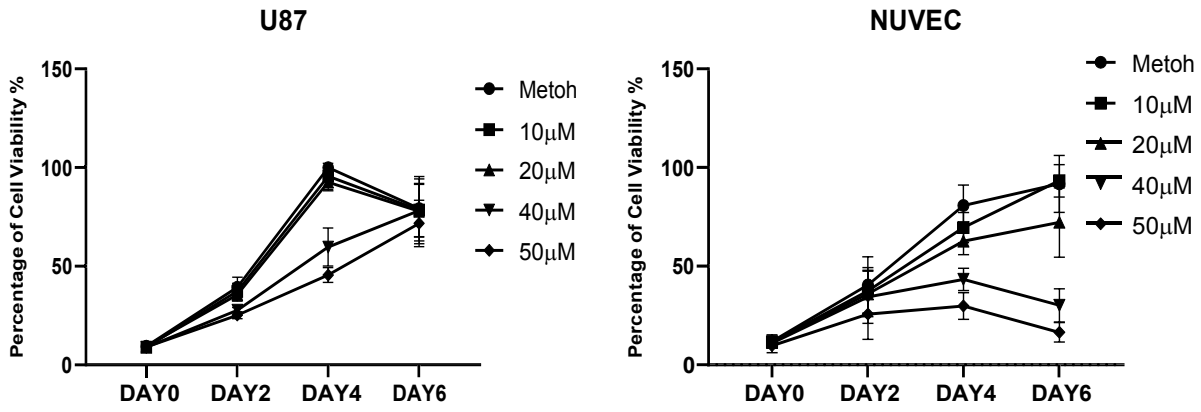

Figure 12： THP therapeutic potential - replicated in all tested models (CTG), THP was added at various concentrations onto JHH520, BTSC233, NCH644, GBM1, U87, and NUVEC the cell survival was monitored using the CTG assay for up to 6 days. At least three independen

3.2.2 Therapeutic effect of THP- characterization of the mode of action assessing cell proliferation Ki67 Proliferation Kit

After detecting the effect of THP on the GBM cells, we defined our THP working concentration as 10 μM. All further experiments were performed with cells treated at that THP drug concentration for 48h and 72h, respectively. To detect the influence of THP on cell proliferation on various GBM cell lines the proliferation marker Ki67 was measured using a desktop cytometer (Guava®Muse® Cell Analyzer). The results revealed significant differences in proliferation in three of five GBM cell lines (Figure 13). JHH520, NCH644, and U87 activity were significantly reduced, after 48h treatment with 10 μM THP. GBM1 and BTSC233 did not show significant differences in their proliferation rate as well as the control line HUVEC. Interestingly, 72h post-treatment almost all cell lines showed significantly reduced proliferation. Only in BTSC233 and in the healthy control HUVE cells no decrease in proliferation were detected. Our results showed that THP at a drug concentration of 10μM could effectively inhibit the proliferation of most glioma stem cells, while this concentration had no significant effect on the cells of normal tissues.

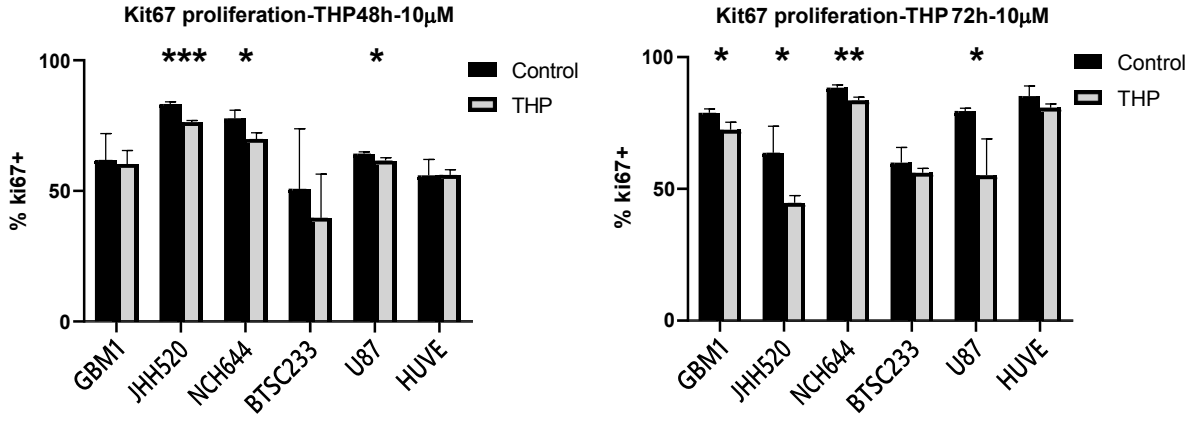

Figure 13： Kit67 proliferation-THP 48/72h-10µM; The significance of the difference between groups was described as * $p < 0.05$, ** $p < 0.01$.

3.2.3 Therapeutic effect of THP- characterization of the mode of action assessing cell cycle progression

To test the influence of THP on the cell cycle we treated all cell lines separately using a concentration of 10 µM THP for 48h, followed by fixation and cell cycle measurement. We coul d not detect any significant differences after 48h of THP treatment in all cell lines. Indicating that the growth and proliferative inhibitory effect of THP on glioma stem cells is probably not related to the cell cycle (Figure 14).

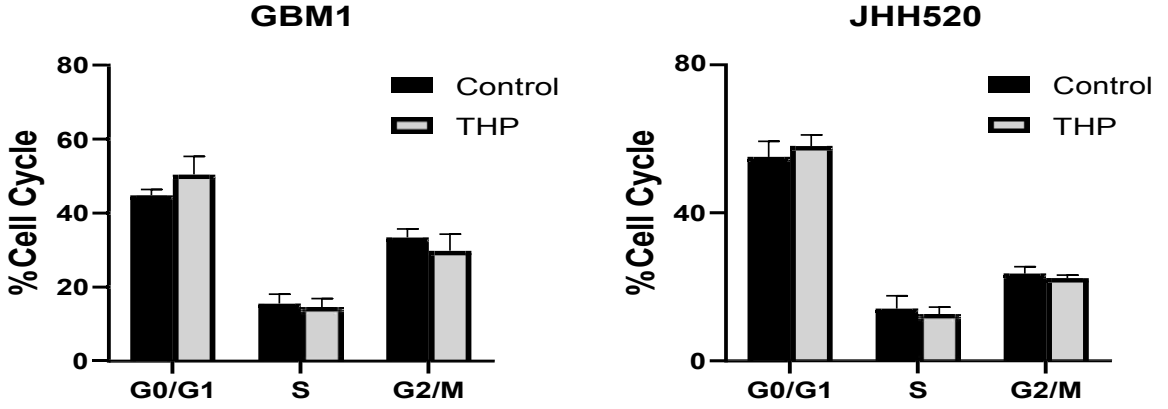

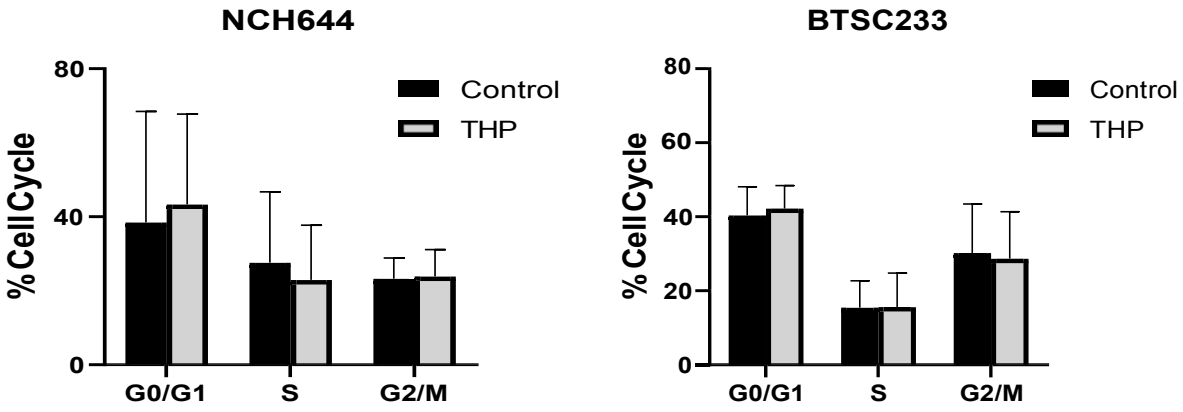

Figure 14: DNA and cell cycle analysis. The cell cycle of the indicated cells was observed after 48h treatment with 10μM THP. Results are represented by cell population in the G1, S, and G2 phases of the cell cycle.

3.2.4 Therapeutic effect of THP- characterization of the mode of action assessing survival focusing on apoptosis

To detect if the observed cell-killing effect was induced by apoptosis all cell lines were treated with THP (10 μM) for 48h and 72h, followed by Annexin-V staining. The results revealed that NCH644, GBM1, and HUVEC do not die due to apoptosis induction 48h nor 72h after treatment. Only a small difference in the number of living cells could be detected. A stronger increase in apoptotic cells was observed in U87 cells after 48h ($p<0.01$) treatment, which was maintained over 72h. Interestingly, in the JHH520 cell, a decrease in an apoptotic cell was detected, which may indicate an anti-apoptotic effect of THP in that cell line. The most profound effect of THP was detected in the cell line BTSC233. Here, 72h after THP treatment the cell line BTSC233 showed a general increase in apoptotic cells. Combined with the above experimental results, the inhibitory effect of THP on certain types of glioma stem cells could be related to the promotion of apoptosis of glioma stem cells (Figure 15).

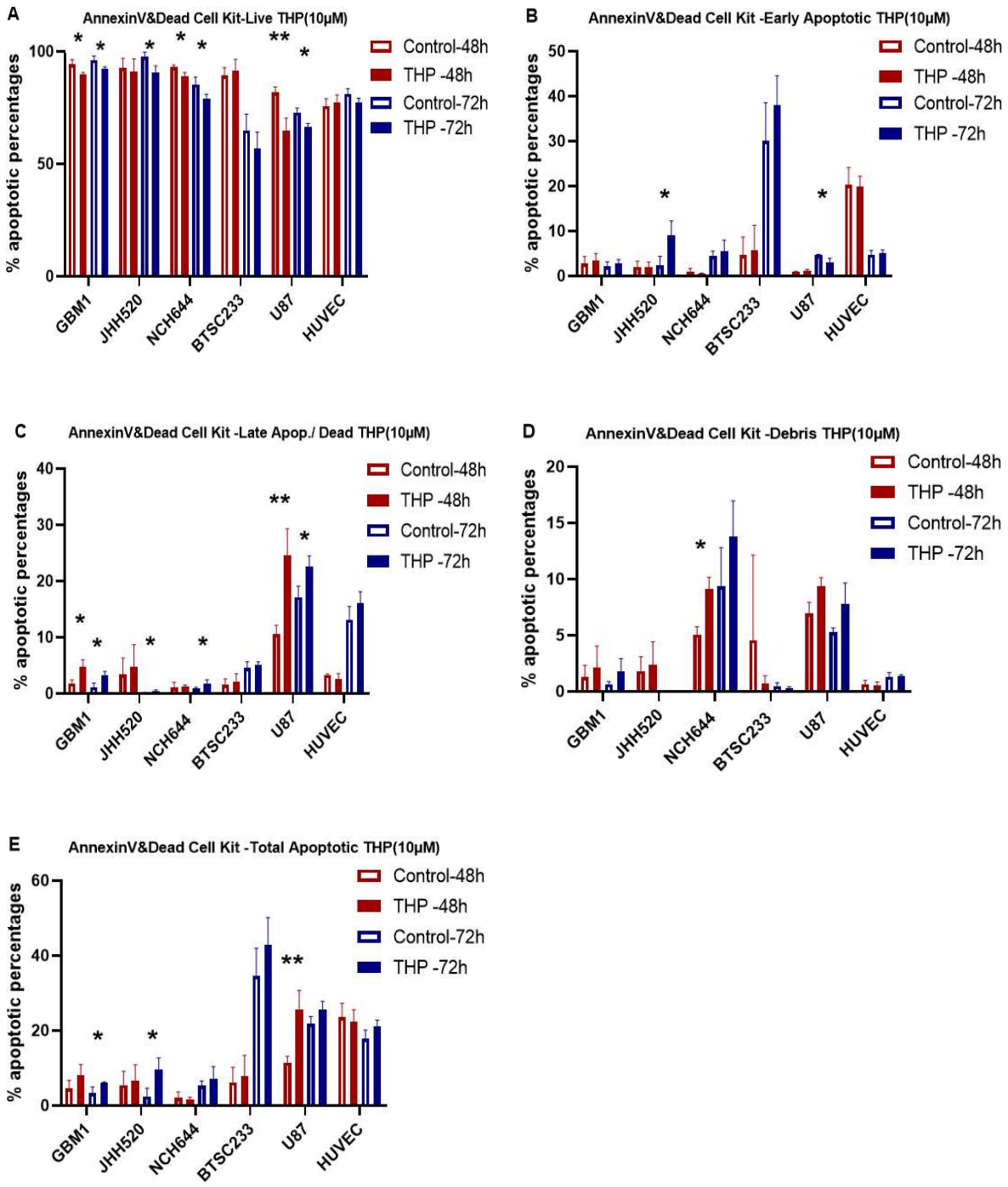

Figure 15: AnnexinV & Dead Cell Kit results after THP (10μM) treatment 48hours (A). AnnexinV & Dead Cell Kit-Live, (B) AnnexinV&Dead Cell Kit -Early Apoptotic, (C) AnnexinV&Dead Cell Kit -Late Apop./ Dead,(D)AnnexinV&Dead Cell Kit -Debris,(E) AnnexinV&Dead Cell Ki

3.2.5 qPCR results after THP 48h

Then qPCR was used to examine the response of THP (10 μM) to different primers on each tumor cell line after 48 hours (Figure 16). The results showed that all three cell lines treated with THP showed different degrees of up- or down-regulation after 48h, but no significant differences were observed.

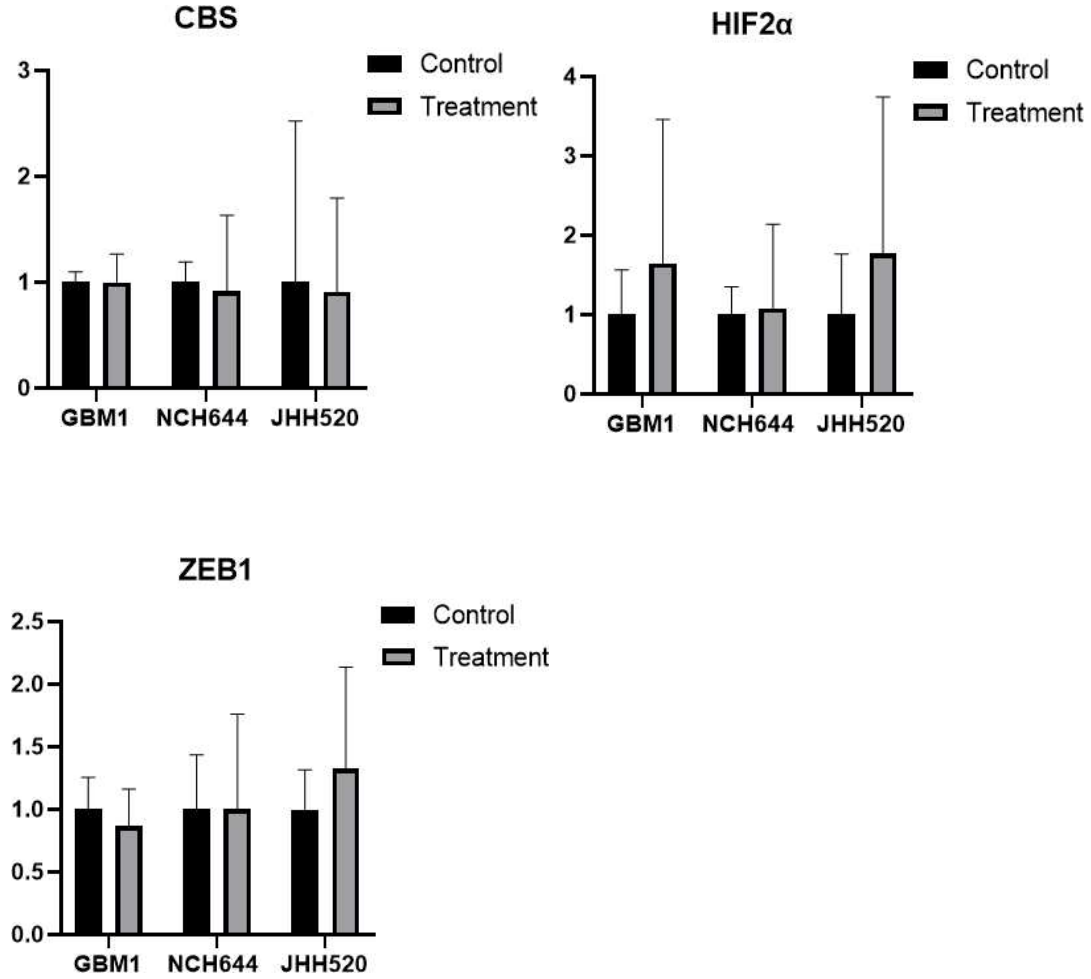

Figure 16: THP was implemented and treatment models were developed (10uM, three independent replicates) (qPCR). The statistical test performed was a one-way ANOVA. The significance of differences between groups was described as * $P < 0.05$

3.2.6 Therapeutic effect of THP- therapeutic trial in vivo using a xenograft rodent model

To test the effect of THP on GBM tumor growth we performed intracranial injection of classical GBM cell line U87-MG and analyzed the tumor regression pattern, tumor cell density, degree of intra-tumor fibrosis, tumor cell degeneration, degree of necrosis, and degree of inflammatory cell response. We used the U87-MG cell line as this is a very accepted brain tumor model worldwide, recapitulating strong cell proliferative growth features when implanted in immune-compromised mice, which is one of the core clinical scenarios glioblastoma is characterized by. After successful cell implantation and proof of tumor presence, the animals were treated either with TMZ or THP alone in the treatment regimens as detailed indicated in table 12.

Gliomas are diffusely distributed within the skull with no clear boundaries. Measurement of tumor size by the naked eye is not possible, and my hospital does not have a biopsy system, so assessment of intracranial tumor size variation is not available. However, we are convinced that the model generation was successful as the animals showed a strong vital decline after some time after the implantation (about 4 weeks), which was not noticed in control animals from the same animal delivery that did not receive implantation of tumor models but just sham treatment (equivalent volume implantation of PBS). We observed that with the increase in the concentration of THP, the body weight, diet, and mental state of the tumor-implanted mice have a trend of improvement. When the tumor-implanted mice showed a refusal to feed, weight loss, and/or depression, the mice were sacrificed by the spinal dislocation method, and the immunohistochemical method was performed on the tumor tissue.

Centripetal degeneration of tumor cells of the THP-treated group can be observed (Figure 17 C-F). In addition, decreased tumor cell density in the surrounding area was accompanied by inflammatory cell infiltration (Figure 17 C-F). At the higher magnification (Figure 17 A1-F1), the infiltration of inflammatory cells in the THP group was more obvious and accompanied by fibrous tissue proliferation (Figure 17 D1), Except for the partial vasodilation in the THP highest concentration group, tumor cells lost their adhesion, and were transformed, fragmented, and vacuolated in the cytoplasm (Figure 17 C, E). Mice treated with TMZ exhibited a significant decrease in tumor cell density, and tumor cell vacuolation and inflammatory cells are visible (Figure 17 F1).

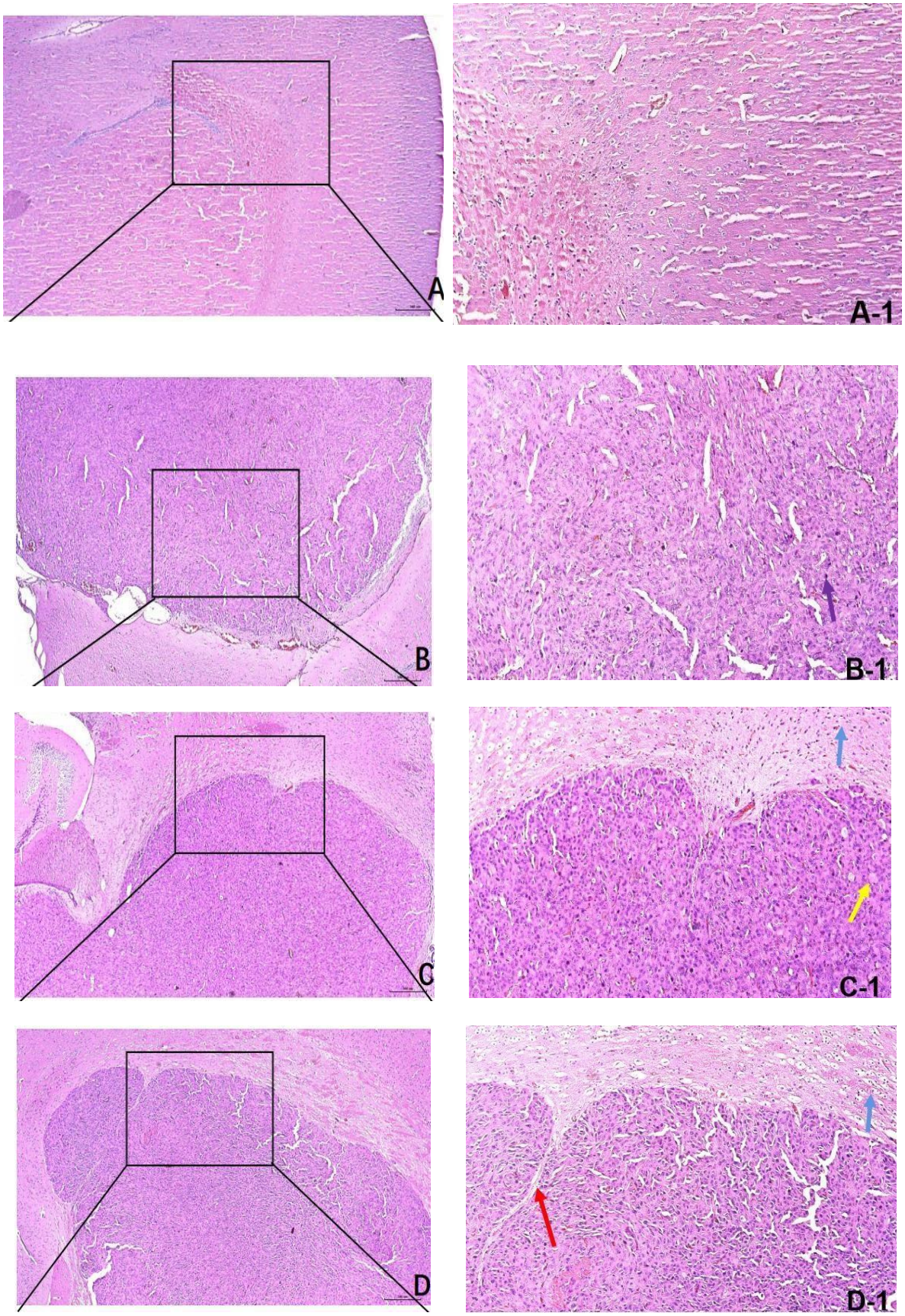
A
A-1
B
B-1
C
C-1
D
D-1

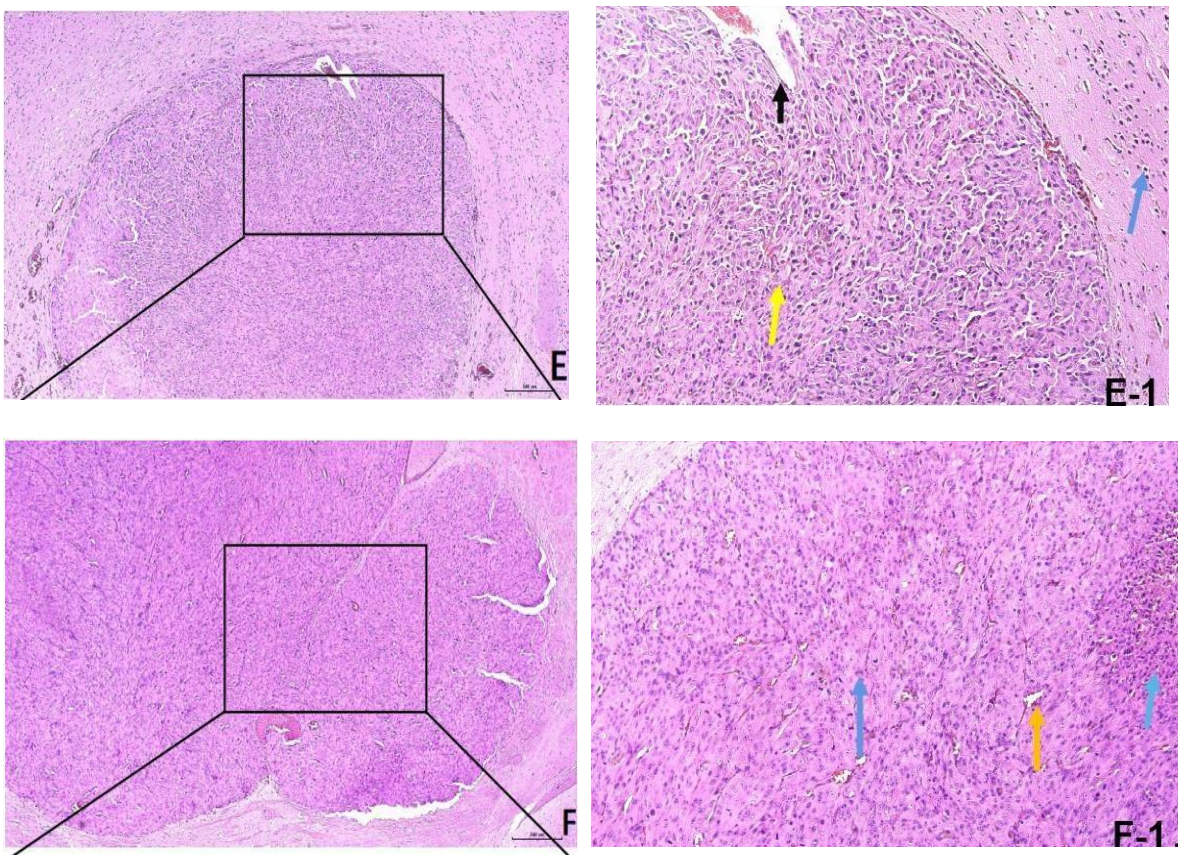

Figure 17： Tumor morphology in different treatment groups at different magnifications (HE staining). A/A1: Normal saline (uninoculated tumor group) (Magnification 40X/100X); B/B1:normal saline (inoculated tumor group) (Magnification 40X/100X); C/C1:THP (general do

While comparing tumor cell density in the THP highest concentration group with the TMZ treated group, significant cell sparing, and cell vacuolization was shown in tumor cells(E-1/F-1/F-2/F-3/F-4). In addition, the group with the highest concentration of THP showed significant mesenchymal fibrovascular expansion in some areas of the tumor, fibrosis in some areas of the tumor tissue margins, loss of tumor cell adhesion as well as small tumor cells scattered at the tumor cell margins; and lymphocytes were seen at the tumor margins (Figure 18). It is noteworthy that the tumor cells in the center of the tumor in the TMZ-treated group showed necrotic apoptosis (Figure 19), which proves that the efficacy of TMZ is indeed excellent.

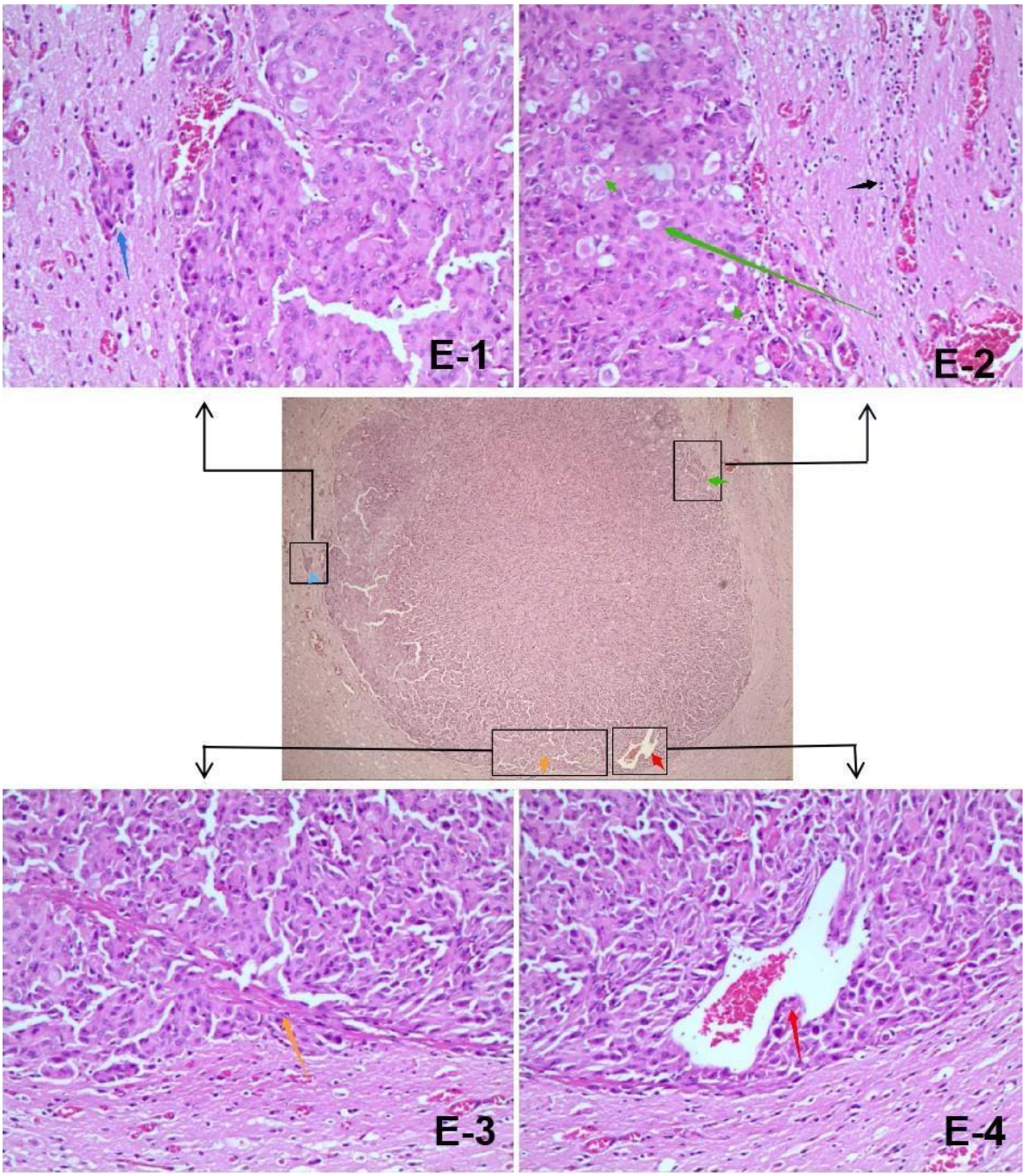

Figure 18： E: tumor morphology of THP maximal drug dose group at magnification 40X (HE staining). E-1/E-2/E-3/E-4: tumor morphology of THP (maximal drug dose group) at magnification 100X (HE staining). Red: dilated mesenchymal fibrovascular in some area

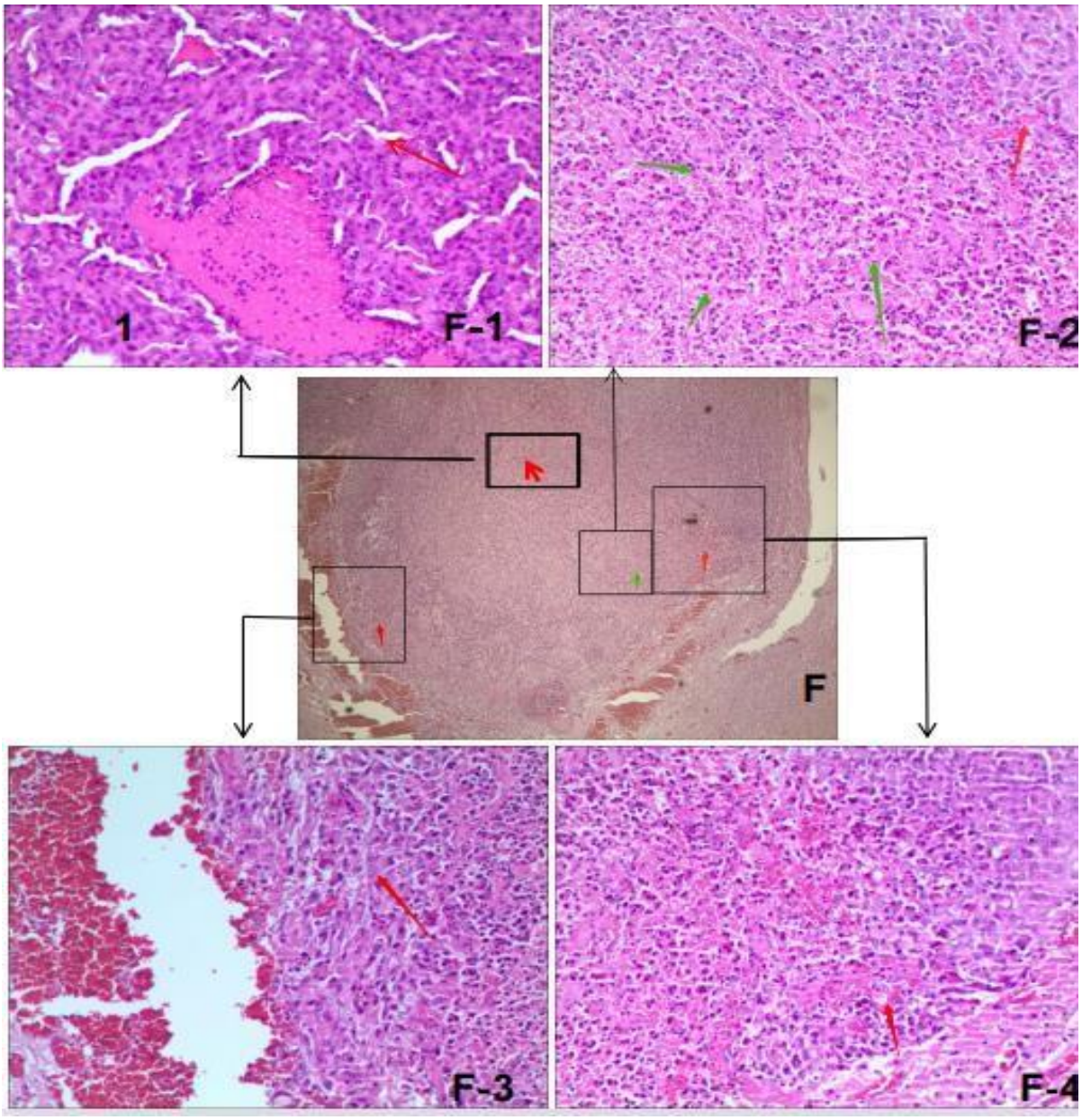

Figure 19： F: tumor morphology of TMZ drug-treated group at 40X magnification (HE staining). F-1/F-2/F-3/F-4: tumor morphology of TMZ drug-treated group at 100X magnification (HE staining). Red: tumor cells are vacuolated and cells appear sparse; green:

Further *in vivo* validation trials, combining TMZ with THP are needed to adequately validate the therapeutic potency of our drug suggestion as an additive in the context of clinical standard of care

3.2.7 Transcriptomic changes of glioma stem cells treated with THP in vitro

To measure and identify the influence of THP on the molecular level we performed RNA sequencing of the three GBM stem cells GBM1, JHH520, and NCH644. The cells were treated with THP (10 μM) for 48h before RNA extraction for non-biological repeat RNA sequencing. Very surpassingly, a total of only five genes were identified that were uniformLy differentially regulated in all three cell lines, four of them were null genes, mutant copies of genes that completely lacked that gene's normal function such as RNA or protein-coding (Figure 20). The fifth identified gene was the Cystathionine beta-synthase-like (CBSL) gene, which was a significant upregulation in all three cell lines (Figure 21). CBSL plays part in the transsulfuration pathway that is important for the elimination of L-methionine and the toxic metaboliteL-homocysteine.

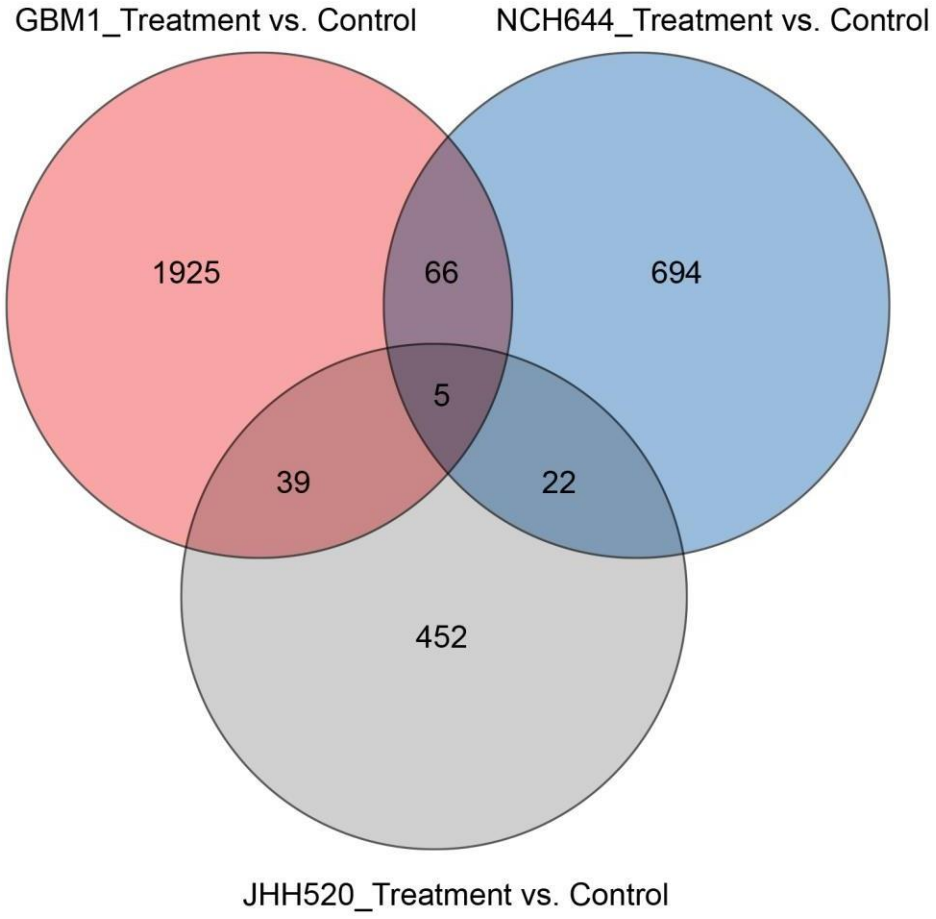

Figure 20： VENN analysis of DEGs after THP treatment 48 hours. Blue represents the GBM1. yellow represents the NCH644, green represents the JHH520.

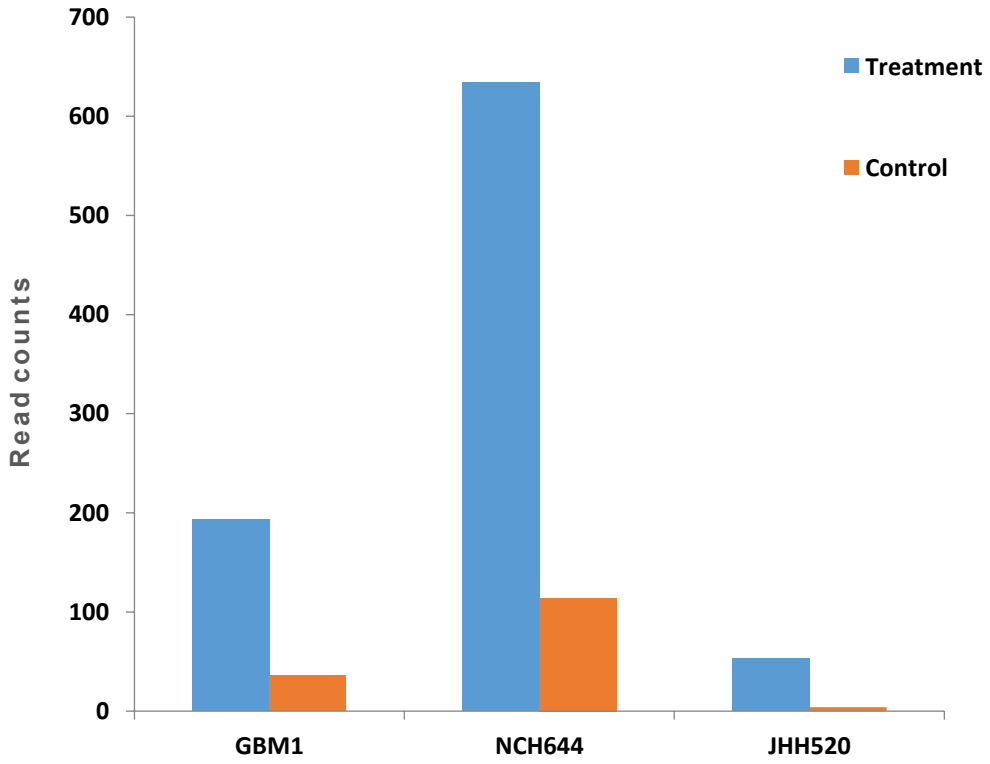

Figure 21: Gene expression of CBSL in GBM1, NCH644, and JHH520 after THP treatment 48 hours.

We next used the obtained 48h, THP treatment RNA sequencing data for a KEGG analysis. Matching the discovery to the earlier mentioned transsulfuration pathway all three cell lines showed different degrees of upregulation in pathways involved in the biosynthesis of amino acids, cysteine and methionine metabolism, and glycine, serine, and threonine metabolism (Figure 22).

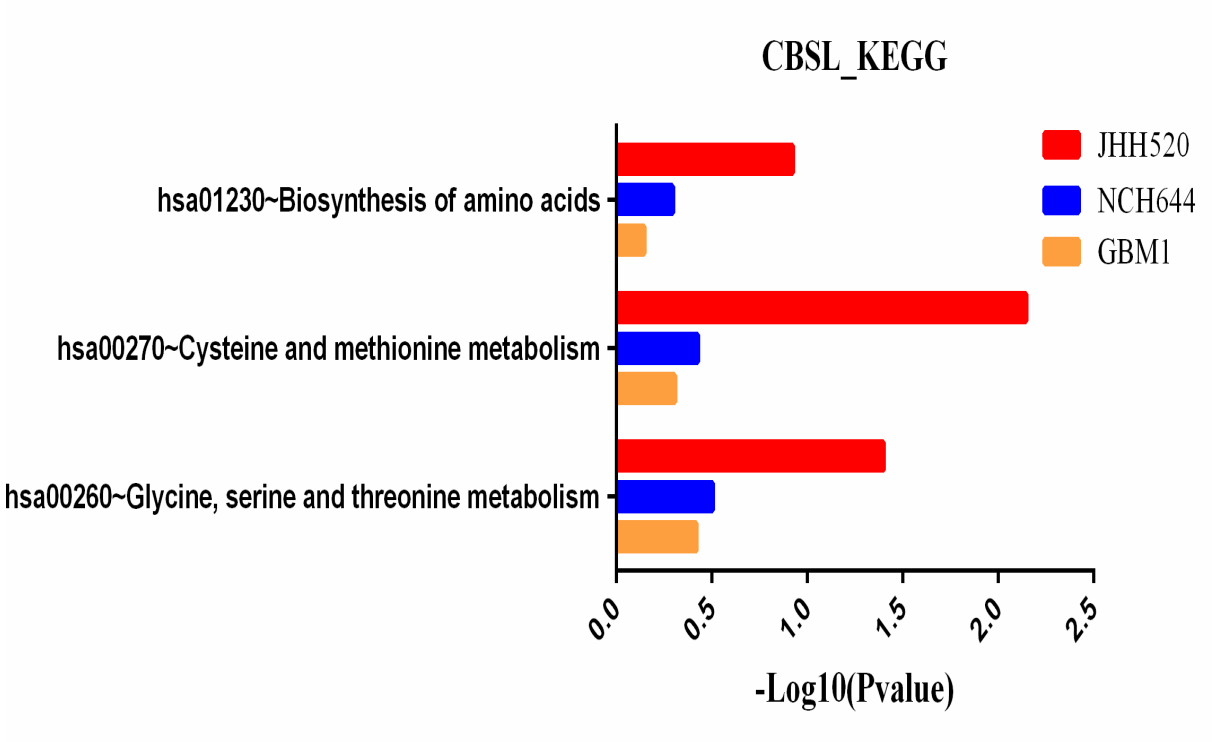

Figure 22： Pathways involved with CBSL got from KEGG enrichment analysis results after THP treatment for 48 hours. Red: JHH520. Blue: NCH644, Orange: GBM.

3.2.8 Western blot results after THP

Western blot was then used to examine the response of THP (10 μM) to CBS protein in each tumor cell line after 72h (Figure 23). The results showed that all three cell lines treated with THP showed varying degrees of up- or down-regulation after 72h, unfortunately, no significant differences were seen.

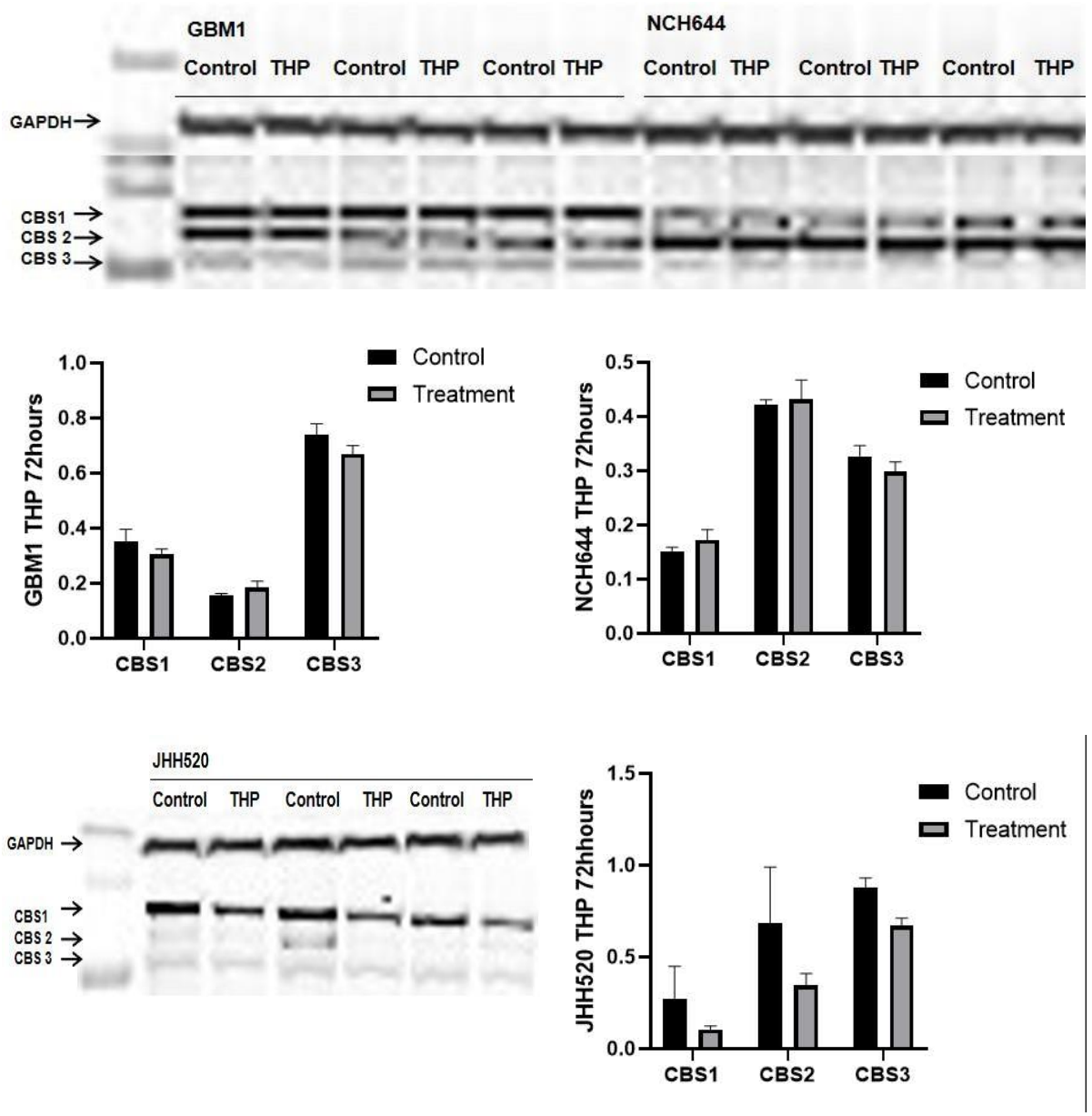

Figure 23： THP 72h western blot. THP was implemented and treatment models were established (10uM, three independent replicates) (Western Blot). The statistical test performed was a one-way ANOVA. The significance of differences between groups was described as * P <0.05.

The response of the NCH644 tumor cell line to THP (10 μM) after 48/72 hours was examined by Western blot (Figure 24). The results showed that CBS time-dependent showed varying degrees of up- or down-regulation after 48/72h. Unfortunately, no significant differences between control and treatment were detected.

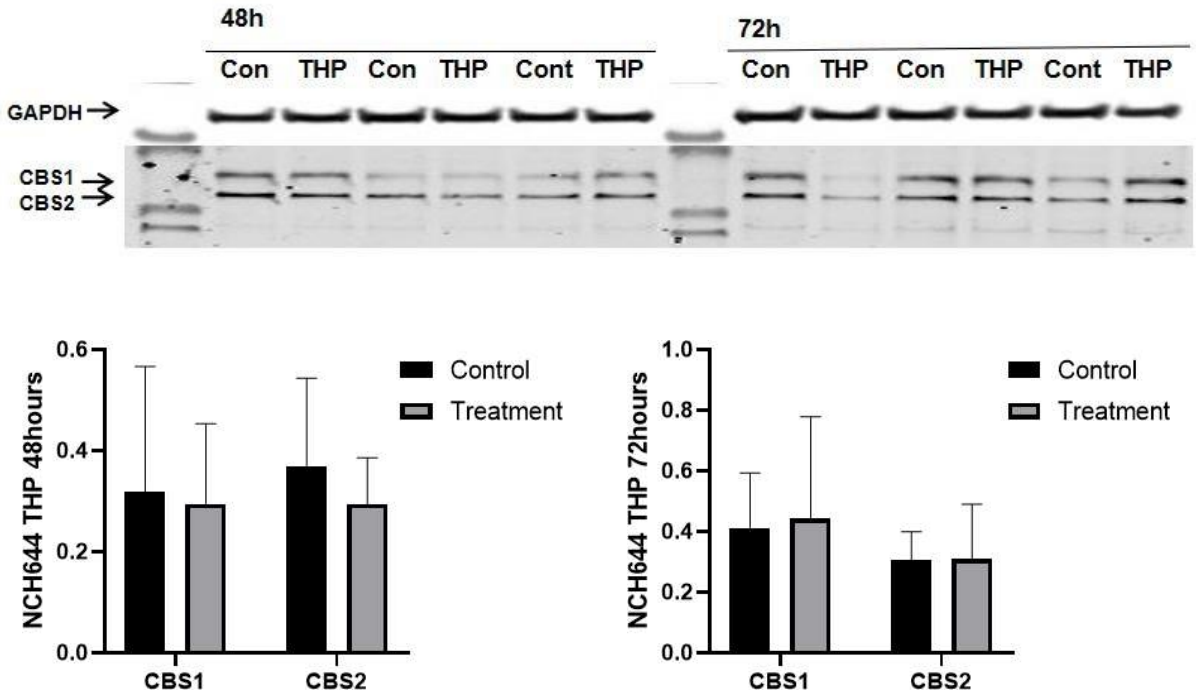

Figure 24: NCH644 THP 48h/72h Western blot. THP was implemented and treatment models were established (10 µM, three independent replicates). The statistical test performed was a one -way ANOVA. The significance of differences between groups was described as * $P < 0$.

3.2.9 Detection of persulfidated and carbonylated proteins afterTHP

We next want to determine the involvement and effect of the CBS protein during THP treatment. We therefore detected the amount of reduced, oxidized and persulfidated cysteines in NCH644 cells 48 h post THP treatment. We could not detect a decrease of the persulfated proteins in the THP treated cells (Figure 25A). However, the ration between reduced and oxidized proteins almost doubled ofter THP (Figure 25 A). We therefore performed blotting experiments with the three GBM cell lines at 48h (Figure 25B) and 72h (Figure 25C) after THP treatment to detect carbonylated proteins. In contrast to unspecified oxidation, carbonylation went down after treatment in NCH644 and JHH520 at both time points. The GBM1 cell line showed slightly elevated amounts of carbonylated proteins after 72h of THP treatment.

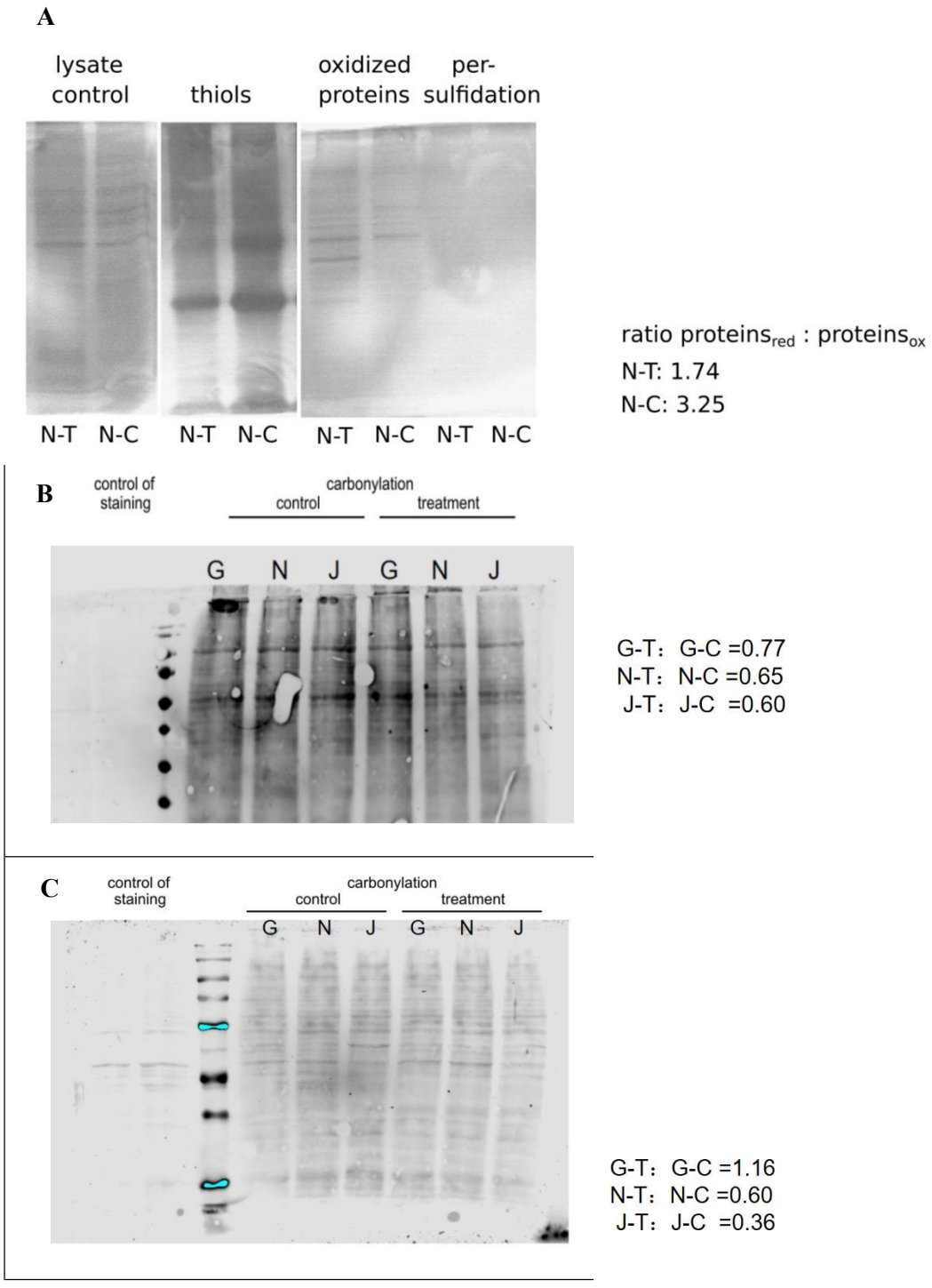

Figure 25： Detection of persulfidated or carbonylated proteins at different time points of THP treatment (A). Detection of persulfidated proteins in NCH644 48h post THP treatment. (B) Oxyblot THP 48h -GBM1/NCH644/JHH520. (C) Oxyblot THP 72h -GBM1/NCH644/JHH520. GBM1 cell line treatment group (G-T); GBM1 cell line control group (G-C)，NCH644 cell line treatment group (N-T); NCH644 cell line control group (N-C)，JHH520 cell line treatment group (J-T); JHH520 cell line control group (J-C).

3.2.10 Extracellular Matrix Gene-Based Prognostic Model for predicting the clinical course of glioblastoma patients.

Univariate Cox regression analysis found that 134 genes were positively associated with the prognosis using the CGGA dataset. 118 genes or 74 genes were found to be positively associated with prognosis in the GSE16011 or the TCGA-GBM data set, respectively. All identified genes are summarized as protective genes.

Similarly, 223 genes, 205 genes, and 211 genes were negatively correlated with prognosis in the CGGA, GSE16011, or TCGA-GBM dataset, respectively. The here identified genes are defined: as risk factors.

Lasso regression and multivariate cox regression revealed that AEBP1, F3, FLNC, IGFBP2, and LDHA were independent risk factors for patient prognosis. The ECM index was obtained by the following formula: [1.0391 × AEBP1] + [0.6346 × F3] + [0.5396 × FLNC] + [2.1276 × IGFBP2] + [2.7396 × LDHA].

The median value of the ECM index was selected to divide the patients into high and low ECM index groups. Survival analysis showed that the low ECM index group had a significantly better prognosis than the high ECM index group. The results of the external validation of the model showed that the same formula was applied to an independent data set, GSE83300, resulting in the model index. ROC analysis showed that the ECM index had a powerful ability to predict GBM survival. We calculated the link between the ECM index and the abundance of immune and stromal cell populations. The results suggested that the samples in the high index group consisted of more endothelial cells and fibroblasts.

GLM, ANN, SVM, KNN, and RF were constructed to predict the survival status of patients 6, 12, 18, 24, 30, and 36 months after the treatment.

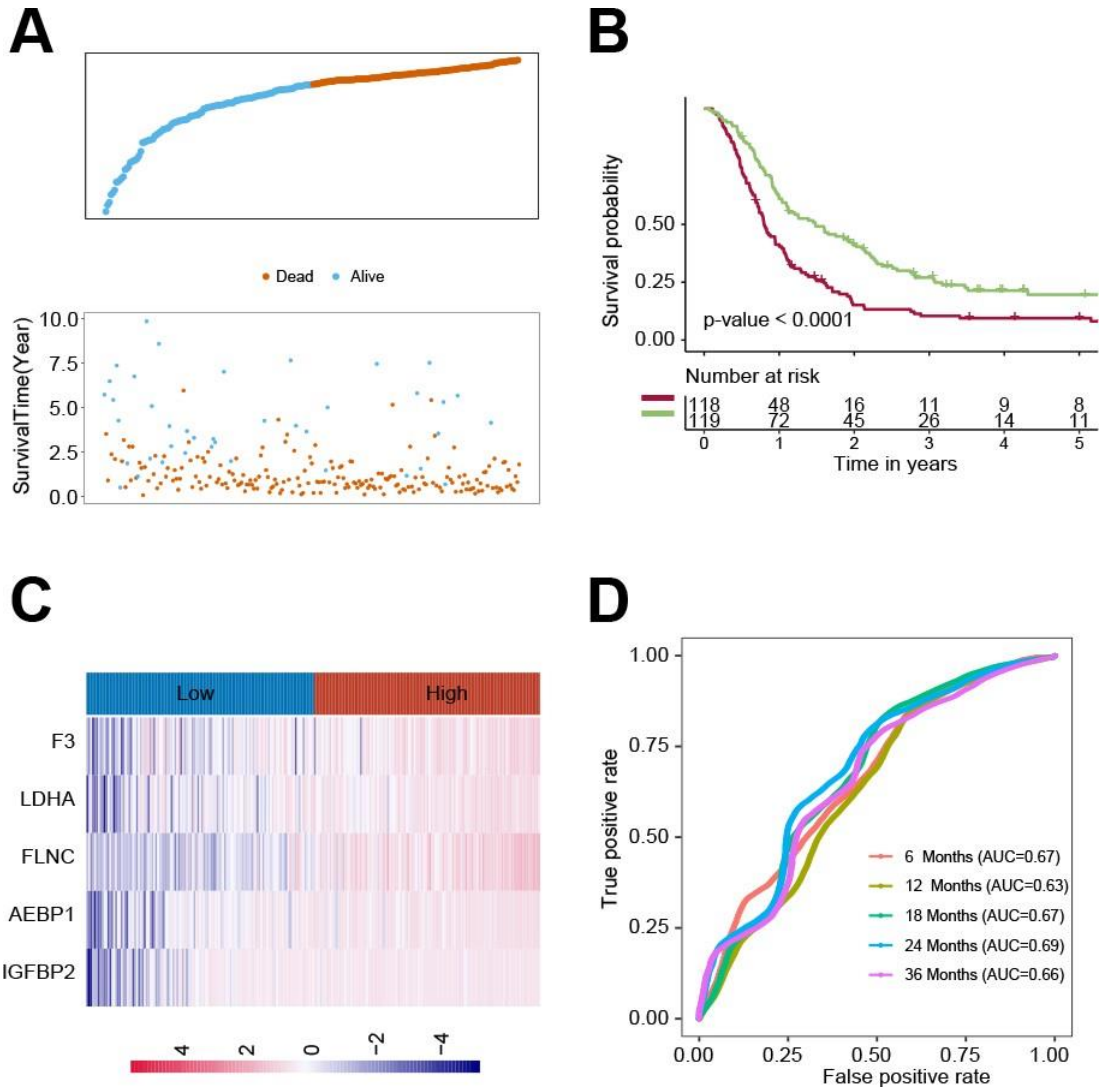

Figure 26: The construction of the ECM index in the CGGA dataset. (A) The ECM index distribution and overall survival status of GBM patients. (B) Kaplan–Meier survival curves of high and low ECM index groups. (C) The gene expression profiles of ECM genes.[122]

The result shows that high AUC values in predicting the survival status and applying it in an independent dataset, this conclusion also consist.

To assist clinical decision-making, we have developed an online tool that allows researchers to calculate the patient's prognosis by visiting the website and entering relevant gene expression levels. The online tool's URL is https://ospg.shinyapps.io/OSPG/.

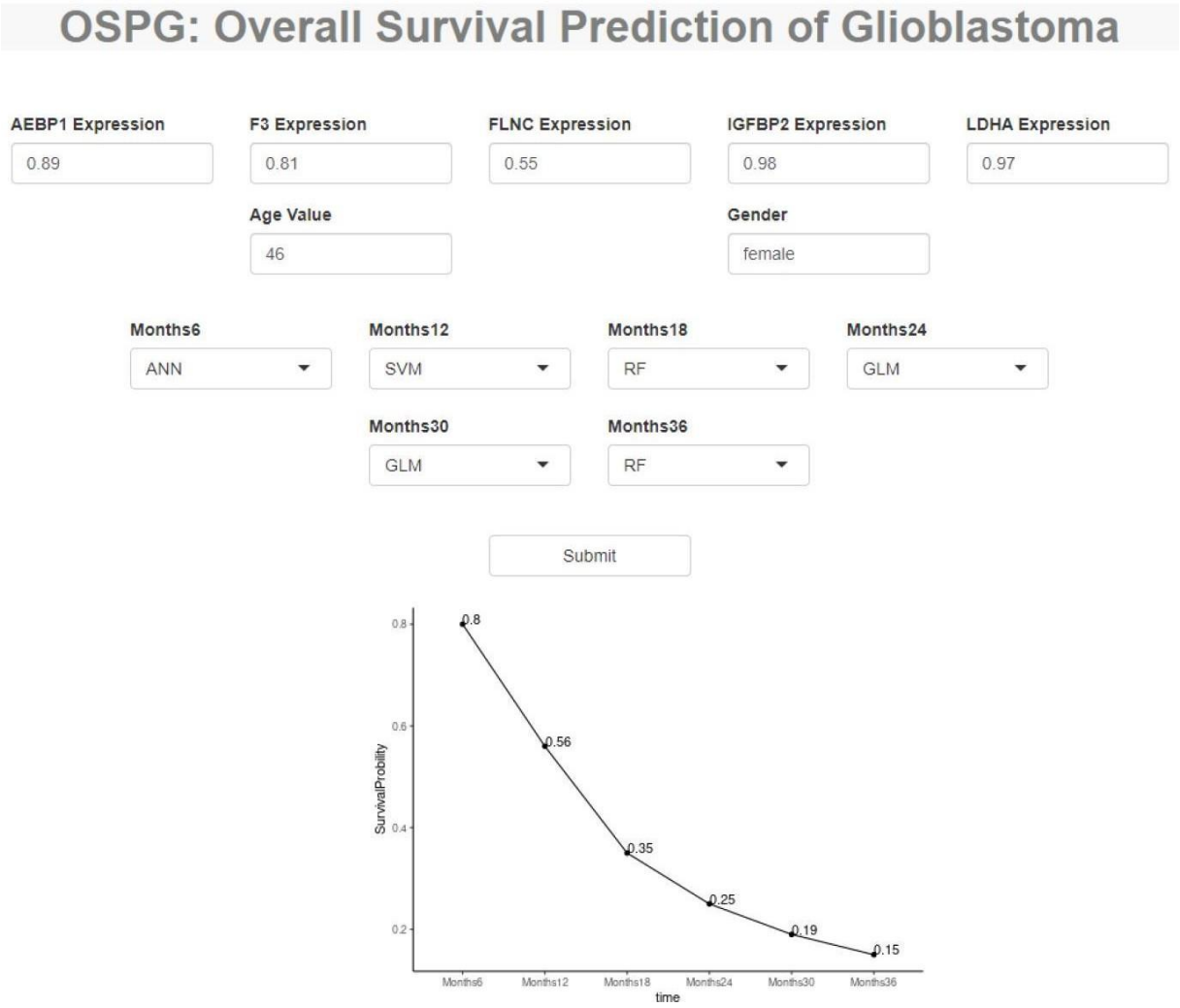

Figure 27： OSPG can be used in four steps: (1) via the website https://ospg.shinyapps.io/OSPG/, (2) inputting the values of five genes including AEBP1, F3, FLNC, IGFBP2, and LDHA (gene expression values range 0 to 1), (3) inputting the values of age and gender (ma)

The work was published as an original article in a scientific, open access journal, entitled “A Novel Extracellular Matrix Gene-Based Prognostic Model to Predict Overall Survive in Patients with Glioblastoma” in the journal “Frontiers in genetics” [122].

4 Discussion

Glioblastoma is the most common malignant primary brain tumor. Overall, the prognosis for patients with this disease is poor, with a median survival of <2 years [4]. Current GBM treatment options include surgery with concomitant radiotherapy, temozolomide therapy, and post-operative adjuvant temozolomide therapy. Another option is offered using TTFields. It provides a local low-intensity alternating electric field, which can also be adjuvant to temozolomide therapy. However, as soon as the tumor has recurred there are no conventional treatments, In such a case the modalities of treatment are surgery, radiotherapy, systemic chemotherapy or bevacizumab, nutritional support, and palliative care depending on the patient's condition [3].

All the above treatments are not very effective in prolonging the survival of GBM patients, and much less in achieving radical control of the disease. This presents us with a major challenge. There are two options: First, the mechanism of the efficacy of existing therapies needs to be further investigated and improved to achieve more targeted treatments. Second, new therapeutic agents need to be found to expand the treatment possibilities for GBM. In this thesis, I present the results studied in each of these two aspects.

4.1 TTFields

TTFields are a unique treatment modality for GBM and other solid tumors. The idea behind TTFields is based on the observation that exposure to ionizing radiation is the only potentially modifiable risk factor for human cancer [10]. Is it therefore possible to achieve a therapeutic effect by changing the electromagnetic field locally around the tumor side? This question was addressed for the first time by Kirson et al in 2004 by showing that alternating electric fields are disrupting cancer cell replication [36].

The advent of TTFields devices for local GBM treatment has confirmed this conjecture and shortly after, the FDA approved the TTFields device as adjuvant treatment for newly-diagnosed patients after completing standard-of-care surgery and chemoradiation [70]. Furthermore, the National Comprehensive Cancer Network (NCCN) added the TTFields device as an option for the treatment of newly-diagnosed GBM[32]. The device can generate an intermediate-frequency alternating electric field and on a molecular level induces a diverse range of intracellular

mechanisms, including microtubule disturbance followed by apoptosis in specific types of cancer cells with few toxic side effects.

In this project, we could verify the supportive effect of TTFields on GBM that was shown earlier by Vargas-Toscano et al [100]. We found a significant reduction in the number of tumor cells and their metabolic activity under TTFields treatment. Our results were also consistent with Moshe Giladi's experimental results. In addition, his team further confirmed that TTFields destroy the mitotic spindle through improper chromosome separation and mitotic mutations in cancer cells [123].

We suggest that the therapeutic effect TTFields on GBM is by reducing the number of cancer cells. To investigate the molecular cause of the decrease in cell number, we performed RNA sequencing. The sequencing results revealed 3 genes, NMRAL2P, AKR1C3, and SRPX2, that were significant upregulation at 48h and 72h post-TTFields. Examination of NMRAL2P, AKR1C3, and SRPX2 in TCGA revealed that NMRAL2P was a null gene and therefore excluded from this study. SRPX2 (sushi repeat-containing protein, X-linked 2), a component of the extracellular matrix, is a known prognostic biomarker in many different cancer cell lines and is associated with poor prognosis in cancer patients [124, 125].

SRPX2 upregulation is also linked to the invasiveness and migration of GBM and suggests that this gene is playing an important role in GBM metastasis through Epithelial to mesenchymal transition (EMT). Interestingly, SPRX2 is a potential downstream gene of the PI3K-Akt pathway via the regulation of both miR-192 and miR-215. Both microRNAs are targets of PI3K-Akt that can down-regulate their expression [126].

That finding is in concordance with our pathway enrichment study that revealed that the PI3K_AKT_ mTOR signaling pathway seems to be downregulated, suggesting that the down-regulation leads to increased release of the microRNAs and increased SPRX2. Furthermore, PI3K/AKT/mTOR signaling is known to modify tumor development and chemo-sensitivity by encouraging proliferation [72].

Moreover, PI3K signaling tended to increase the expression of matrix metalloproteinase (MMP), and members such as MMP2 and MMP9 were superior in promoting ECM degradation and migration and infiltration [127].

The third gene we found to be differentially expressed upon TTFields was a member of the Aldo-Keto Reductase Family, AKR1C3. AKR1C3 catalyzes both androgen and estrogen metabolism and deregulated AKR1C3 expression has been associated with multiple human cancers [128]. Furthermore, it was shown that elevated levels of AKR1C3 in esophageal cancer cells lead to radioresistance and could explain the higher expression in our cells as it may act as a rescue mechanism for the GBM cells under TTFields

[129]. This study also showed that in AKR1C3-elevated cells the oxidative stress marker (ROS) was elevated as well as DNA damage was increased. In the GBM cell line increased expression of the AKR1C gene products is also implicated in chemoresistance and cell proliferation processes [130]. Glioma patients who have high AKR1C3 expression tend to have worse clinical prognosis in terms of OS, DSS, and PFI, suggesting that AKR1C3 is closely related to patient prognosis [131].

Furthermore, we indirectly confirmed the possible involvement of AKR1C3 in the regulation of the PI3K pathway by analyzing the correlation between AKR1C3 and PTEN, a key gene in the PI3K pathway, and our results suggested that AKR1C3 was positively correlated with PTEN with a correlation of 0.252. We found that the PI3K/AKT/mTOR signaling pathway would be significantly inhibited after TTFields action in our previous HALLMARK pathway enrichment analysis. We finally speculate that TTFields may regulate the PI3K/AKT/mTOR signaling pathway by regulating AKR1C3. But this must be verified by detecting the relevant protein expression of the pathways. Our results are not in concordance with others, which suggests that PTEN is an important gene that inhibits the PI3K/AKT/mTOR signaling pathway[77].

Our RNA sequencing results revealed the opposite and showed that no significant changes were found in PTEN, while AKR1C3, which is positively correlated with PTEN, was significantly upregulated. Therefore, we speculate that TTFields inhibit the PI3K/AKT/mTOR signaling pathway by replacing PTEN with AKR1C3 to achieve cell number reduction. However, the exact mechanism of corroboration remains to be investigated.

The PI3K-pathway seems to be the connecting point between all of the identified genes but was not the only pathway that was significantly down-regulated in our HALLMARK pathway enrichment analysis. In total 12 pathways were identified, namely: MYC_Target_V1 and

MYC_Target_V2, E2F_Targets, G2M_Checkpoint, mTORC1_signaling, oxidative phosphorylation, spermatogenesis, androgen response, mitotic spindle formation, cholesterol homeostasis, DNA repair, and the above mentioned PI3K/AKT/mTOR signaling pathway.

In detail, MYC targets v1 and v2 are associated with worse survival in Estrogen-positive/HER2-negative breast cancer subtypes maybe too high mutation scores, and also in general with higher cell proliferation in cancer cells [132]. Since the MYC oncogene is known to control multiple aspects of cell regulation it was not a surprise that this pathway is detected to be deregulated in the GBM cell lines. Furthermore, almost similar deregulated pathways were detected in low-grade glioma patients, namely pathways of the G2M checkpoint, E2F targets, mitotic spindle, and Myc target v1 [133].

All pathways were increased in the high-expression KIF4A shad a negative effect on prognosis. At least E2F-target gene overexpression is correlated with a poor prognosis in cancer patients by promoting chromosome instability [134]. Of course, the mTORC1_signaling and PI3K/AKT/mTOR signaling pathways are strongly connected since signaling functions of mTOR are distributed between at least two distinct mTOR protein complexes: mTORC1 and mTORC2, which are targets for mTOR inhibitors such as rapamycin [135].

This pathway is highly analyzed in the field of brain cancer. A connection between oxidative phosphorylation, DNA repair, and androgen response pathway could be established via AKR1C3 and the PI3K/AKT/mTOR pathway. AKR1C enzymes constitute a family of oxidoreductases that catalyze NADPH-dependent reduction of a wide variety of substrates and was shown to regulate ligand occupancy and trans-activation of androgen-, estrogen- and progesterone receptors in certain cancer types [136, 137].

The detection of the involvement of the genes involved in the mitotic spindle formation was expected since this is the main mode of action of TTFields, the disruption of the normal assembly of spindle microtubules. The major mechanism in how all these pathways act together in the event of TTFields treatment has still to be revealed. However, taken together for this part of the thesis, I have shown that the in-vitro system is suitable to study the TTFields effect on suspension in vitro models, in this case specifically for brain tumor stem cells grown in neurosphere media. To the best of our knowledge, there is little evidence published on these aspects. Secondly, we show evidence that TTFields impair the growth and survival of stem cell fraction of GBM, across all molecular subtypes of the tumor. In the wake of personalized medicine and

the use of molecular signatures of tumor tissue in nowadays-routine clinical neuropathological diagnostics, we believe this might support the application of this research also in the future for a variety of glioma patients.

We notice that more frequently brain tumor patients become a case in molecular tumor boards, to find the most suitable treatment option for each patient. TTFields might be a general therapy for all subtypes. It remains to be investigated if combination therapy, modulating the activity of the identified putative downstream signal mediators of TTFields are therapeutic relevant, or if the changes in expression of the described networks can be confirmed in more preclinical models of the disease, such as more cell models or in an animal model. The company Novocure also provides a TTFields application device to be used on mice, termed inovivo^{TM} system. Ide- ally, tumor specimens of patients that have been treated with TTFields should be studied, i.e. retrieved from biopsy / resection material from tumor recurrences.

4.2 Trihexyphenidyl

The blood-brain barrier is a protective membrane responsible for brain homeostasis and pre- venting most antibodies, proteins, peptides, and small molecules from crossing the BBB into the bloodstream [20]. Due to the presence of the blood-brain barrier, many drugs are unable to lead to effective treatments for intracranial tumors such as glioblastoma [21]. Given the still devastating clinical outcome of the current standard of care, this imposes a very high demand for new pharmacological mediated interventions for treating this disease. My colleagues in pre- vious studies have found that THP, an ACh receptor antagonist used in the symptomatic treat- ment of Parkinson's disease, can inhibit the growth of GBM [100].

Partly considered as a confirmatory study, we now wanted to replicate and validate this finding in a larger number of biological models in addition to pinpointing some aspects of its mecha- nism of action on brain cancer cells.

We delivered strong evidence that this therapy might be followed up as a clinical trial. Both *in vitro* and *in vivo* experiments showed that THP had an inhibitory effect

on GBM cell amplifi- cation. Importantly, based on our in vitro results, likewise, as TTFields, THP acts similarly potent on tumor models from different molecular subtypes, although our tested collection of biological models is rather small and needs further validation with increased sample size.

To further investigate the mechanism of GBM cell reduction, we performed Ki67 staining to detect a change in cell proliferation as well as analyzed the cell cycle and the occurrence of apoptotic cells. Indeed, we could indicate that the decrease in cell numbers was associated with apoptosis. But we could not connect THP treatment to changes in the cell cycle changes. The experimental results suggest that THP may achieve therapeutic effects by inhibiting the proliferation of GBM cells and promoting the apoptosis of GBM cells. As we used stem cell models of the disease, the results of apoptosis induction are particularly promising, as those cells are usually very resistant to treatments[138], as we have shown in various tests before testing the resistance of the same models as used in this trial to exposure to a standard of care therapy (TMZ and radiation therapy)[139].

To further analyze the effects of the molecular level mRNA sequencing on the RNA extracts of the cells under THP treatment vs. control intervention was performed and we identified only a total of five significantly changed genes (all upregulated) uniformly presented in all three cell lines. Four of these genes were null genes, therefore we focused on the gene encoding cystathionine beta-synthase (CBS). This gene acts as a homotetramer to catalyze the conversion of homocysteine to cystathionine, the first step in the transsulfuration pathway. CBS may function to either promote or suppress tumor growth, depending on the cancer cell type[110].

Previous studies have shown that CBS promotes lymph node metastasis in gallbladder adenocarcinomas and squamous cell/ adenosquamous carcinoma [140]. Liu Ya et al found that the expression of CBS was significantly upregulated in ESCC and positively related to TNM stage and lymph node metastasis. They found that CBS could promote tumor cell growth and proliferation to increase the aggressiveness of ESCC cells [141]. In the brain, CBS is expressed by glia and astrocytes[108], which are the cells from which gliomas arise. Neural stem cells also express CBS and the addition of the substrate L-cysteine to culture media stimulated the in vitro differentiation of neural stem cells to neurons and astroglia, whereas knockdown of CBS expression by small interfering RNA suppressed L-cysteine-induced stem cell differentiation [109].

The results of Naoharu Takano's study showed that reduced CBS expression in gliomas increased HIF-2α protein levels and HIF-2 target gene expression, thereby promoting the formation of glioma tumors [110]. Our experimental results demonstrate the role of CBS in GBM in the opposite direction. And it further suggests that CBS genes have a central role in the

development of GBM. Further studies, applying laboratory assays that test CBS on protein level or enzymatic function were applied but did not show a clear picture for confirming the findings on transcript level. We believe that this might be due to the relatively long half-life of the protein in this cell under normoxic conditions. Further studies with cells that survive a long-term treatment with THP might allow further insights. It would be interesting to establish genetic models with CBS overexpression or CBS suppression or even gene knock-out, to validate the relevance of CBS activity for mediating therapeutic effects of THP treatment in GBM.

The fact that we did not notice a clear dysregulation of the putative target of THP indicates the drug effects are based on off-target effects. This goes well in line with the hitherto plethora of described mode of actions of this substance in different diseases. Nevertheless, even if we cannot validate the target specificity at this point, the presented data further adds to the growing body of evidence that using neurotransmitter targeting agents might be particular attractive route for developing new cancer therapies. Not only limited to the central nervous system, but it is also known that microenvironment of many solid cancers is in part composed my nerve structures. Recent discoveries of direct cell-to-cell interactions of cancer cells with neurons, such as through synaptic-like structures termed tumor microtubes, showed that these nerve structure inputs have pronounced effects on cancer survival and progression, possibly also mediating resistance to therapy and evasion of host immune surveillance[142].

In a larger picture, the results on THP are associated with somewhat Cancer Neuroscience field, considered one of the most understudied and innovative cancer research areas of the moment. The prognosis of GBM is very poor; only about 5% of patients survive more than 5 years, and it is critical to identify possible biomarkers to predict the prognosis of GBM. In this study, we determined five prognostic ECM genes were used to calculate the ECM index, and a machine learning model was further constructed to predict the survival of GBM patients at 6, 12, 18, 24, 30 and 36 months after treatment situation. To promote the clinical application of the model, we also provide a web server to guide clinical decision-making.

Although this work is solely based on correlative data and presents data mining results, we hypothesize that those results are of help to deliver improve future patient stratification. Tumor patients, suffering from a particularly aggressive subtype of the tumor – featuring a prediction of the super short remaining of their life - might be particularly welcoming to test new treatment interventions that are not yet approved or even tested in humans for treating the disease they

are suffering from. Correlating to the wet-lab results in this thesis, this means that particular negative prognostic overall delivered by ECM gene expression signature might suggest applying THP/TTF therapy as an addition to the standard of care. Of note, verifying any additive or synergistic effects of the THP intervention with such standard of care therapy needs to be tested in experimental models, before execution of *first-in-man* trials.

5 References

1. Furnari, F.B., et al., *Malignant astrocytic glioma: genetics, biology, and paths to treatment.* Genes & development, 2007. **21**(21): p. 2683-2710.
2. Liu, S., et al., *Progress and prospect in tumor treating fields treatment of glioblastoma.* Biomedicine & Pharmacotherapy, 2021. **141**: p. 111810.
3. Ostrom, Q.T., et al., *CBTRUS statistical report: primary brain and other central nervous system tumors diagnosed in the United States in 2012–2016.* Neuro-oncology, 2019. **21**(Supplement_5): p. v1-v100.
4. Tan, A.C., et al., *Management of glioblastoma: State of the art and future directions.* CA: a cancer journal for clinicians, 2020. **70**(4): p. 299-312.
5. Louis, D.N., et al., *The 2016 World Health Organization classification of tu- mors of the central nervous system: a summary.* Acta neuropathologica, 2016. **131**(6): p. 803-820.
6. Huse, J.T., E. Holland, and L.M. DeAngelis, *Glioblastoma: molecular analysis and clinical implications.* Annual review of medicine, 2013. **64**: p. 59-70.
7. Kalkan, R., *Glioblastoma stem cells as a new therapeutic target for glioblas- toma.* Clinical Medicine Insights: Oncology, 2015. **9**: p. CMO. S30271.
8. Cruceru, M.L., et al., *Therapy targets in glioblastoma and cancer stem cells: lessons from haematopoietic neoplasms.* Journal of Cellular and Molecular Medicine, 2013. **17**(10): p. 1218-1235.
9. Mellinghoff, I.K., et al., *Molecular determinants of the response of glioblasto- mas to EGFR kinase inhibitors.* New England Journal of Medicine, 2005. **353**(19): p. 2012-2024.
10. Fisher, J.L., et al., *Epidemiology of brain tumors.* Neurologic clinics, 2007. **25**(4): p. 867-890.
11. Amirian, E.S., et al., *Approaching a scientific consensus on the association between allergies and glioma risk: a report from the glioma international case- control study.* Cancer Epidemiology and Prevention Biomarkers, 2016. **25**(2): p. 282-290.
12. Scheurer, M.E., et al., *Familial aggregation of glioma: a pooled analysis.* American journal of epidemiology, 2010. **172**(10): p. 1099-1107.
13. Vienne-Jumeau, A., C. Tafani, and D. Ricard, *Environmental risk factors of pri- mary brain tumors: A review.* Revue neurologique, 2019. **175**(10): p. 664-678.
14. Galldiks, N., et al., *The use of amino acid PET and conventional MRI for moni- toring of brain tumor therapy.* NeuroImage: Clinical, 2017. **13**: p. 386-394.
15. Molinaro, A.M., et al., *Association of maximal extent of resection of contrast-enhanced and non–contrast-enhanced tumor with survival within molecular subgroups of patients with newly diagnosed glioblastoma.* JAMA oncology, 2020. **6**(4): p. 495-503.
16. Stummer, W., et al., *Fluorescence-guided surgery with 5-aminolevulinic acid for resection of malignant glioma: a randomised controlled multicentre phase III trial.* The lancet oncology, 2006. **7**(5): p. 392-401.
17. Eigenbrod, S., et al., *Molecular stereotactic biopsy technique improves diag- nostic accuracy and enables personalized treatment strategies in glioma pa- tients.* Acta neurochirurgica, 2014. **156**(8): p. 1427-1440.

18. Stupp, R., et al., *Effects of radiotherapy with concomitant and adjuvant te- mozolomide versus radiotherapy alone on survival in glioblastoma in a ran- domised phase III study: 5-year analysis of the EORTC-NCIC trial.* The lancet oncology, 2009. **10**(5): p. 459-466.
19. Chakravarti, A., et al., *Temozolomide-mediated radiation enhancement in glio- blastoma: a report on underlying mechanisms.* Clinical Cancer Research, 2006. **12**(15): p. 4738-4746.
20. Zhou, Y., et al., *Crossing the blood-brain barrier with nanoparticles.* Journal of controlled release, 2018. **270**: p. 290-303.
21. Pardridge, W.M., *Drug transport across the blood–brain barrier.* Journal of cer- ebral blood flow & metabolism, 2012. **32**(11): p. 1959-1972.
22. Wild-Bode, C., et al., *Sublethal irradiation promotes migration and invasive- ness of glioma cells: implications for radiotherapy of human glioblastoma.* Cancer research, 2001. **61**(6): p. 2744-2750.
23. Wick, W., et al., *Prevention of irradiation-induced glioma cell invasion by te- mozolomide involves caspase 3 activity and cleavage of focal adhesion ki- nase.* Cancer Research, 2002. **62**(6): p. 1915-1919.
24. Djedid, R., et al., *Combining bevacizumab with temozolomide increases the antitumor efficacy of temozolomide in human glioblastoma preclinical models.* 2009. **72**(5): p. 1.
25. Katayama, et al., *DNA damaging agent-induced autophagy produces a cyto- protective adenosine triphosphate surge in malignant glioma cells.* Cell Death & Differentiation, 2007.
26. Roos, W., et al., *Apoptosis in malignant glioma cells triggered by the te- mozolomide-induced DNA lesion O6-methylguanine.* Oncogene, 2007. **26**(2): p. 186-197.
27. Lefranc, F., J. Brotchi, and R. Kiss, *Possible future issues in the treatment of glioblastomas: special emphasis on cell migration and the resistance of mi- grating glioblastoma cells to apoptosis.* Journal of clinical oncology, 2005. **23**(10): p. 2411-2422.
28. Lefranc, F., V. Facchini, and R. Kiss, *Proautophagic drugs: a novel means to combat apoptosis-resistant cancers, with a special emphasis on glioblasto- mas.* The oncologist, 2007. **12**(12): p. 1395-1403.
29. Blough, M.D., M.C. Zlatescu, and J.G. Cairncross, *O6-methylguanine-DNA methyltransferase regulation by p53 in astrocytic cells.* Cancer research, 2007. **67**(2): p. 580-584.
30. Trivedi, R.N., et al., *The role of base excision repair in the sensitivity and re- sistance to temozolomide-mediated cell death.* Cancer research, 2005. **65**(14): p. 6394-6400.
31. Friedman, H.S., et al., *Methylator resistance mediated by mismatch repair de- ficiency in a glioblastoma multiforme xenograft.* Cancer research, 1997. **57**(14): p. 2933-2936.
32. Fabian, D., et al., *Treatment of glioblastoma (GBM) with the addition of tumor-treating fields (TTF): a review.* Cancers, 2019. **11**(2): p. 174.
33. Stupp, R., et al., *Effect of tumor-treating fields plus maintenance te- mozolomide vs maintenance temozolomide alone on survival in patients with glioblastoma: a randomized clinical trial.* Jama, 2017. **318**(23): p. 2306-2316.

34. Kirson, E.D., et al., *Alternating electric fields arrest cell proliferation in animal tumor models and human brain tumors.* Proceedings of the National Academy of Sciences, 2007. **104**(24): p. 10152-10157.
35. Pless, M. and U. Weinberg, *Tumor treating fields: concept, evidence and fu- ture.* Expert opinion on investigational drugs, 2011. **20**(8): p. 1099-1106.
36. Kirson, E.D., et al., *Disruption of cancer cell replication by alternating electric fields.* Cancer research, 2004. **64**(9): p. 3288-3295.
37. Wu, P., et al., *Integrated genomic analysis identifies clinically relevant sub- types of renal clear cell carcinoma.* BMC cancer, 2018. **18**(1): p. 1-9.
38. Capper, D., et al., *DNA methylation-based classification of central nervous system tumours.* Nature, 2018. **555**(7697): p. 469-474.
39. Nickel, A., et al., *Longitudinal stability of molecular alterations and drug re- sponse profiles in tumor spheroid cell lines enables reproducible analyses.* Bi- omedicine & Pharmacotherapy, 2021. **144**: p. 112278.
40. Kirson, E.D., et al., *Alternating electric fields (TTFields) inhibit metastatic spread of solid tumors to the lungs.* Clinical & experimental metastasis, 2009. **26**(7): p. 633-640.
41. Pless, M., et al., *A phase I/II trial of Tumor Treating Fields (TTFields) therapy in combination with pemetrexed for advanced non-small cell lung cancer.* Lung cancer, 2013. **81**(3): p. 445-450.
42. Schneiderman, R.S., et al., *TTFields alone and in combination with chemo-therapeutic agents effectively reduce the viability of MDR cell sub-lines that over-express ABC transporters.* BMC cancer, 2010. **10**(1): p. 1-7.
43. Choe, K., *Analysis of RTOG-RPA Scores in the Phase 3 EF-14 Trial of Tumor Treating Fields with Temozolomide (TTFields/TMZ) Versus TMZ Alone in Newly Diagnosed Glioblastoma.* International Journal of Radiation Oncology, Biology, Physics, 2018. **102**(3): p. S48.
44. Odia, Y. and F. Iwamoto, *ATIM-08. TRIAL IN PROGRESS: CA209-9Y8 PHASE 2 TRIAL OF TUMOR TREATING FIELDS (TTFS), NIVOLUMAB PLUS/MINUS IPILIMUMAB FOR BEVACIZUMAB-NAÏVE, RECURRENT GLI- OBLASTOMA.* Neuro-Oncology, 2019. **21**(Suppl 6): p. vi3.
45. Mehta, M., et al., *Critical review of the addition of tumor treating fields (TTFields) to the existing standard of care for newly diagnosed glioblastoma patients.* Critical reviews in oncology/hematology, 2017. **111**: p. 60-65.
46. Halasz, L.M. and T. Mitin, *Tumor-treating fields: answering the concern about quality of life.* JAMA oncology, 2018. **4**(4): p. 504-505.
47. Clague, D. and E. Wheeler, *Dielectrophoretic manipulation of macromole- cules: The electric field.* Physical review E, 2001. **64**(2): p. 026605.
48. Gonzalez, C.F. and V.T. Remcho, *Harnessing dielectric forces for separations of cells, fine particles and macromolecules.* Journal of Chromatography A, 2005. **1079**(1-2): p. 59-68.
49. Gera, N., et al., *Tumor treating fields perturb the localization of septins and cause aberrant mitotic exit.* PloS one, 2015. **10**(5): p. e0125269.
50. Stingele, S., et al., *Global analysis of genome, transcriptome and proteome re- veals the response to aneuploidy in human cells.* Molecular systems biology, 2012. **8**(1): p. 608.
51. Lee, Y.-J., et al., *5-Fluorouracil as a tumor-treating field-sensitizer in colon cancer therapy.* Cancers, 2019. **11**(12): p. 1999.

52. Hönscheid, P., K. Datta, and M.H. Muders, *Autophagy: detection, regulation and its role in cancer and therapy response.* International journal of radiation biology, 2014. **90**(8): p. 628-635.
53. Voloshin, T., et al., *Alternating electric fields (TTFields) in combination with paclitaxel are therapeutically effective against ovarian cancer cells in vitro and in vivo.* International journal of cancer, 2016. **139**(12): p. 2850-2858.
54. Giladi, M., et al., *Tumor treating fields (TTFields) delay DNA damage repair following radiation treatment of glioma cells.* Radiation Oncology, 2017. **12**(1): p. 1-13.
55. Carrieri, F.A., et al., *Tumor treating fields: at the crossroads between physics and biology for cancer treatment.* Frontiers in oncology, 2020: p. 1991.
56. Zhao, W., et al., *The BRCA tumor suppressor network in chromosome dam- age repair by homologous recombination.* Annual review of biochemistry, 2019. **88**: p. 221-245.
57. Karanam, N.K., et al., *Tumor-treating fields elicit a conditional vulnerability to ionizing radiation via the downregulation of BRCA1 signaling and reduced DNA double-strand break repair capacity in non-small cell lung cancer cell lines.* Cell death & disease, 2017. **8**(3): p. e2711-e2711.
58. Thiery, J.P., et al., *Epithelial-mesenchymal transitions in development and dis- ease.* cell, 2009. **139**(5): p. 871-890.
59. Weller, M., et al., *Glioma.* Nature reviews Disease primers, 2015. **1**(1): p. 1-18.
60. Voloshin, T., et al., *Tumor Treating Fields (TTFields) Hinder Cancer Cell Motil- ity through Regulation of Microtubule and Actin Dynamics.* Cancers, 2020. **12**(10): p. 3016.
61. Li, X., F. Yang, and B. Rubinsky, *A theoretical study on the biophysical mech- anisms by which tumor treating fields affect tumor cells during mitosis.* IEEE Transactions on Biomedical Engineering, 2020. **67**(9): p. 2594-2602.
62. Quail, D.F. and J.A. Joyce, *The microenvironmental landscape of brain tu- mors.* Cancer cell, 2017. **31**(3): p. 326-341.
63. Dai, S., et al., *The PD-1/PD-Ls pathway and autoimmune diseases.* Cellular immunology, 2014. **290**(1): p. 72-79.
64. Voloshin, T., et al., *Tumor-treating fields (TTFields) induce immunogenic cell death resulting in enhanced antitumor efficacy when combined with anti-PD-1 therapy.* Cancer Immunology, Immunotherapy, 2020. **69**(7): p. 1191-1204.
65. Chang, E., et al., *Tumor treating fields increases membrane permeability in gli- oblastoma cells.* Cell death discovery, 2018. **4**(1): p. 1-13.
66. Kessler, A., et al., *Blood brain barrier (BBB) integrity is affected by tumor treat- ing fields (TTFields) in vitro and in vivo.* International Journal of Radiation On- cology, Biology, Physics, 2019. **105**(1): p. S162-S163.
67. Chang, E., et al., *Combining the glioblastoma cell membrane-permeabilizing effect of tumor treating fields with chemotherapy*. 2020, AACR.
68. Christofk, H.R., et al., *The M2 splice isoform of pyruvate kinase is important for cancer metabolism and tumour growth.* Nature, 2008. **452**(7184): p. 230- 233.
69. Patel, C.B., et al., *Tumor treating fields (TTFields) impairs aberrant glycolysis in glioblastoma as evaluated by [18F] DASA-23, a non-invasive probe of py- ruvate kinase M2 (PKM2) expression.* Neoplasia, 2021. **23**(1): p. 58-67.

70. Hong, P., et al., *Tumor treating fields: a comprehensive overview of the under- lying molecular mechanism.* Expert review of molecular diagnostics, 2021: p. 1-10.
71. Monson, C., et al., *BIOM-41. Genetic markers correlated with progression-free survival times in glioblastoma patients undergoing treatment with tumor treat- ing fields.* Neuro-Oncology, 2020. **22**(Suppl 2): p. ii10.
72. Gao, N., et al., *Role of PI3K/AKT/mTOR signaling in the cell cycle progression of human prostate cancer.* Biochemical and biophysical research communica- tions, 2003. **310**(4): p. 1124-1132.
73. Ersahin, T., N. Tuncbag, and R. Cetin-Atalay, *The PI3K/AKT/mTOR interactive pathway.* Molecular BioSystems, 2015. **11**(7): p. 1946-1954.
74. Liu, X., et al., *PI3K in cancer: its structure, activation modes and role in shap- ing tumor microenvironment.* Future Oncology, 2018. **14**(7): p. 665-674.
75. Guo, H., et al., *The PI3K/AKT pathway and renal cell carcinoma.* Journal of genetics and genomics, 2015. **42**(7): p. 343-353.
76. Fan, W., et al., *Elevated levels of p-Mnk1, p-eIF4E and p-p70S6K proteins are associated with tumor recurrence and poor prognosis in astrocytomas.* Journal of neuro-oncology, 2017. **131**(3): p. 485-493.
77. Malek, M., et al., *PTEN regulates PI (3, 4) P2 signaling downstream of class I PI3K.* Molecular cell, 2017. **68**(3): p. 566-580. e10.
78. Li, A., et al., *PTEN, insulin resistance and cancer.* Current Pharmaceutical De- sign, 2017. **23**(25): p. 3667-3676.
79. Manning, B.D. and A. Toker, *AKT/PKB signaling: navigating the network.* Cell, 2017. **169**(3): p. 381-405.
80. Akhmetzyanova, E., et al., *Different approaches to modulation of microglia phenotypes after spinal cord injury.* Frontiers in systems neuroscience, 2019: p. 37.
81. Kim, Y.C. and K.-L. Guan, *mTOR: a pharmacologic target for autophagy regu- lation.* The Journal of clinical investigation, 2015. **125**(1): p. 25-32.
82. Polchi, A., et al., *mTOR signaling and neural stem cells: The tuberous sclero- sis complex model.* International journal of molecular sciences, 2018. **19**(5): p. 1474.
83. Mecca, C., et al., *Targeting mTOR in glioblastoma: rationale and preclini- cal/clinical evidence.* Disease Markers, 2018. **2018**.
84. Li, J., et al., *A network‐based analysis for mining the risk pathways in glioblas- toma.* Oncology Letters, 2019. **18**(3): p. 2712-2717.
85. Wick, W., et al., *Phase II study of radiotherapy and temsirolimus versus radi- ochemotherapy with temozolomide in patients with newly diagnosed glioblas- toma without MGMT promoter hypermethylation (EORTC 26082).* Clinical can- cer research, 2016. **22**(19): p. 4797-4806.
86. Jez, J.M., T.G. Flynn, and T.M. Penning, *A new nomenclature for the aldo- keto reductase superfamily.* Biochemical pharmacology, 1997. **54**(6): p. 639- 647.
87. Zhong, T., et al., *Aldo-keto reductase 1C3 (AKR1C3) is associated with the doxorubicin resistance in human breast cancer via PTEN loss.* Biomedicine & Pharmacotherapy, 2015. **69**: p. 317-325.

88. Ragel, B.T., et al., *Identification of hypoxia-induced genes in a malignant gli- oma cell line (U-251) by cDNA microarray analysis.* Neurosurgical review, 2007. **30**(3): p. 181-187.
89. Novotna, R., et al., *Inactivation of the anticancer drugs doxorubicin and oracin by aldo–keto reductase (AKR) 1C3.* Toxicology letters, 2008. **181**(1): p. 1-6.
90. Liu, C., et al., *Intracrine androgens and AKR1C3 activation confer resistance to enzalutamide in prostate cancer.* Cancer research, 2015. **75**(7): p. 1413- 1422.
91. Liu, Y., et al., *Overview of AKR1C3: Inhibitor achievements and disease in- sights.* Journal of medicinal chemistry, 2020. **63**(20): p. 11305-11329.
92. Orayj, K. and E. Lane, *Patterns and determinants of prescribing for Parkin- son's disease: a systematic literature review.* Parkinson's Disease, 2019. **2019**.
93. Brocks, D.R., *Anticholinergic drugs used in Parkinson's disease: An over- looked class of drugs from a pharmacokinetic perspective.* J Pharm Pharm Sci, 1999. **2**(2): p. 39-46.
94. Romeo, D.M., et al., *Treatment of dystonia using trihexyphenidyl in Costello syndrome.* Brain sciences, 2020. **10**(7): p. 450.
95. Surathi, P., et al., *Prescribing pattern for Parkinson's disease in Indian com- munity before referral to tertiary center.* Canadian Journal of Neurological Sci- ences, 2017. **44**(6): p. 705-710.
96. Chiappini, S., et al., *Misuse of Anticholinergic Medications: A Systematic Re- view.* Biomedicines, 2022. **10**(2): p. 355.
97. Harvey, A.R., et al., *Trihexyphenidyl for dystonia in cerebral palsy.* Cochrane Database of Systematic Reviews, 2018(5).
98. Torrents, R., et al., *Misuse of Trihexyphenidyl (Artane) on Réunion Island.* Journal of Clinical Psychopharmacology, 2018. **38**(3): p. 250-253.
99. Ji, B.-S. and Y. Gao, *Protective effect of trihexyphenidyl on hydrogen perox- ide-induced oxidative damage in PC12 cells.* Neuroscience letters, 2008. **437**(1): p. 50-54.
100. Vargas-Toscano, A., et al., *Robot technology identifies a Parkinsonian thera- peutics repurpose to target stem cells of glioblastoma.* CNS oncology, 2020. **9**(2): p. CNS58.
101. Venkataramani, V., et al., *Glutamatergic synaptic input to glioma cells drives brain tumour progression.* Nature, 2019. **573**(7775): p. 532-538.
102. Monje, M., *Synaptic communication in brain cancer.* Cancer research, 2020. **80**(14): p. 2979-2982.
103. Monje, M., et al., *Roadmap for the emerging field of cancer neuroscience.* Cell, 2020. **181**(2): p. 219-222.
104. Thompson, E.G. and H. Sontheimer, *Acetylcholine receptor activation as a modulator of glioblastoma invasion.* Cells, 2019. **8**(10): p. 1203.
105. Kajimura, M., et al., *Interactions of multiple gas-transducing systems: hall- marks and uncertainties of CO, NO, and H2S gas biology.* Antioxidants & re- dox signaling, 2010. **13**(2): p. 157-192.
106. Watanabe, M., et al., *Mice deficient in cystathionine beta-synthase: animal models for mild and severe homocyst (e) inemia.* Proceedings of the National Academy of Sciences, 1995. **92**(5): p. 1585-1589.

107. Bhattacharyya, S., et al., *Cystathionine beta-synthase (CBS) contributes to ad- vanced ovarian cancer progression and drug resistance.* PloS one, 2013. **8**(11): p. e79167.
108. Morikawa, T., et al., *Hypoxic regulation of the cerebral microcirculation is me- diated by a carbon monoxide-sensitive hydrogen sulfide pathway.* Proceed- ings of the National Academy of Sciences, 2012. **109**(4): p. 1293-1298.
109. Wang, Z., et al., *L-Cysteine promotes the proliferation and differentiation of neural stem cells via the CBS/H2S pathway.* Neuroscience, 2013. **237**: p. 106- 117.
110. Takano, N., et al., *Decreased expression of cystathionine β-synthase pro- motes glioma tumorigenesis.* Molecular Cancer Research, 2014. **12**(10): p. 1398-1406.
111. Wróbel, M., P. Bronowicka-Adamska, and A. Bentke, *Hydrogen sulfide gener- ation from l-cysteine in the human glioblastoma-astrocytoma U-87 MG and neuroblastoma SHSY5Y cell lines.* Acta Biochimica Polonica, 2017. **64**(1): p. 171-176.
112. Zhao, H., et al., *Frequent epigenetic silencing of the folate-metabolising gene cystathionine-beta-synthase in gastrointestinal cancer.* PloS one, 2012. **7**(11): p. e49683.
113. Szabo, C., et al., *Tumor-derived hydrogen sulfide, produced by cystathionine- β-synthase, stimulates bioenergetics, cell proliferation, and angiogenesis in colon cancer.* Proceedings of the National Academy of Sciences, 2013. **110**(30): p. 12474-12479.
114. Zhang, Y., et al., *Overexpression of CBS/H2S inhibits proliferation and metas- tasis of colon cancer cells through downregulation of CD44.* Cancer Cell Inter- national, 2022. **22**(1): p. 1-12.
115. Al-Hajj, M., et al., *Prospective identification of tumorigenic breast cancer cells.* Proceedings of the National Academy of Sciences, 2003. **100**(7): p. 3983- 3988.
116. Zhu, P., et al., *Angiopoietin-like 4 protein elevates the prosurvival intracellular O2−: H2O2 ratio and confers anoikis resistance to tumors.* Cancer cell, 2011. **19**(3): p. 401-415.
117. Desai, S., S. Laskar, and B. Pandey, *Autocrine IL-8 and VEGF mediate epi- thelial–mesenchymal transition and invasiveness via p38/JNK-ATF-2 signal- ling in A549 lung cancer cells.* Cellular Signalling, 2013. **25**(9): p. 1780-1791.
118. Zhao, J., et al., *Trihexyphenidyl induced malignant hyperthermia in a patient with Parkinson's disease complicated with pneumonia: A case report.* Medi- cine, 2020. **99**(20).
119. Rajesh, K.M., V. Sinnathamby, and A.N. Sakthi, *Neuroleptic malignant syn- drome masked by cerebral malaria.* Case Reports, 2013. **2013**: p. bcr2013009061.
120. Downs, A.M., et al., *Trihexyphenidyl rescues the deficit in dopamine neuro- transmission in a mouse model of DYT1 dystonia.* Neurobiology of disease, 2019. **125**: p. 115-122.
121. Nair, A.B. and S. Jacob, *A simple practice guide for dose conversion between animals and human.* Journal of basic and clinical pharmacy, 2016. **7**(2): p. 27.

122. Qian, C., et al., *A Novel Extracellular Matrix Gene-Based Prognostic Model to Predict Overall Survive in Patients With Glioblastoma.* Frontiers in Genetics, 2022. **13**.
123. Giladi, M., et al., *Mitotic spindle disruption by alternating electric fields leads to improper chromosome segregation and mitotic catastrophe in cancer cells.* Scientific reports, 2015. **5**(1): p. 1-16.
124. Tang, H., et al., *SRPX2 enhances the epithelial–mesenchymal transition and temozolomide resistance in glioblastoma cells.* Cellular and molecular neurobi- ology, 2016. **36**(7): p. 1067-1076.
125. Wu, Z., et al., *SRPX2 promotes cell proliferation and invasion in osteosarcoma through regulating hippo signaling pathway.* OncoTargets and therapy, 2020. **13**: p. 1737.
126. Zhao, J., J. Xu, and R. Zhang, *SRPX2 regulates colon cancer cell metabolism by miR-192/215 via PI3K-Akt.* American journal of translational research, 2018. **10**(2): p. 483.
127. Gao, Z., et al., *SRPX2 boosts pancreatic cancer chemoresistance by activat- ing PI3K/AKT axis.* Open medicine, 2020. **15**(1): p. 1072-1082.
128. Lewis, M.J., J.P. Wiebe, and J.G. Heathcote, *Expression of progesterone metabolizing enzyme genes (AKR1C1, AKR1C2, AKR1C3, SRD5A1, SRD5A2) is altered in human breast carcinoma.* BMC cancer, 2004. **4**(1): p. 1-12.
129. Xiong, W., et al., *Elevated expression of AKR1C3 increases resistance of can- cer cells to ionizing radiation via modulation of oxidative stress.* PloS one, 2014. **9**(11): p. e111911.
130. Le Calvé, B., et al., *Long-term in vitro treatment of human glioblastoma cells with temozolomide increases resistance in vivo through up-regulation of GLUT transporter and aldo-keto reductase enzyme AKR1C expression.* Neoplasia, 2010. **12**(9): p. 727-739.
131. Hermawan, A. and H. Putri, *Systematic analysis of potential targets of the cur- cumin analog pentagamavunon-1 (PGV-1) in overcoming resistance of glio- blastoma cells to bevacizumab.* Saudi Pharmaceutical Journal, 2021. **29**(11): p. 1289-1302.
132. Bredel, M., et al., *A network model of a cooperative genetic landscape in brain tumors.* Jama, 2009. **302**(3): p. 261-275.
133. Cho, S.Y., et al., *Integrative analysis of KIF4A, 9, 18A, and 23 and their clini- cal significance in low-grade glioma and glioblastoma.* Scientific reports, 2019. **9**(1): p. 1-14.
134. Thangavelu, P.U., et al., *Overexpression of the E2F target gene CENPI pro- motes chromosome instability and predicts poor prognosis in estrogen recep- tor-positive breast cancer.* Oncotarget, 2017. **8**(37): p. 62167.
135. Fan, Q.-W. and W.A. Weiss, *Inhibition of PI3K-Akt-mTOR signaling in glioblastoma by mTORC1/2 inhibitors*, in *mTOR*. 2012, Springer. p. 349-359.
136. Zub, K.A., et al., *Modulation of cell metabolic pathways and oxidative stress signaling contribute to acquired melphalan resistance in multiple myeloma cells.* PloS one, 2015. **10**(3): p. e0119857.
137. Penning, T.M. and J.E. Drury, *Human aldo–keto reductases: function, gene regulation, and single nucleotide polymorphisms.* Archives of biochemistry and biophysics, 2007. **464**(2): p. 241-250.

138. Vargas-Toscano, A., et al., *Rapalink-1 targets glioblastoma stem cells and acts synergistically with tumor treating fields to reduce resistance against temozolomide.* Cancers, 2020. **12**(12): p. 3859.
139. Suwala, A.K., et al., *Inhibition of Wnt/beta-catenin signaling downregulates expression of aldehyde dehydrogenase isoform 3A1 (ALDH3A1) to reduce re- sistance against temozolomide in glioblastoma in vitro.* Oncotarget, 2018. **9**(32): p. 22703.
140. Li, D., et al., *Clinical significance of CBS and CCL21 in gallbladder adenocarcinomas and squamous cell/adenosquamous carcinomas.* Applied Immunohistochemistry & Molecular Morphology, 2020. **28**(2): p. 103-110.
141. Liu, Y., et al., *Cystathionine-β-synthase (CBS)/H2S System Promotes Lymph Node Metastasis of Esophageal Squamous Cell Carcinoma (ESCC) by Acti- vating SIRT1*. Carcinogenesis, 2022.
142. Zahalka, A.H. and P.S. Frenette, *Nerves in cancer.* Nature Reviews Cancer, 2020. **20**(3): p. 143-157.

Acknowledgments

First and foremost, I am very grateful to Prof. Dr. Ulf Kahlert for giving me this opportunity to engage in scientific research. He opened a door of scientific research for me, which changed my life and profoundly impacted my future clinical work. Thanks for taking care of my life in the past three years. Without his patience and help, I am unsure whether I can hold on till now.

Thank Prof. Dr. Carsten Berndt for giving me the opportunity to do experiments in his lab. I will never forget and appreciate his patient guidance.

Thank Dilaware, who helped me to start my research. Thank him for his guidance and help during the experiments.

To Ann Christin, I am eternally grateful for her kindness and patience. Thanks for helping me during the final period of my German life and letting me feel how friendly German people were. I wish her always to be happy and optimistic!

Additionally, I thank my neurosurgery colleagues Di Zhu in China and my project partner Enxi Xu. Due to their professional advice, the animal experiment of the project was completed in China, which laid the critical foundation for the application of THP in glioma.

I will never forget the great painter Michael's beers, games, and outgoings. Thank him for making me feel warm at home. He is the only person in Germany who remembers my birthday. Let our friendship last forever.

I thank my good friends Xuanchen Li, and Ke Li for their company and help. We will all remember this unforgettable study journey and are glad to have them.

I would like to thank my good friends Yannan Liu and Bo Yu for caring for my family in China and giving me support and help when I meet difficulties!

I would like to thank my good friends Haiqian Yu, Jing Qi, Heng Chen, Mingming Cui and Chuanxin Su for helping me to solve lots of difficulties in my life here.

Last but not least, thanks to my family, my wife, Ms Huo Shuran and my lovely son Mr Du Heda. Their supports are my biggest motivation to get an MD diploma. My biggest regret is that I could not accompany them for these three years, and I will use the rest of my life to be with them.